AN INVESTIGATION OF LATERAL SUPPORT SYSTEMS BY THE FINITE ELEMENT METHOD

by

Troy Clark

BSc Eng (Civil)

A thesis submitted in partial fulfilment of the requirements for the degree of Master of Science in Engineering.

Department of Civil Engineering

in association with

Centre for Research in Computational and Applied Mechanics

University of Cape Town

December 1993

Declaration

This is to certify that the calculations, results and other work presented in this thesis are essentially my own work, and that no part of it has been submitted for a degree at any other university

Troy Clark

December 1993

Acknowledgements

I would like to express my appreciation to the following people:

- My supervisors, Dr F Scheele for his help and expertise in the field of lateral support system engineering and Dr GP Mitchell for the assistance given to me with regard to finite element analysis. I would like to thank both my supervisors particularly for their patience throughout the course of my studies.
- The supervisors and students of the CERECAM computer room for their suggestions and help.
- My parents for assisting me financially and for their encouragement.
- My house mates at 10 Perth Rd for their friendship and support.

Abstract

The design of lateral support systems, in the context of surface excavations, are usually done using conventional (classical) methods of analysis. For these design procedures limit state assumptions are made concerning the lateral earth pressures acting on the structure to determine the support system characteristics. No information with regard to the deformation of the soil adjacent to the structure can be provided. The objective of this thesis is to examine the finite element method of analysis as an alternative design tool which is adaptable to a wide range of situations.

Finite element models are developed to investigate the influence of the plastic flow rule, wall friction and the soil type on the behaviour of a cantilever support system. Subsequently, the effect of wall stiffness, prop stiffness and the application of prop loads on the performance of a multiple level support system is examined. The results from these studies focus on wall displacements, lateral earth pressures, bending moments, plastic strain patterns and surface settlements behind the wall.

The investigation provides extensive information about the entire soil-structure interaction of the system. This potential of the finite element method can be used in the optimization of support system design.

A case study of a cantilever type and a multiple level supported wall is carried out using both conventional and finite element analysis methods. The lateral earth pressure distributions behind the multiple level supported wall calculated by the finite element method indicate the simple geometric shape assumed in the conventional analysis is not appropriate in this specific situation. The influence of the difference in these lateral pressures on bending moments and prop forces is demonstrated.

A definition of a factor of safety is proposed based on the dissipated plastic strain energy in the soil surrounding a cantilever type wall system. A preliminary study of this measure is made to evaluate its suitability for an expression of the stability of lateral support systems analysed using the finite element method.

Table of Contents

List of Figures

List of Tables

List of Symbols

Earth pressure:

Δ_a	displacement mobilizing active pressures
Δ_p	displacement mobilizing passive pressures
K_0	coefficient of at-rest, horizontal earth pressure
K_{ah}	coefficient of active, horizontal earth pressure
K_{ph}	coefficient of passive, horizontal earth pressure
e_{ah}	horizontal active earth pressure
e_{ph}	horizontal passive earth pressure
e_{ach}	horizontal cohesive active earth pressure
e_{pch}	horizontal cohesive passive earth pressure
E_{ah}	horizontal active earth thrust
E_{ph}	horizontal passive earth thrust

Wall friction:

μ	coefficient of wall friction
δ	angle of wall friction
δ_a	angle of wall friction on the active side of the structure
δ_p	angle of wall friction on the passive side of the structure

Material parameters:

ϕ	internal angle of friction of soil (Mohr-Coulomb)
c	cohesion of soil (Mohr-Coulomb)
β	internal angle of friction of soil (Drucker-Prager)
ψ	dilation angle soil (Drucker-Prager)
d	cohesion of soil (Drucker-Prager)
E	Young's modulus
I	moment of inertia
EI	bending stiffness

Description of stress:

σ_h	horizontal stress
σ_v	vertical stress

γ	density
z	depth below the ground surface
Z	maximum depth of excavation below the ground surface

Plasticity theory:

$\dot{\varepsilon}$	classical small strain rate tensor
$\dot{\varepsilon}^{el}$	elastic strain rate tensor
$\dot{\varepsilon}^{pl}$	plastic strain rate tensor
$\dot{\sigma}$	stress rate tensor
τ	shear stress tensor
D	elasticity tensor
$\mathbf{D}^*$	tangent modulus
$\dot{\lambda}$	plastic multiplier
$f(\sigma, H_\alpha)$	yield function
$g(\sigma, H_\alpha)$	flow potential
p	equivalent pressure stress
q	von Mises equivalent stress
r	third stress invariant
t	deviatoric stress measure
S	deviatoric stress
I	identity tensor
K	ratio of yield stress in triaxial tension to the yield stress in triaxial compression

Factor of safety:

GFS	generalized factor of safety
TSE	total strain energy
TUSE	total ultimate strain energy at failure
W^{pl}	plastic work
DE	dissipated plastic strain energy
UDE	Ultimate dissipated plastic strain energy at failure
FS	factor of safety
n	material parameter

CHAPTER 1
INTRODUCTION

1.1 BACKGROUND TO THIS INVESTIGATION

Lateral support systems are used to support earth where deep excavations have been performed. Deep excavations may be required, for example, in the construction of deep basements for high rise buildings, of subways or tunnels. A lateral support system consists of some type of wall retaining the soil and usually includes wall supports. There are a wide variety of wall and support types available in current practice.

For deep excavations in congested urban environments it is important that the analyst makes reliable predictions of the magnitudes of wall displacements. The wall deformations are one of the serviceability criterion in the lateral support system design because it may cause movements of the structures adjacent to the excavation. Conventional design techniques are not able to make reliable predictions about the behaviour of the system and therefore the need for more advanced techniques, such as the finite element method, exist.

The loading of the structure, in the form of earth pressure, is exerted by the supported material and is a function of the shear strength of the material, the deformation of the support system, inclination of the wall, surcharge loading and the level of the water table (Code of Practice, 1989). Design of lateral support systems is usually done using conventional (classical) methods of analysis. There are widely applied design assumptions concerning earth pressures acting on the system.

The conventional design methods have enabled designers to obtain satisfactory designs for cantilever walls and for relatively rigid walls. The designs are often, however, inaccurate for flexible structures in multiple level supported systems. Since the real earth pressure distribution deviates significantly from the classical distribution at failure, the assumption of a redistributed lateral pressure of simple geometrical shape is recommended for design purposes. The finite element method is capable of taking into account the relevant variables (e.g. soil characteristics, wall stiffness, wall friction, strut loads etc.) and can be used to analyse the system and accurately predict the real load on the system. It can therefore be used as a tool to investigate what influence the different parameters have on the earth pressures exerted on the structure. This information can help the designer in making a good assumption of redistributed shape for the particular soil and structure characteristics under consideration.

During the design process by conventional methods a factor of safety is accommodated in the design of a lateral support system, to guarantee the stability of the structure. A

suitable expression for a factor of safety needs to be developed if the finite element method, representing the numerical approximation of equilibrium, is to be used for design purposes.

1.2 OBJECTIVES

The main objective of this investigation is to use the finite element method to assess the design principles employed by conventional design methods. A secondary goal is to demonstrate the amount of information that the finite element method provides to help the designer in the design process.

The approach taken is to firstly investigate the influence of the plastic flow rule, wall friction and the soil type on the performance of a cantilever support system. Secondly, the effect of wall stiffness, prop stiffness and the application of prop loads on the performance of a multiple level support system is examined. The discussion of the results from these studies focus on wall displacements, lateral earth pressures, bending moments, failure patterns and settlements.

The calculation of lateral earth pressures, in particular, assist the designer in understanding the influence of the various parameters and enable the designer to make a good assumption of a redistributed shape when using the conventional approach. An understanding of how the various parameters influence the bending moments also assist the designer in optimizing the design, enabling a cost effective solution that meets the design criterion. The failure and settlement patterns cannot be calculated by conventional methods, although being important considerations, but are shown to be readily available from the finite element analysis.

A case study of two selected problems is then carried out, namely of a cantilever wall and a multiple level supported wall. The problems are analysed by both the finite element method and a conventional method. The assumptions of lateral earth pressure distribution made in the conventional approach are compared to the distributions calculated by the finite element method and the effect that the differences have on the response of the support systems are considered. Particular consideration is given to bending moments and prop forces. The cases studies also help to illustrate the advantages and disadvantages of the two approaches.

A further aim is to begin a study of a factor of safety that can be applied in finite element analysis. A proposed definition of a factor of safety is made based on the dissipated plastic strain energy in the soil surrounding a cantilever type wall system. A study of this measure

is made to evaluate its suitability for an expression of the stability of lateral support systems.

1.3 THESIS OUTLINE

Chapter 2 of this thesis discusses the literature that contributes to the modelling of support systems by the finite element method. The principles of the design of lateral support systems is also discussed briefly.

A description of the finite element models and the analysis procedures used to simulate construction is given in Chapter 3. For the purpose of the investigation, finite element models are developed that include the necessary features to perform the investigation. These serve as examples of what a model of a lateral support system should include to adequately predict the behaviour of the system.

In Chapter 4 the influence of the plastic flow rule and the effect of wall friction are investigated. Thereafter, different soil types are investigated using a model of a cantilever wall. The soil conditions chosen are isotropic and anisotropic sand and homogeneous clay.

Chapter 5 follows on with an investigation of the influence that wall stiffness, prop stiffness and additional prop loads have on the performance of a multiple level support system. The results are presented in terms of wall displacements, earth pressure distribution, bending moment distributions, failure patterns and settlements.

In order to demonstrate the capabilities of the finite element method, Chapter 6 includes a case study of a cantilever wall and of a multiple level supported wall is carried out. They are analysed by a conventional method and by the finite element method and comparisons made. The examples serve to illustrate how significantly the assumptions about earth pressures made during the conventional analysis can affect the design of the system.

The issue of safety factors is discussed in Chapter 7 and a preliminary definition of a factor of safety for the design of support systems by the finite element method is proposed. The quantity dissipated plastic strain energy is investigated as a measure for the purposes of introducing a factor of safety. The performance of the proposed definition is demonstrated for the case of a cantilever wall installed in three different soil types. A full study of the factor of safety is, however beyond the scope of this investigation.

Finally, Chapter 8 presents the conclusions and recommendations made based on the investigation as well as some suggestions on further work in this field.

CHAPTER 2
LITERATURE REVIEW

2.1 INTRODUCTION

The finite element studies published to date in the field of lateral support system engineering have largely been in the form of case studies or investigations of specific problems. Each case study focuses on the influence of one or two aspects of the support system. It should be noted that generally each problem has different boundary conditions, soil properties, a different wall type and other features specific to the situation. For this reason, the discussion in this chapter deals with each case study in turn under a heading that indicates the focus of interest. A brief description of the finite element model is included so that the findings can be evaluated in that particular context. During the discussion of the case studies, specific mention is made of any aspect that is relevant to the finite element model that was developed for this investigation.

2.2 OVERVIEW OF THE TYPES OF LATERAL SUPPORT SYSTEMS

In the past twenty years there has been a growth in the methods and products for retaining structures. In order to give a brief overview of the types of support systems used in practice a classification scheme is given in Table 2.1. The earth support systems are divided into two main categories, namely internally and externally stabilized systems. Externally stabilized systems use an external structural wall to achieve the stability of the supported earth mass and internally stabilized systems involve reinforcing the soil mass beyond the potential region of failure, and in doing so strengthening the critical shear zone.

Externally Stabilized Systems		Internally Stabilized Systems	
In-Situ	Gravity	Reinforced Soil	In-Situ Reinforcement
Downward	Upward	Upward	Downward
Construction Method		Construction Method	
Sheet piles	Massive wall (un-reinforced)	(Wide variety of reinforcing components)	Soil nailing
Soldier piles	Reinforced (cantilever)		
Cast-in-situ	Counterfort		
Bored-in-place	Gabion		
	Crib etc.		
Braced	Anchored	Hybrid Systems	

Table 2.1: Classification scheme for lateral support systems.

The traditional support systems are almost all externally reinforced. Gravity walls may be in the form of a cantilever type structure or precast structural elements where the earth is supported by the weight and stiffness of the structure. Temporary in-situ walls can be supported by bracing in the form of struts. More permanent support is provided by anchors which are grouted into the soil outside of the zone of potential failure. Figure 2.1 shows a schematic of a braced and an anchored support system.

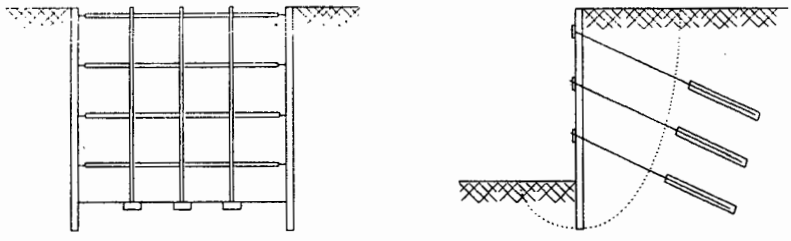

Braced sheet pile wall Anchored sheet pile wall

Figure 2.1: Examples of multiple supported wall structures.

The focus of this dissertation is on externally stabilized systems, specifically braced support systems. These are most commonly installed in the construction of long and narrow excavations where props extend between two opposite wall structures.

Design and construction of these lateral support systems can be analysed by advanced computer based methods, such as the finite element method, to optimize the design of the system and to evaluate ground movements. A review of selected case studies, subsequently undertaken in this chapter, shows that the method has been successfully used in practical design and for the purposes of predicting the performance of lateral support systems.

2.3 DESIGN PRINCIPLES FOR CONVENTIONAL METHODS

The first stage of the analysis by conventional methods is to determine the earth pressures acting on the structure. These are dependent on the deformation of the support system. The movement of the structure causes shear stresses to be mobilized in the adjacent soil material until the stresses reach a limiting value, namely the shear strength of the material. Movements towards the excavation result in a decrease in the earth pressure exerted by the supported soil. When sufficient movement has occurred to mobilize the maximum shear strength of the supported material the earth pressure reaches a limiting value known as active earth pressure. Similarly, movements towards the supporting soil result in an increase in earth pressure to a limiting value known as the passive earth pressure. If there is no wall movement at all, the earth pressure exerted on the support system is known as

the earth pressure at-rest. The coefficients of earth pressure K_0, K_a, and K_p at these three stages, with respect to wall movements, are shown in Figure 2.2.

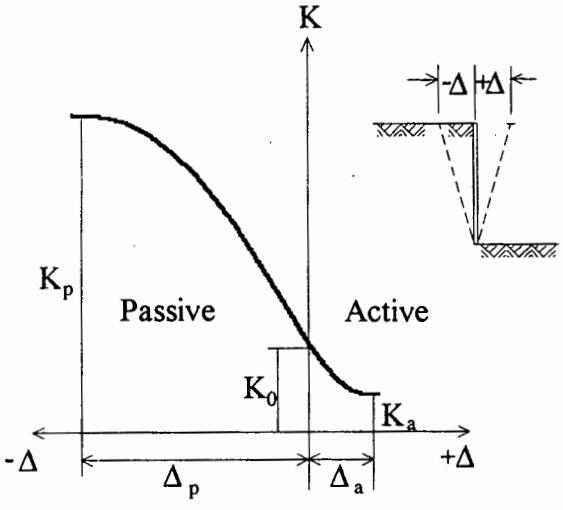

Figure 2.2: Relationship between wall movement and coefficient of earth pressure [after Winterkorn and Fang (1975)]

The classical earth pressure theories (Rankine or Coulomb) are based on limit considerations. This means that at failure earth pressures are fully mobilized and the full active and passive earth pressure conditions exist. These approaches cannot be used to predict deformations and the finite element method is suggested as a suitable method for doing so.

The objective of the design of support systems is to ensure the stability of the systems and thus restrict wall movements. Stability is the equilibrium of activating and resisting forces. Activating forces include the weight of the supported material, water pressure, surcharge loading, induced loading, seismic forces etc. Resisting forces include passive resistance, resistance of the retaining structure, strut or anchor loads and shear resistance within the supporting material.

Lateral support systems are designed to resist the forces acting on the structure within a margin of safety. No single design method is recommended.

In general, the design principles of cantilever or strutted/anchored walls are as follows:

(a) Evaluation of the lateral pressures exerted on the wall.
    It is noted that the classical earth pressure distribution can only be expected in certain circumstances and it is recommended that provision is made for earth pressure redistribution.
(b) Check equilibrium of the horizontal and vertical forces.
(c) Check moment equilibrium of the complete structure.

(d) Compute the shear and bending moments due to the applied lateral pressures.
(e) Design the structural members and elements in accordance with the calculated values. Including the design of ground anchors.
(f) Evaluate the overall stability and stability against wedge or sliding block failure.

Further specific recommendations are made with regard to earth pressure redistribution for anchored walls. The commonly applied redistribution patterns for single and double level supported walls are shown in Figure 2.3. The design of the support system which includes the calculation of prop forces is based on the assumption of redistributed earth pressures.

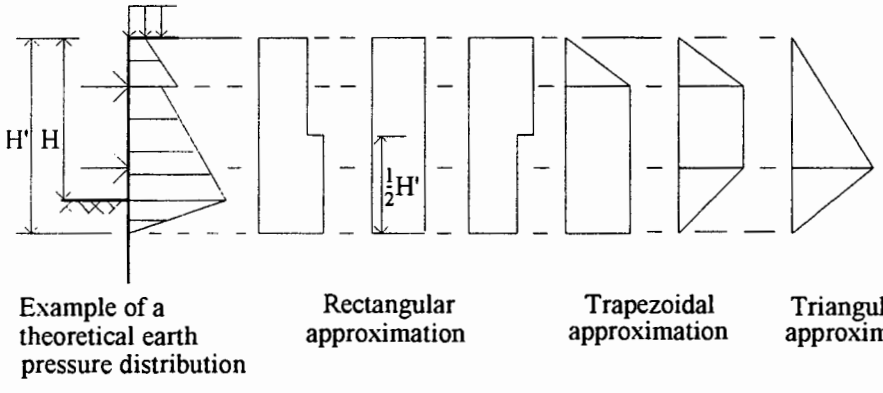

Figure 2.3: Simplified earth pressure distributions [after Code of Practice (1989)]

2.4 CASE STUDIES: GENERAL FINDINGS ON THE INFLUENCE OF VARIOUS PARAMETERS

This section deals with the various influences that were investigated which included initial pressures and soil/structure contact conditions; construction technique; wall stiffness and supported walls in general.

2.4.1 Initial Pressures and Soil/Structure Contact Conditions

An effort to improve the finite element modelling of lateral support systems was made by Félix *et al* (1982). This was carried out by comparing the full scale measurements undertaken during the Le Havre harbour quay wall construction with the results of the quay wall analysis obtained by Blivet *et al* (1981) . The aspects of the finite element model that were addressed related to:

- the stresses at the wall soil interface just after the diaphragm wall installation. Measurements revealed values that were higher than the values for horizontal stress obtained from calculations based on $\sigma_h = K_0 \sigma_v$;
- the introduction of interface elements to allow sliding and separation to occur between the soil and structure.

The quay wall was constructed in a fine grained, cohesionless sand and angle of internal friction of $\phi' = 45°$. The horizontal earth pressure coefficient at-rest was $K_0 = 0.45$. The Young's modulus of the soil increases with depth according to the relation:
$E = 230\ (\sigma'_3)^{0.58}$ MPa, where σ'_3 is the pre-consolidation stress applied in a triaxial test which was similar to the vertical in-situ stress. The coefficient of 230 is an empirical value.

The concrete quay wall was constructed with the dimensions 1.2 m by 24.5 m deep. A layer of grouted anchors was installed with a prestressed force of horizontal component equal to 583 kN/m. The sequence of construction was accurately simulated in the analysis where excavation was carried out to a final depth of 16.5 m.

In the finite element model of Blivet *et al*, (1981) an elastic perfectly plastic constitutive soil model with a Mohr-Coulomb yield criterion was applied. Soil and wall elements were modelled using 8-noded plane strain elements. Line elements were used to represent the anchors and the nodes representing the grouted anchor length were pinned to the soil elements. The contact between wall and soil was assumed to be perfect allowing no relative movement. The initial stresses in the soil were assumed to be those of the undisturbed material i.e. defined by the unit weight of the material and the earth pressure coefficient at-rest K_0.

The results of the analysis showed that the earth pressures at-rest were lower than the measured values. Upon the anchor prestressing the wall displacements above the anchor level were directed away from the excavation, whereas the measured results indicated displacements towards the excavation. After the excavation had been completed to the design depth results indicated local peak values of earth pressure and bending moments at the anchor level and between the anchor and the base of the excavation. The computed values of effective earth pressures generally underestimated the measured ones.

The improvements made to the original model were:

- The installation of the wall into the soil in two steps in order to include the effects of prestressing the soil during the construction of the diaphragm wall. The wall was introduced in the first step with properties equal to zero (i.e. introducing a space of the same dimensions as the wall). The wall was then introduced with the properties of concrete and placed under compressive stress. The resulting lateral stresses were higher than those of the at-rest condition.
- To allow relative sliding between wall and soil, interface elements with a friction law between soil and wall elements were inserted.

The results from the model by Félix *et al*, (1982), which included these improvements, showed for the stage after prestressing the anchors that the wall displacements were

due to the contribution of the increased initial stresses, however, the results for the *final* stage of excavation predicted a wall displacement of parallel translation rather than rotation about the anchor level which the measured results demonstrated. The effect of increasing the initial stresses seemed to be the cause of the poor agreement. The results of bending moment distributions and earth pressures seemed to improve the agreement with the measured values qualitatively.

The findings of this work showed that the influence of initial stresses were significant although not fully understood, and that the introduction of adequate interface elements between wall and soil lead to an improved performance of the model.

2.4.2 Construction Technique

During the simulation of excavation, consideration needs to be given to the "construction technique". Smith and Ho (1992) use the term "to describe variables such as stiffness of struts, depth of excavation steps and the order of placement of struts".

The authors performed a case study of an excavation in a multi-layered soil consisting of sand and soft clay overlying a stiff clay. The soil was modelled using an elastic perfectly plastic Mohr-Coulomb criterion. The four-level supported sheet pile wall that was used to support the soil was 24 m deep and the excavation depth was 9 m. Interface elements were included between soil and structure.

The variables considered to simulate various construction techniques were wall stiffness, order of strut installation and strut stiffness. Four different walls with a bending stiffness of, 34, 54, 87 and 135 MNm^2/m were investigated. In the construction sequence, four different methods were used, each varying the number of struts and the order of strut placement. Two extremes of strut stiffness coefficient were used, namely 20 000 kN/m and 2000 kN/m.
The study investigated the influence on the maximum wall deflection only.

The results from finite element analyses indicated that the influence of wall stiffness increased the maximum wall deflection by about 70% increasing the wall bending stiffness from EI = 34 MNm^2/m to 135 MNm^2/m. There were only small increases in deflection with the inclusion of more struts and this trend held for all wall and strut stiffness values considered. The effect of low strut stiffness for this case was increased maximum wall deflections by 50% and increased bending moments at the mid span by up to 50%.

A brief investigation of plastic hinging of the wall structure was made by the authors by setting a plastic limit to the wall material. The redistribution of forces caused by the formation of a plastic hinge increased the bending moment in other levels of the wall which

gave an indication where further plastic hinges would form. The effect of plastic hinging in the case study showed an increase in maximum wall deflection by about 20%.

The conclusions drawn from this work were that the correct simulation of the construction technique is at least as important as adequately characterising the soil. Also that the influence of plastic hinging was found to be an important consideration under conditions where wall deflections are sufficiently high to cause the yielding of the wall, such as excavations with an applied surcharge load.

2.4.3 Wall Stiffness

The problem of designing supported, flexible walls by the conventional method is that redistribution of earth pressures occur resulting in earth pressure distributions that deviate from classical earth pressure distributions. The influence of wall stiffness has therefore been a topic of some interest.

A finite element analysis of a single anchored wall in sand was undertaken by Egger (1975). The analysis was performed for a flexible sheet pile wall and a stiff, concrete diaphragm wall where the ratio of stiffness is 1:100. The excavation was performed in stages and the anchor was prestressed.

The wall behaved as a cantilever system before the anchor was installed and results showed two main trends. Firstly, for the flexible wall, the depth over which passive earth pressures were mobilized was much shallower than for a stiff wall. Secondly, prestressing the anchor caused an increase in the earth pressure behind the wall at the level of the anchorage. This increase in earth pressure is concentrated in the region immediately behind the anchor for the flexible wall, whereas for the stiff wall it is more spread out over a greater region of the wall height. These two trends continued throughout the excavation stages.

The effect of wall stiffness was also studied by Potts and Fourie (1985). The parameters involved in the study were the coefficient of earth pressure at-rest K_0 and the wall stiffness. The results were compared with the works of Rowe (1952) and Terzaghi (1954). Four walls of different stiffness were chosen to represent a 'rigid' wall, a diaphragm wall, a sheet pile wall and a 'soft' wall. Bending stiffness of EI = 2.3×10^6, 2.3×10^3, 78 and 23 MNm^2/m, respectively, were assigned to the various wall types.

The finite element analyses modelled a 20m deep, single propped retaining wall in a cohesionless sand. A Mohr-Coulomb constitutive model was used with a fully associative flow rule. The details of the soil/structure interface were not described. The Young's

modulus was assumed to be increasing with depth according to the relation E = 6000Z kN/m²/m, where Z is the depth below ground surface. The prop was inserted at the top of the wall and excavation was simulated by the removal of layers until a maximum depth was reached. Analyses for all four walls were performed for both K_0 = 0.5 and K_0 = 2.0. It should be noted that K_0 values for sand do not under normal circumstances exceed unity, however K_0 values as high as this do occur in overconsolidated clays.

The results of wall displacements for the K_0 = 2.0 case range from the mode rotation about the top for the 'rigid' wall to large displacements at mid-height for the soft wall causing the wall to 'bulge' out. The rotation about the top mode is less pronounced for the K_0 = 0.5 case. Active earth pressures for the K_0 = 2.0 case and the rigid wall showed a parabolic distribution with a maximum value at mid-height of the wall, whereas the active earth pressure distribution for the soft wall clearly demonstrated arching between the prop level and the excavation level. The results for the diaphragm wall and the sheet pile wall, with respect to wall displacement and active earth pressure distribution, fitted in between these two extremes.

For K_0 = 0.5 the active earth pressure for a 'rigid' wall showed the classical triangular distribution whereas the results from the analyses with the other three walls showed a similar trend as for the K_0 = 2 case.

Bending moment distributions demonstrated that for K_0 = 2.0 the bending moments for the 'rigid' wall and the diaphragm wall were much higher than those predicted by the conventional analysis. In all other situations the bending moments were lower than those found by conventional analysis. The trends observed for bending moments were also true for prop forces.

The results obtained from the finite element analysis were compared with the results taken from Rowe's data. They are presented to demonstrate the effects of wall flexibility in a graph of bending moment reduction factor $\frac{M}{M_{LE}}$ against the logarithm of wall flexibility number $\rho = \frac{H^4}{EI}$, where M is the maximum observed moment and M_{LE} is the bending moment calculated by the limit equilibrium method and H is the height of the wall. The material properties used in the theoretical analysis were comparable to those used in the experimental tests. The authors noted that Rowe's reduction factor does not take into account the influence of K_0.

Good quantitative agreement was found between the theoretical results and the experimental results for the case of K_0 = 0.5. The values of the moment reduction factor

for cases where $K_0 > 0.5$ were greater than those for $K_0 = 0.5$. This increase was shown to be more pronounced with an increase in wall stiffness. These results describe the same trend in moment reduction factor as predicted by Rowe, (1952).

To summarize the main findings of this study of a propped embedded retaining wall it can be said that for the case of a low K_0 the predicted bending moments for the walls over the range of stiffness considered were lower than those found by the conventional method. The stiffer the wall the closer the bending moments approach the values found by the conventional method. For the case of high K_0 the bending moments and prop forces for stiff walls greatly exceeded those found by the conventional method. The finite element method therefore demonstrates its ability to facilitate a more efficient design and to include the effects that initial earth pressures have which are not adequately predicted by the conventional method.

Potts and Day (1990) consider the effects of wall flexibility with respect to economic considerations. Three typical excavations in the London area were analysed to see if sheet pile walls could have been used instead of diaphragm retaining walls. Sheet pile walls are more flexible and therefore allow more stress redistribution at the expense of increased wall displacements. The results from the excavations they simulated clearly showed the redistribution of stresses when a wall of lower stiffness was used. The findings of the study were that sheet pile walls were generally capable of replacing the diaphragm walls, considering structural aspects only, and were more economically viable.

2.4.4 Supported Walls in General

The finite element method is useful in the design of anchored walls to ensure reliability and to optimize wall design. Many analyses have been done as case studies of completed support system constructions which include field observations, or as preliminary design analyses.

Murakami *et al* (1988) performed a case study on an excavation in soft undrained clay in Osaka. The performance of an anchored sheet pile wall and the effect of anchor rupture was analysed by the finite element method. A potentially dangerous situation was identified when an anchor which has been installed suddenly ruptures. The load of this anchor gets redistributed to the adjacent supports and this may lead to the failure of the system. The excavation analysis was also used to investigate the mechanism of load redistribution through an experiment involving anchor release.

The length of the sheet pile wall was 16 m and the depth of the excavation was 10.4 m. The finite element specifications were not described in detail. Four levels of anchors were

installed at 2 m intervals with the grouted part of the anchor length situated in layers of stiffer material. The design anchor loads are calculated such that each row of anchors supported its lower row portion of the wall. A prestress load of 85% of the design load was applied at anchor installation.

During the exercise of releasing the anchors the following sequence was followed: anchors in the bottom row were released one at a time and the load redistribution to the adjacent anchors measured; material was then backfilled to 0.5 m below the next row of anchors. Anchors in the row above were then released successively with load redistribution again being measured; the process was repeated until all anchors were released.

An examination of the results of load redistribution showed that most of the load was redistributed downward to the lower ground and only a very small percentage to the adjacent anchors. The observed trend was as the number of rows got fewer the greater the load redistribution to adjacent anchors. The most extreme case was therefore when only the top row of anchors remained and almost 10% of the load was redistributed to adjacent anchors. The wall was found to be safe and the maximum load redistribution due to anchor rupture was about 20 kN.

Wall displacements, surface settlements and lateral pressure calculations showed good agreement with measured values during the excavation stages. The shape of the earth pressure distribution behind the wall changed from the classical triangular distribution at rest to a trapezoidal distribution with the installation of the anchors. The effect of preloading the anchors was an increase in earth pressure at the anchor level and a decrease just below the anchor level. The case study demonstrated the soil-structure interaction of an anchored wall and the mechanism of load redistribution.

Another construction that was simulated by the finite element method was of a braced excavation in saturated, anisotropic clay in Chicago. Finno *et al* (1991) reported a simulation of the construction using a coupled finite element formulation to solve for ground movements, pore water pressures and wall deflections. The paper stressed the importance of accurately modelling the construction procedure, including sheet pile installation, and the constitutive behaviour of the soil. This particular case was identified as an interesting test for the capabilities of the finite element method in modelling lateral support systems because of the unexpected responses of the system during construction. These responses were the effect of sheet pile installation, rapid changes in pore water pressure and the development of two incipient shear surfaces on the active side of the wall.

The soil conditions on the site were a rubble fill overlying a series of clay layers. The clay behaviour was simulated using the Modified Cam Clay model and eight-noded elements

with pore pressure degrees of freedom at the corners. Interface elements were included between the soil and wall beam elements. The total length of sheet pile wall was 19 m and the maximum excavation depth was 12 m. It was felt that the modelling of the sheet pile installation was necessary, instead of the conventional approach of assuming the support wall already in place with no disturbance of the in situ soil mass. The time given for the dissipation of pore water pressures was also included.

The sheet pile installation was modelled by displacing two columns of nodes, that initially have the same position, away from one another by an amount equal to the equivalent width of the sheet pile section. One column of nodes is then removed and restraints removed from the other and the beam elements for the sheet pile wall are included. An appropriate shear stiffness for the wall-soil interface is applied.

The values of measured results of earth movement during the sheet pile wall installation compared well with computed results as did results of pore water pressure, where installation induced an increase in pore water pressures adjacent to the wall followed by a gradual decrease. The ground movements adjacent to the sheet pile wall affected a wider soil mass than in the computed results.

During the excavation and bracing stages of excavation, computed lateral ground movements agreed reasonably well with measured values. The opposite sides of the excavation show different displacement patterns and the authors highlight the advantage of modelling the whole problem in the case of narrow braced excavation. The cantilever stage showed good agreement but the trend of movements differed during the first level of strut installation. The computed values under-predicted above the mid span of the wall and over-predicted below. A more detailed look at the strain contours during this stage showed that the computed results compare reasonably well although they showed lower values spread over a wider area. This difference also results in a difference in settlements, where smaller settlements are computed near the wall and larger values away from the wall when compared to the measured results. What was significant about the strain contours was that the computed pattern did not capture the incipient shear surface that the measured pattern exhibits. This did not however, prevent the model from giving reasonable results.

The pore water pressure calculations also did not reflect the sudden drop in pressure at certain stages of the excavation which are suggested by the authors to be the stages where strain localization is initiated. Computed results were higher than measured results at the end of the excavation.

The authors analysis of these results were that they demonstrated two main weaknesses in lateral support simulation. Those were the incorrect assumptions of K_0 conditions after assuming that the sheet pile wall is already in place, and the inability of commonly used constitutive models to permit strain localization. They also demonstrated through a parameter study the importance of good simulation of construction procedures and the accurate modelling of the soil. In particular, a soil model capable of modelling anisotropic clays was important in this analysis.

An analysis of a deep excavation for an underground parking garage, in a stratified soil in Boston was performed by Whittle *et al* (1993). The authors introduced their paper by giving a brief review of the important aspects of modelling support systems of this nature that have been reported in previously documented case studies.

A summary of the factors that the authors recommend the analyst should pay careful attention to are as follows:

- Initial conditions in the ground including stratigraphy, initial stress state and the ground-water flow regime. These can all influence the mode of deformation of the wall;
- Selection of engineering properties which requires adequate laboratory and field characterization of engineering properties of soil in all layers, and appropriate constitutive modelling of the soil where behaviour controlled by effective stresses is preferred;
- The construction process should be simulated as closely as possible. Aspects which are often neglected are modelling the installation of the sheet pile wall, dewatering and real-time simulation of coupled flow and deformation in the soil;
- Correct analytical procedures for the simulation of incremental excavation should be included in the finite element program.

The underground parking garage structure comprised a reinforced concrete wall 0.9 m thick and 26 m deep. The soil profile consisted of layers of soil which were from top down: fill, clay, sand, till, weathered argillite and sound argillite. The wall was supported by a roof slab at the top and floor slabs at 3 m intervals to a depth of 16.8 m. The elastoplastic model used Drucker-Prager failure criterion with a non-associated flow rule. A mixed finite element formulation was used to describe flow and deformation in the soil. Construction procedures are followed as closely as possible although the wall is 'wished-in-place' i.e. no simulation of the effects of installing the wall was attempted.

Computed results of wall movements compared well with measured values until the third floor was constructed. From this stage the analysis significantly under-predicted the

maximum displacements. The comparison of settlements between computed and measured results was good until the installation of the third level when the computed values over-predicted the settlements measured. There were large differences in results when a comparison of predicted and observed pore water pressures was made. The reason was thought to be in the choice of permeability properties.

In order to try and improve the performance of the model two main modifications were made: floor slab shrinkage was simulated; and a constant pore water pressure condition was specified in the intact argillite. These modifications led to greatly improved results from the analysis for lateral movements, settlements and pore water pressures.

The effect of the post construction shrinkage of the concrete floor slabs contributed most to the differences between predicted and measured results. This should be a consideration in analyses of a similar nature. It is clear from this case study that an accurate description of soil properties should be invested in to limit the uncertainties in the problem.

CHAPTER 3
THE FINITE ELEMENT MODEL

3.1 INTRODUCTION

For the purposes of this investigation two basic models were developed. The first is a model of a flexible wall installed in soil for excavation analyses involving flexible retaining walls, for example, a sheet pile wall. The second is of a rigid wall installed in soil for analyses of excavations adjacent to, for example, a concrete diaphragm wall. These two wall types were selected so that the investigation could cover a wide range of wall types. The geometric differences between a relatively thin steel sheet pile wall and a thick concrete diaphragm wall necessitated two models.

In this chapter these two models are described together with the reasons for the decisions made during the model development. The analysis procedure used for simulating the excavation by the downward construction method is described and finally, a summary of the constitutive model that is used to model the soil is given.

Certain aspects of lateral support systems have been identified in the literature as being important to model accurately. These are as follows:

- Initial conditions in the ground including stratigraphy and initial stress state;
- soil parameters (values should be selected conservatively if there is uncertainty about their real value);
- adequate representation of the constitutive behaviour of the soil;
- accurate simulation of the construction procedures involved.

Special emphasis was placed on these aspects of the finite element model and they are dealt with in this chapter, except for the soil parameters which are discussed in Chapter 4.

3.2 FLEXIBLE WALL MODEL

3.2.1 Finite Element Representation

The problem domain consists of a flexible wall which is assumed to be already installed in horizontal ground. The boundaries are chosen far enough away from the wall so that the behaviour of the wall structure, due to loading, will not be influenced by the boundary conditions. The mesh is discretized with a higher degree of refinement in those areas of the soil where plastic deformations occur. The elements in these regions need to be sufficiently small for an accurate solution. These regions occur immediately adjacent to the wall where, intuitively, the regions of largest deformations can be expected. The layout of the mesh, including the dimensions of the problem are shown in Figure 3.1.

The problem was solved using the non-linear, multi-purpose, finite element program ABAQUS (Hibbitt, Karlsson and Sorenson, 1992). The soil elements are modelled using four-noded, quadrilateral, reduced integration, plane strain elements with hourglass control. Hourglass control is required for this problem to ensure that spurious zero energy modes associated with the 'hourglass' modes does not arise. The wall is represented by two-noded linear beam elements.

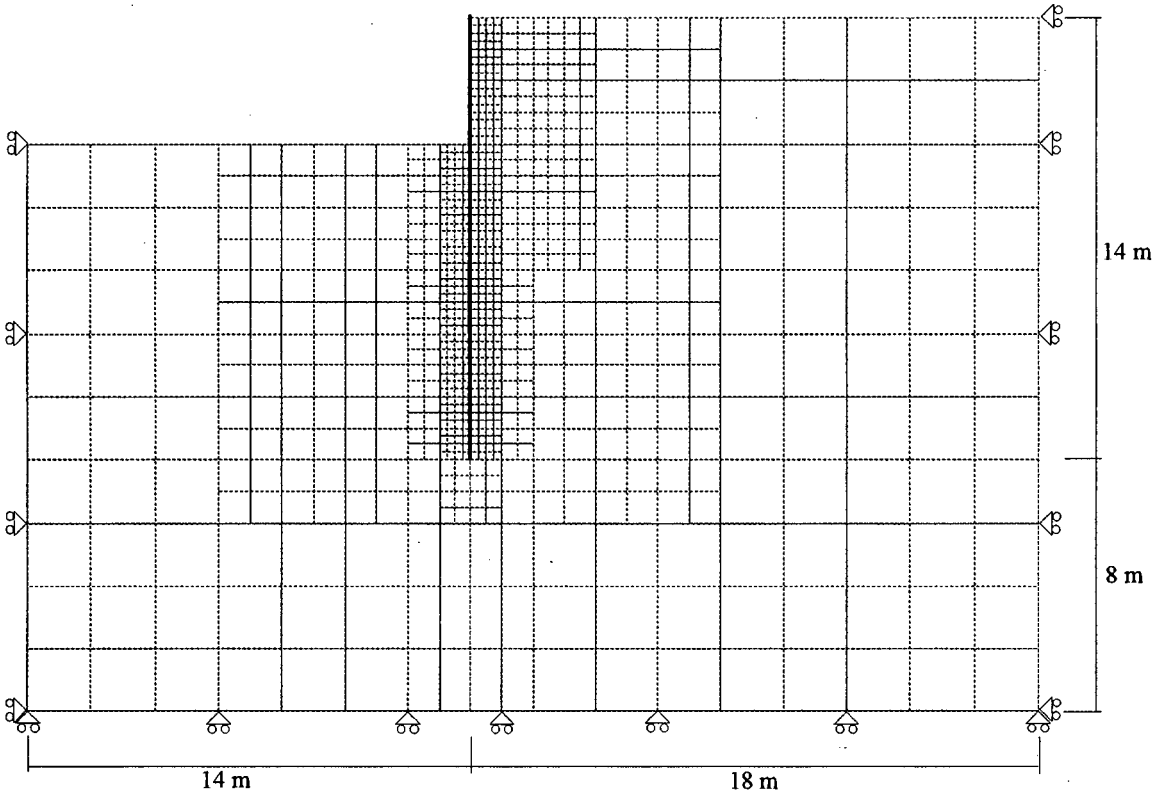

Figure 3.1: Mesh layout of the flexible wall model after 4 m of excavation, including dimensions and boundary conditions.

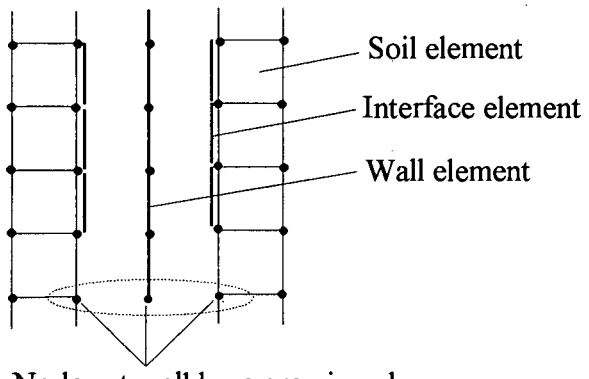

Figure 3.2: Detail of soil-wall interface and wall base constraint.

Interface elements are placed between the soil and the wall elements on either side of the structure. These elements are implemented to allow soil-structure interaction which involves relative sliding, and possibly separation between the soil and the wall. The interface elements are attached to the soil elements by sharing nodes with soil elements. The nodes defining the wall beam elements correspond geometrically to the interface element nodes. The wall is then defined

as the boundary along which the interface elements could slide. To model the soil-structure interaction of a retaining wall, interface elements are required on both sides of the wall. No interface elements are required in contact with the lowest wall element, since the wall-soil interface conditions are taken care of by the interface elements as shown in Figure 3.2 which is a schematic of the finite element model of the wall and adjacent soil elements in detail. It should be noted that the contact zone between wall and soil is exploded sideways and that the nodes of both interfaces and the wall nodes have, in fact, the same co-ordinates.

It is necessary to incorporate the frictional effects that occur between the wall and the soil into the model. This is achieved by using the classical Coulomb friction model, available in the ABAQUS code, in conjunction with the interface elements. The friction model is based on a penalty method that allows some relative motion, called 'elastic slip', when the interface should be sticking. The allowable 'elastic slip' is kept to a small fraction of the characteristic length of the interface element (set to 5 mm per 1 m length as recommended in the ABAQUS *User Manual*). A coefficient of friction is required for the friction model that is based on the properties of the materials that are interacting. The value of the friction coefficient, μ, is chosen according to the recommendations for conventional design practice, namely $\mu = \tan\frac{2}{3}\phi$, where ϕ is the internal friction angle of the soil.

3.2.2 Wall Supports

For the investigation of multiple level supported systems, the prop supports are represented by spring elements. The forces exerted by the supports are as a result of the deformation of the wall and thus the spring deforms according to the equation $F = ku$ where k is the spring stiffness coefficient, and u is the spring deformation. When a spring is introduced into the model one end node is attached to the wall and the other end node is fully fixed as a boundary condition in the same horizontal plane.

3.2.3 Boundary Conditions and Loading

The left and right boundaries of the model are constrained horizontally. These edges are free to move vertically to allow for settlements under gravity loading and heaving due to the relief of load that occurs during excavation. The bottom edge of the mesh is constrained vertically. The boundary conditions are shown in Figure 3.1.

A method to tie the wall to the soil is also required. The procedure used is that the node at the base of the wall is attached (i.e. constrained horizontally and vertically) to the soil nodes at those co-ordinates as shown in Figure 3.2.

Constraints are used at the boundaries that separate elements of different levels of refinement. A linear type of constraint is required for this model because the elements are first-order elements. Figure 3.3 illustrates the method where the degrees of freedom of the nodes m_1 and m_2 are constrained to be interpolated linearly along the edges of the larger elements.

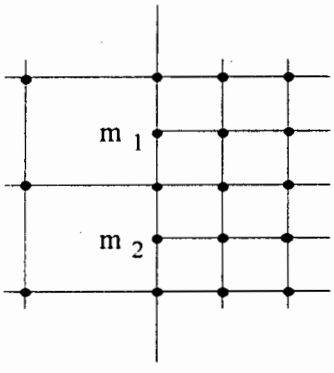

Figure 3.3: Schematic illustrating constraints used in mesh refinement.

Gravity loading is applied to the soil mass and the initial stress state of the soil is described according to the equations of at-rest earth pressure. The vertical stresses are calculated from $\sigma_v = \gamma z$, where z is the depth below the ground surface and the horizontal stresses are found from $\sigma_h = K_0 \sigma_v$, where K_0 is the horizontal coefficient of at-rest earth pressure. The first step of the analysis is used to ensure that this initial state is in equilibrium with the gravity load. For this step the coefficient of friction between wall and soil must be set to zero. The following step of the analysis the real coefficient of friction is introduced.

3.3 RIGID WALL MODEL

The rigid wall model is, in principle, similar to the flexible wall model except for the elements used to model the wall. In this case the elements used to represent the rigid wall are similar to the soil elements (4-noded, quadrilateral, reduced integration, plane strain elements with hourglass control). The mesh plot of the rigid wall model, including the dimensions is shown in Figure 3.4.

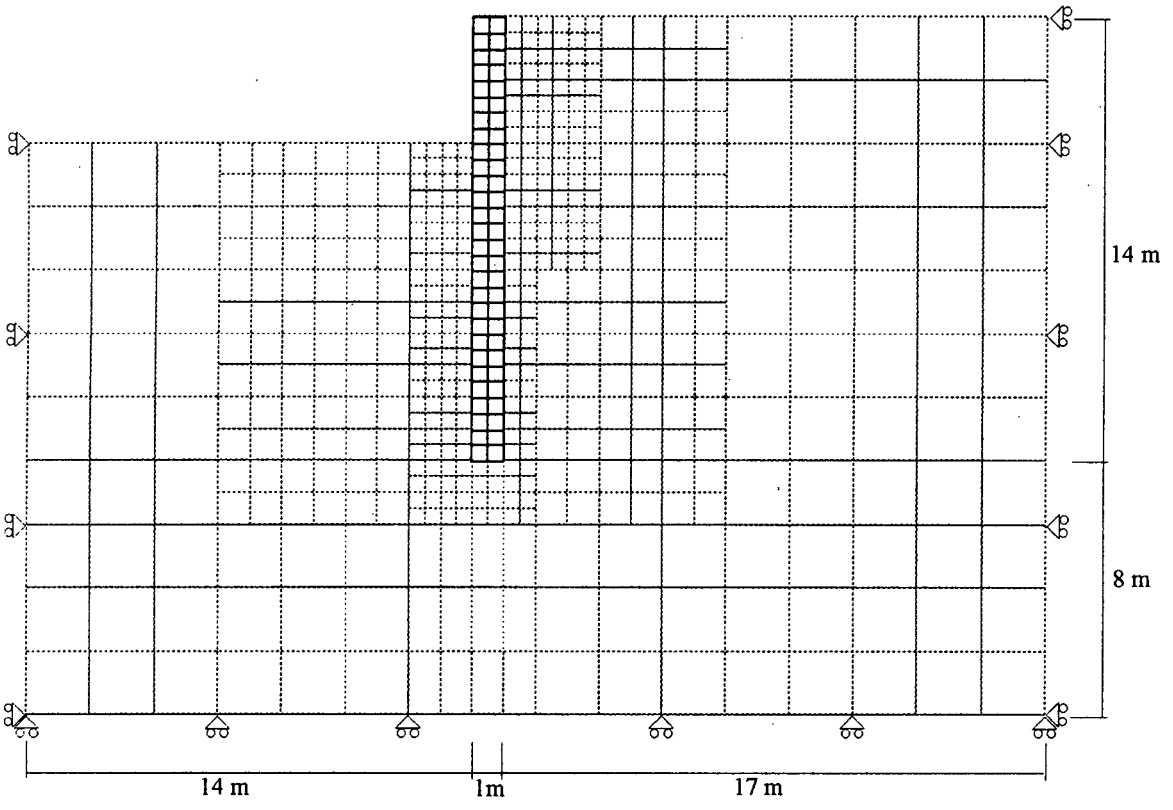

Figure 3.4: Mesh layout of the rigid wall model after 4 m of excavation, including dimensions and boundary conditions.

The rigid wall model requires a similar definition of the interfaces between wall and soil. The interface element boundaries are defined as the nodes on each side of the wall and each boundary is associated with the nodes of the soil with which it is in contact. At the base of the wall, the middle and corner nodes are pinned to the soil nodes that have the same co-ordinates. The arrangement is illustrated in Figure 3.5. Again, no interface elements are required on the soil elements in contact with the lowest wall elements.

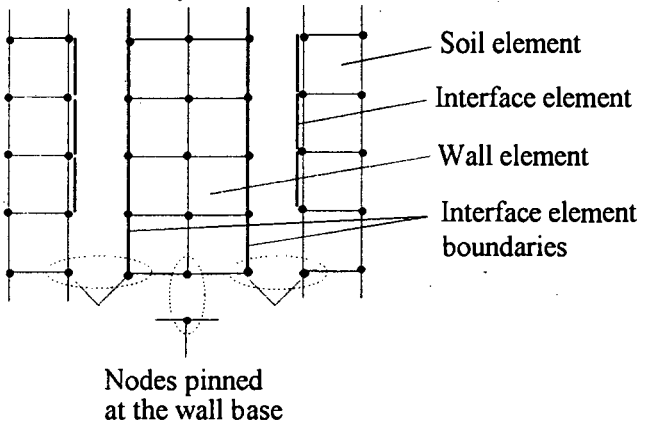

Figure 3.5: Detail of wall-soil interface and wall base constraint for the rigid wall model.

3.4 SIMULATION OF THE CONSTRUCTION PROCEDURE

3.4.1 Simulation of excavation

The presence of interface elements between the wall and the soil requires a special two step procedure for simulating excavation. The first step involves the removal of the interface elements. To achieve a solution, only the nodes of the interface elements that are to be removed, and the corresponding nodes on the interface boundary, are fixed. In the second step, these fixities are released and the soil elements to be excavated are removed. ABAQUS applies nodal forces equal to the reaction forces at the boundary of the removed elements and ramps these forces down, i.e. decreases the nodal forces over a number of increments, until they reach zero.

Layers of elements, representing a 1 m depth of soil, and their associated interface elements are removed one at a time. For the analysis of cantilever walls this is repeated until a solution cannot be achieved during the excavation step. An attempt is then made to remove a layer 0.5 m deep so that the maximum depth of excavation can be calculated to the nearest 0.5 m The last successful excavation depth solved for is considered to be the maximum depth of excavation just prior to the failure of the system.

3.4.2 Simulation of support installation

In ABAQUS new elements cannot be introduced during the analysis once the analysis is under way. Therefore all the spring elements, that represent the wall supports, are included in the original model before the analysis is started and are removed after the equilibrium check of initial stress conditions. Once the layers of soil elements have been removed to 1 m below the relevant prop level the prop installation is simulated by re-introducing the relevant spring element into the model. At this stage the spring elements are re-introduced and will be stressed since some wall displacement has occurred. The props, therefore, exert an initial load. The procedure of excavation and prop installation is repeated until all the wall supports are in place and the design depth reached. The final load of the supports is exerted at this stage.

A modified procedure is used to simulate the prestressing of props. Additional loads are applied to the props to simulate a similar soil/structure interaction which takes place when soil anchors are prestressed. In anchor practice, the prestress loads are usually applied after installation. The prestress loads are a recommended percentage of the anchor working load (i.e. the calculated load that the anchor exerts at the design depth, including a factor of safety). The method of calculating the working loads cannot be the same as the method employed by conventional design methods since the finite element method is an

equilibrium based solution scheme, and factors of safety cannot be included in the support forces.

The procedure used to simulate prop prestressing in this investigation is performed in two stages. Firstly, the magnitude of the applied loads are calculated as follows. An analysis is carried out (without any additional applied loads) to obtain the initial load exerted by the supports after installation and final load at the design depth. The applied loads are then calculated arbitrarily as a proportion of the difference between initial and final loads. Secondly, another analysis is then performed and the additional displacements required to exert the applied loads are prescribed to the fixed end of the spring elements in the analysis step following the installation of the support.

3.5 DRUCKER-PRAGER CONSTITUTIVE MODEL

An extended Drucker-Prager plasticity model based on the classical rate independent elastic-plastic formulation, available in the ABAQUS code, is used in this study. This material model is suitable for modelling granular materials such as sand.

3.5.1 Basic Equations of Elastic-Plastic Formulation

The notation used in this section uses bold symbols to denote tensors and standard symbols to denote scalar quantities. The strain rate is decomposed into an elastic and a plastic part;

$$\dot{\boldsymbol{\varepsilon}} = \dot{\boldsymbol{\varepsilon}}^{el} + \dot{\boldsymbol{\varepsilon}}^{pl},$$

where $\dot{\boldsymbol{\varepsilon}}$ is the classical small strain rate tensor.

Under elastic conditions the stress rate is given by,

$$\dot{\boldsymbol{\sigma}} = \mathbf{D}\,\dot{\boldsymbol{\varepsilon}}^{el},$$

where **D** is the elasticity tensor.

Elastic deformation occurs when the yield function $f(\boldsymbol{\sigma}, H_\alpha) < 0$. When the material undergoes plastic deformation the inelastic part of the deformation is derived from the flow potential, $g(\boldsymbol{\sigma}, H_\alpha)$ and is defined by,

$$\dot{\boldsymbol{\varepsilon}}^{pl} = \dot{\lambda}\frac{\partial g}{\partial \boldsymbol{\sigma}}.$$

The flow potential, g, and the yield function, f, are both a function of the stress state, $\boldsymbol{\sigma}$, and hardening parameter, H_α. Plastic consistency is ensured by applying the conditions:

$$f\,\dot{\lambda} = 0; \qquad f \le 0; \text{ and } \quad \dot{\lambda} \ge 0.$$

Plastic deformation therefore occurs under loading conditions when $f = 0$. The enforcement of this constraint defining the elastic range determines the value of the plastic multiplier, $\dot{\lambda}$.

Combining the above equations and applying appropriate manipulations (ABAQUS *Theory Manual*) gives the relationship between stress and total strain rates as,

$$\dot{\sigma} = \mathbf{D}^{*}\dot{\varepsilon},$$

where $\mathbf{D}^{*}$ is the tangent modulus dependent on the current state of the material.

3.5.2 The Drucker-Prager Plasticity Model

The definition of the Drucker-Prager yield surface utilizes three stress invariants defined as:

the equivalent pressure stress, $p = -\frac{1}{3}\,\mathrm{trace}(\sigma)$;

the von Mises equivalent stress, $q = \sqrt{\frac{3}{2}\,\mathbf{S}:\mathbf{S}}$;

and the third stress invariant, $r^3 = \frac{9}{2}\,\mathbf{S}\,.\,\mathbf{S}:\mathbf{S}$, where the deviatoric stress $\mathbf{S} = \sigma + p\,\mathbf{I}$ with $\mathbf{I}$ being the identity tensor. The symbol . is used to denote the tensor product and : denotes the scalar product.

Another definition used is a deviatoric stress measure,

$t = \frac{1}{2}q\left[1+\frac{1}{K} - \left(1 - \frac{1}{K}\right)\left(\frac{r}{q}\right)^3\right]$,where K is the ratio of yield stress in triaxial tension to the yield stress in triaxial compression.

The Drucker-Prager yield function is defined in terms of these definitions as,

$$f = t - \tan\beta - d = 0,$$

where d measures the cohesion of the material and is defined as a function of the equivalent plastic strain; β is the friction angle of the material in the p-t stress plane, as indicated in Figure 3.6.

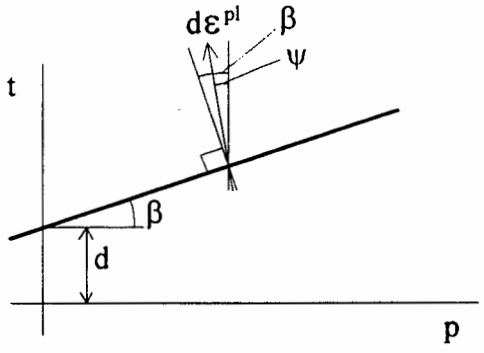

Figure 3.6: Yield surface in the p-t plane.

For plane strain problems K = 1 which implies the yield surface is the von Mises circle in the deviatoric principal stress plane (the Π-plane). In this case the yield stresses in triaxial tension and compression are the same and the deviatoric stress measure t = q. The yield function can therefore be expressed as,

$$f = q - \tan\beta - d = 0.$$

A plot of typical yield surfaces in the principal deviatoric stress plane are presented in Figure 3.7.

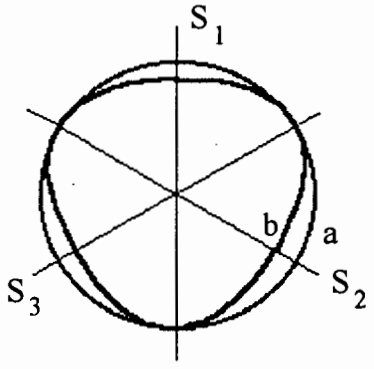

Curve	K
a	1.0
b	0.8

Figure 3.7: Typical yield surfaces in the deviatoric plane.

3.5.3 Flow rule for the Drucker-Prager model

The flow potential g is chosen for this model as

$$g = t - p \tan\psi,$$

where ψ is the dilation angle in the p-t plane.

For granular materials, to ensure that the volumetric expansion of the material is not over-predicted, a non-associated flow is usually used. With a non-associative flow rule the flow is normal to the yield surface in the Π-plane but at an angle ψ to the t-axis in the p-t plane. Figure 3.6 shows a typical situation of non-associated flow where $\psi < \beta$. Associated flow is given by setting $\psi = \beta$. If the flow is described by $\psi = 0$ then the change in equivalent pressure stress p is zero and is therefore referred to as non-dilatant flow since there is no plastic volume change. When a non-associative flow rule is implemented the stiffness matrix in the finite element solution algorithm is non-symmetric.

3.5.4 Matching Drucker-Prager and Mohr-Coulomb Plane Strain Response

In general geotechnical engineering practice the typical values of cohesion and the friction angle for soil materials are given in terms of Mohr-Coulomb parameters. It is possible to transform the Mohr-Coulomb parameters into equivalent Drucker-Prager parameters. The problem under consideration is a plane strain problem and the constitutive model parameters can be matched to provide the same flow and failure response in plane strain. The behaviour is only required to be matched in one plane and therefore the assumption of setting K = 1 can be made.

The yield surface for the Mohr-Coulomb constitutive model is defined as,

$$f = \tau \cos\phi + \sigma \sin\phi - c \cos\phi$$

By comparing the two expressions for the yield surface the following equations can be derived:

$$\sin\phi = \frac{\tan\beta\,\sqrt{3\left(9 - \tan^2\psi\right)}}{9 - \tan\beta\,\tan\psi}$$

$$c\cos\phi = \frac{\sqrt{3\left(9 - \tan^2\psi\right)}}{9 - \tan\beta\,\tan\psi}\,d$$

A further simplification can be made for the two extreme cases of associated flow and non-dilatant flow.

For associated flow ($\psi = \beta$) the previous equations simplify to:

$$\tan\beta = \frac{\sqrt{3}\sin\phi}{\sqrt{1 + \tfrac{1}{3}\sin^2\phi}} \qquad \text{and} \qquad \frac{d}{c} = \frac{\sqrt{3}\cos\phi}{\sqrt{1 + \tfrac{1}{3}\sin^2\phi}}$$

and for non-dilatant flow they give:

$$\tan\beta = \sqrt{3}\sin\phi \qquad \text{and} \qquad \frac{d}{c} = \sqrt{3}\cos\phi$$

Corresponding values for the friction angle β and cohesion d of the Drucker-Prager model can now be calculated given the Mohr-Coulomb parameters of friction angle ϕ and cohesion c. The derivation of the equations is given in the ABAQUS *Theory Manual*.

CHAPTER 4
STUDY OF VARIOUS INFLUENCES ON CANTILEVER SUPPORT SYSTEMS

4.1 INTRODUCTION

In the literature review given in Chapter 2 some of the important aspects of the finite element analysis of lateral support systems were discussed. In many cases the papers reviewed were case studies which contain limited information about the values of the parameters that were used. A series of finite element analyses, based on the models described in Chapter 3, were undertaken to study various influences on a lateral support system. In this chapter selected results from analyses of a typical cantilever sheet pile wall are presented and discussed.

The aspects of the analyses considered are the depth of excavation, wall displacements and the development of the lateral earth pressure distribution. The results are discussed in the light of the application of:

- various plastic flow rules;
- the choice of wall friction and
- a selection of different soil types.

The bending moment distributions for cantilever walls are, in general, similar in shape and not very informative. For this reason, only the magnitude of the maximum bending moments are considered in the discussion.

4.2 PLASTIC FLOW RULE

As mentioned in the discussion of the Drucker-Prager soil model in Chapter 3, soil behaviour is generally not accurately described by fully associative flow. A fully associative flow rule over-estimates the volumetric behaviour of a soil. In order to demonstrate the effect that the choice of flow rule has on an excavation analysis, three different flow rules are applied. These include the two extremes of a fully associative flow and a non-dilatant flow, with a non-associative flow rule of $\psi = \frac{1}{2}\beta$ between the two limits. Non-dilatant flow is a special case of non-associative flow where the dilation angle equals zero. The soil used in the analysis is a cohesionless sand, however, a nominal value for cohesion of 1 kPa is assigned to avoid the numerical difficulties associated with a cohesion of zero when implementing Drucker-Prager model. The values of the parameters used are tabulated in Table 4.1.

Flow Rule	Mohr-Coulomb		Drucker-Prager		
	Friction angle, ϕ	Cohesion, c [kPa]	Friction angle, β	Cohesion, d [kPa]	Dilation angle, ψ
Associative flow	35°	1	43.3°	1.37	43.3°
Non-associative flow	35°	1	44.05°	1.39	22.03°
Non-dilatant flow	35°	1	44.81°	1.42	0°

Table 4.1: Soil parameters of a sand used for different flow rules.

A typical sheet pile wall section (standard LARSSEN 4B) is used for all the cantilever wall studies. The section has a bending stiffness of EI = 8.07 x 10^4 kNm^2/m.

a) Excavation depth

Each excavation analysis is completed to the nearest 0.5 m of maximum depth, as described in the procedure for excavation in Chapter 3. An inspection of these results demonstrate clearly the influence that the choice of flow rule has on the maximum attainable excavation depth. The material with non-dilatant flow can only be excavated to 3 m whereas the material with associative flow can be excavated to a depth of 7 m. The analysis with the non-associative material indicates an excavation limit of 5 m which is close to what would be expected in practice. As a rule of thumb, Winterkorn and Fang (1975) recommend that the maximum depth that a cantilever wall should support is about 4.5 m.

It should be noted that the results from the investigation of the flow rule presented in this section are at the maximum excavation depth and not at the same depth. This is because the results for all choices of flow rule are almost identical at the same depth of excavation. The maximum excavation depth evaluated using different flow rules clearly demonstrates the effect of the volumetric assumption implied in the respective flow rules on the stability of the wall.

b) Wall displacements

The wall displacements are shown in Figure 4.1. The figure serves to illustrate not only the magnitude of the wall displacements, but also the modes of wall displacement as excavation progresses. Initially, the mode of displacement can be described as parallel translation, thereafter the amount of bending increases and the point of maximum

curvature moves progressively down as the excavation increases. Therefore, the magnitude of wall displacement increases rapidly with excavation depth.

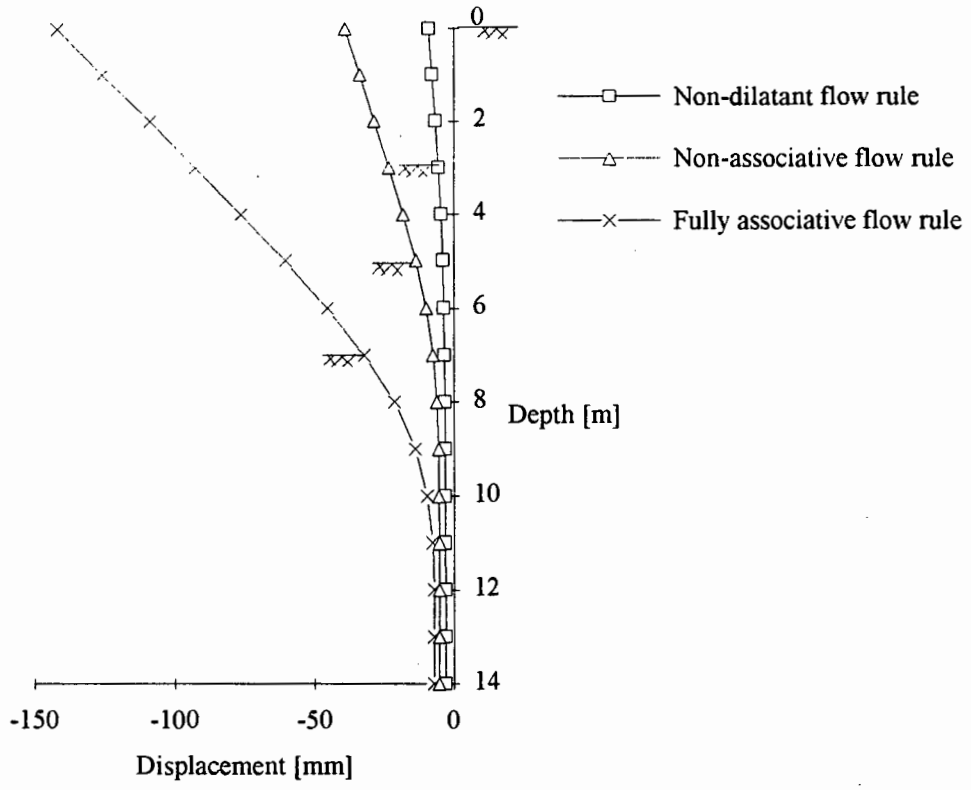

Figure 4.1: Wall displacements in sand characterized by three different flow rules.

c) Lateral earth pressures

The magnitudes of wall displacements below the excavation levels are greater with increasing excavation depth. This causes the depth over which active and passive earth pressures are mobilized to be greater as the excavation depth increases. The earth pressure distributions just prior to the failure state are shown in Figure 4.2 for the three assumed flow rules.

The values of the coefficients of the horizontal component of earth pressure K_{ah} and K_{ph} can be calculated from the gradient of the earth pressure distributions. The active earth pressures are mobilized in the supported soil behind the excavation, with a transition back to at-rest earth pressure conditions below the base of the excavation. The gradient of the active earth pressure distribution over this depth indicates a decrease in the earth pressures relative to the at-rest earth pressure conditions, i.e. $K_{ah} < K_0$. This is in agreement with earth pressure theory.

Passive pressures are mobilized in front of the wall immediately below the base of the excavation. These conditions exist over a depth where sufficient wall displacements

towards the excavation have occurred to produce failure. Again, at a certain depth, a transition back to at-rest conditions is observed. The gradient of the passive earth pressure distribution indicates that the rate of change of earth pressure with depth is much greater than for the at-rest earth pressure conditions, i.e. $K_{ph} > K_0$. The at-rest earth pressure conditions exist where zero or insignificant wall displacements occur.

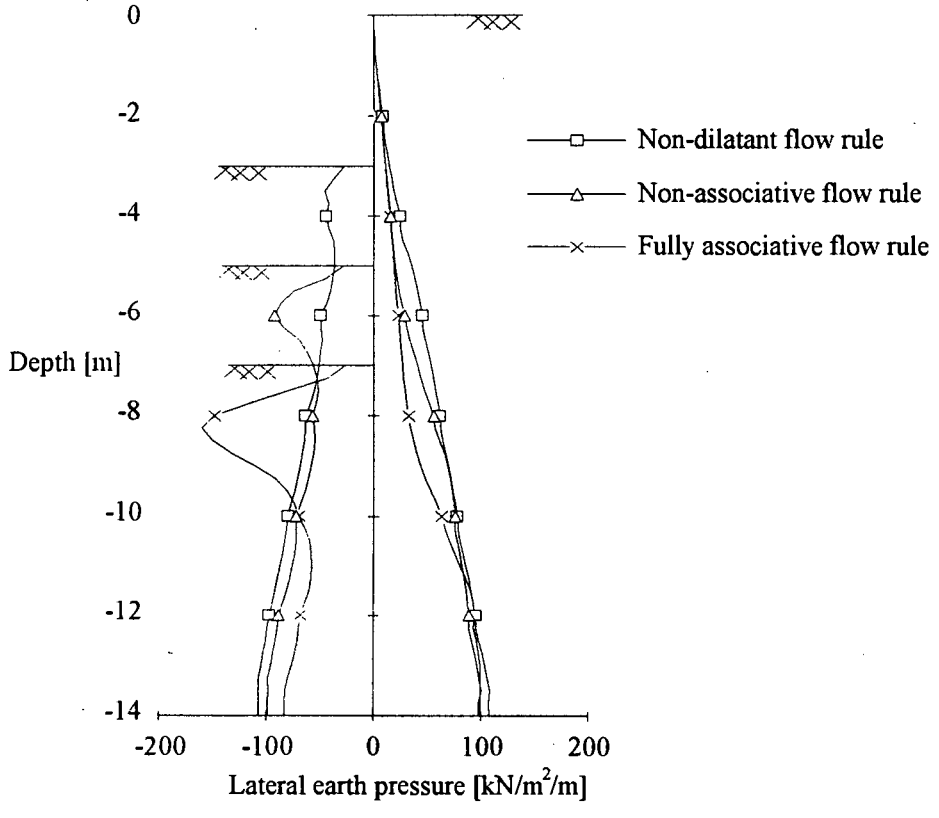

Figure 4.2: Lateral earth pressure distributions in sand characterized by three different flow rules.

This example of a cantilever wall shows that the depth of excavation is most limited if the assumption of non-dilatant flow is made. It can therefore be predicted that the choice of flow rule will also play an important role in the investigation of supported wall systems.

4.3 WALL FRICTION

The influence of frictional effects that occur between the soil and the wall is investigated by performing two excavation analyses, one including and the other excluding wall friction. The soil parameters for the sand presented in Table 4.1 were used, together with the non-associative flow rule $\psi = \frac{1}{2}\beta$. The effects of wall friction can be incorporated into the analysis by introducing a suitable coefficient of friction to the interface between the wall and soil. In conventional design the value for the coefficient of friction is

calculated from the equation $\mu = \tan \delta$, where δ, the wall friction angle = $\frac{2}{3}\phi$, the internal angle of friction of the soil.

a) Wall displacements

The influence of friction expressed in terms of wall displacements are shown in Figure 4.3. These results show that the wall displacements at the same level of excavation for the analysis which excluded frictional effects (i.e. $\mu = 0$) are greater than when wall friction is included. In both cases the modes of wall displacement are a combination of parallel translation and bending. The point of maximum wall flexure is lower for the case of no wall friction and the amount of bending is greater. The greater magnitude of wall displacements indicates that the depth over which passive earth pressures are mobilized should be greater for the frictionless wall.

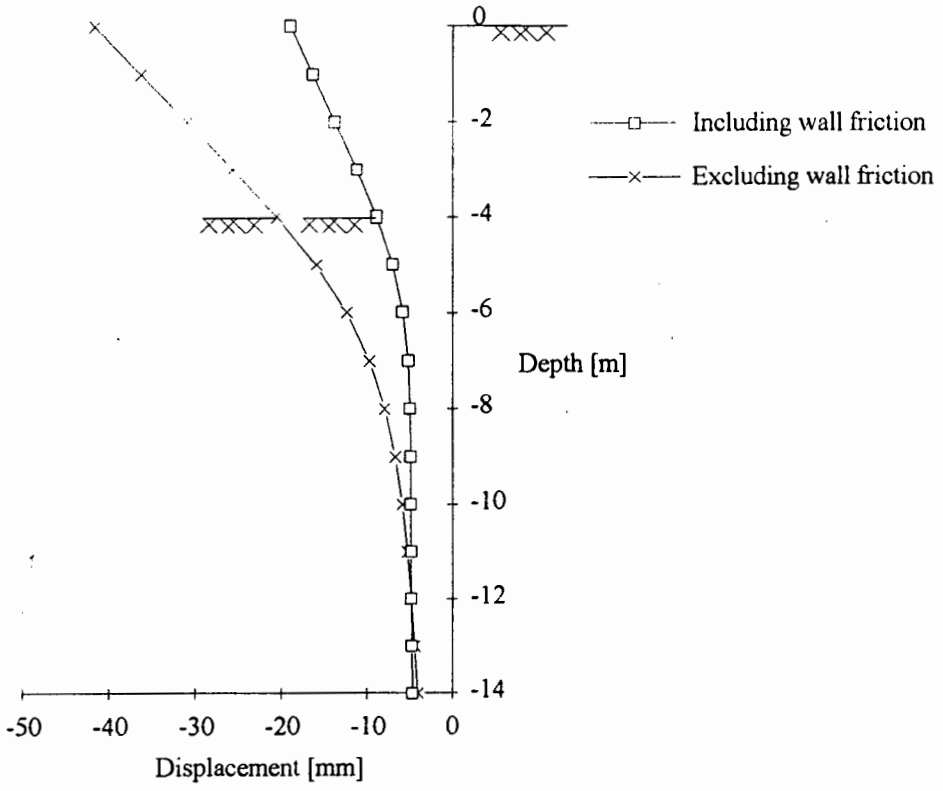

Figure 4.3: Wall displacements in sand including and excluding wall frictional effects.

b) Lateral earth pressures

The comparison of the earth pressure distributions for the two analyses, presented in Figure 4.4, show that the passive earth pressure coefficient, K_{ph}, is smaller for the solution which excludes frictional effects. The case that includes wall friction gives $K_{ph} = 5.2$ and for the case that excluded frictional effects $K_{ph} = 2.7$.

In conventional design the coefficients of lateral earth pressure, K_{ph} and K_{ah}, can be calculated from general equations. These may be equations from Coulomb theory which assumes straight failure surfaces or from the equations of Caquot and Kérisel, (1948) which assume curved failure surfaces. Curved failure surfaces generally occur when the internal angle of friction $\phi \geq 35°$. These equations include parameters δ_a and δ_p which represent the wall friction angles assuming an earth pressure distribution at failure. It is of interest to compare the values calculated from the results by the finite element method to the values calculated based on theory. The values for K_{ph} calculated from the equations of Caquot and Kérisel are 7.6 when wall friction angle $\delta_p = \frac{2}{3}\phi$ and 3.7 when $\delta_p = 0$ (respecting the appropriate sign convention). The values calculated from the results of the finite element analysis are lower, indicating that there has not been sufficient wall displacement to fully mobilize the passive pressures. However, the trend of K_{ph} increasing for an increase in wall friction is described consistently by both approaches.

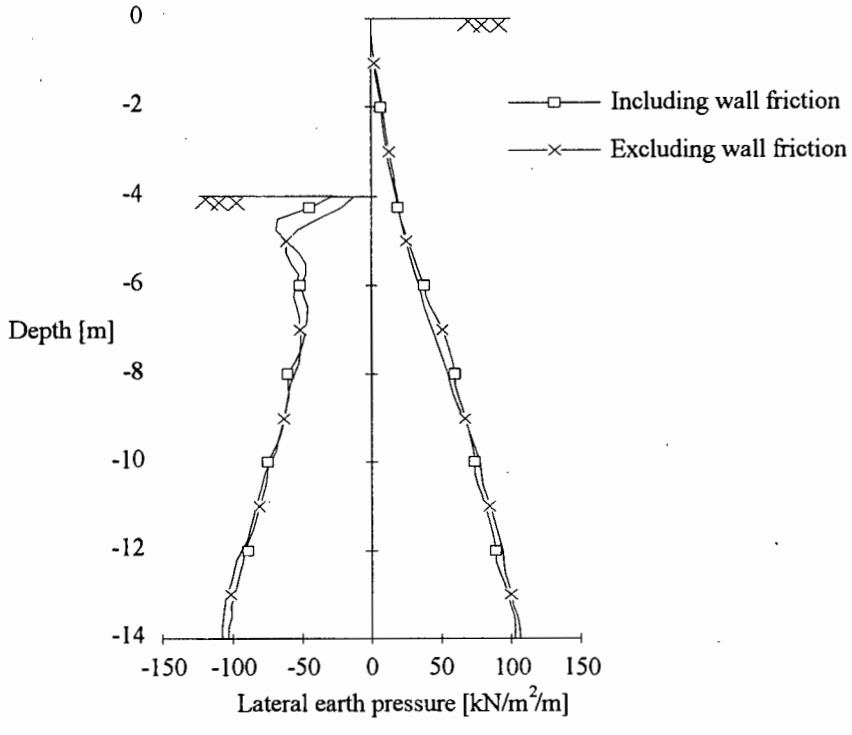

Figure 4.4: Lateral earth pressure distributions in sand including and excluding wall frictional effects.

It is important to note that when frictional effects are included in the analysis an additional 1 m can be excavated before the solution algorithm fails to converge The additional excavation is possible because the lateral resistance on the passive side of the wall is greater. An implication for the designer is that if the coefficient of friction is uncertain then a more conservative assumption of wall friction would be closer to zero.

4.4 SOIL TYPE AND PROPERTIES

To examine the influence of the shear parameters and the homogeneity of the soil stiffness on the behaviour of the support system, three different types of soil have been selected: a homogeneous, isotropic sand of low cohesion; an anisotropic sand with a low cohesion; and a homogeneous, isotropic clay of high cohesion. Anisotropy is characterised by an increasing Young's modulus with depth. As in the previous analyses the cantilever wall installed in these soils are investigated employing a non-associative flow rule ($\psi = \frac{1}{2}\beta$) and wall friction of $\mu = \tan \frac{2}{3} \phi$ except for the clay where a more representative value would be $\mu = \tan \frac{1}{2} \phi$.

Again a low cohesion is assigned to avoid any numerical difficulties during the solution procedure. The soil parameters for these three soils are listed in Table 4.2. The shear parameters in terms of Mohr-Coulomb failure criterion which are generally applied in geotechnical engineering are converted to the equivalent values of the Drucker-Prager model.

The anisotropic sand is assumed to be stratified with strata of 2 m thickness with a Young's modulus that increased with depth Z according to the relationship $E = 4000\,(Z)^{0.9}$ [kN/m^2 / m]. This relation was developed to give values for Young's modulus that fall within the range of typical values for sand of increasing densities with depth (Bowles, 1988). Other researchers (Félix *et al,* 1982; Potts and Fourie, 1985) applied similar relationships to obtain an increase in stiffness of the soil with depth.

Description	Density	Mohr-Coulomb		Drucker-Prager			Young's Modulus,
	γ [kN/m^3]	Friction angle, ϕ	Cohesion, c [kPa]	Friction angle, β	Cohesion, d [kPa]	Dilation angle, ψ	E [MPa]
Homogeneous, isotropic sand	18	35°	1	44°	1.39	22°	30
Homogeneous, isotropic clay	19	25°	30	35.8°	46.37	17.9°	30
Anisotropic sand	18	35°	1	44°	1.39	22°	4 (Z) $^{0.9}$ *

Table 4.2: Soil parameters for the three selected soil types.

[* Z is the depth below the ground surface]

a) Soil model verification

In order to increase confidence in the soil model that is used the values of the earth pressure coefficients provide a readily available check. The values calculated from the results of the finite element analyses can be compared to the values calculated by Caquot and Kérisel (1948). The latter values are used in conventional design as 'input' to calculate an assumed earth pressure distribution at failure. The values derived from the finite element method are calculated from the gradients of earth pressure distribution and are therefore 'output' values.

For comparison, the respective coefficients are listed in Table 4.3 (a). These values correspond to the stages of excavation when the support system is in a failure state. Failure in the finite element analyses is assumed to occur at the excavation depth that fails to achieve convergence of the solution, as said before.

Description	Determined from results by the finite element method		Calculations based on values from Caquot and Kérisel	
	K_{ah}	K_{ph}	K_{ah}	K_{ph}
Anisotropic sand	0.23	5.2	0.23	7.6
Clay	0.35	3.8	0.35	3.7

Table 4.3 (a): Table of comparison between values calculated from the finite element analysis results and values from Caquot and Kérisel, (1948).

Another verification can be made in terms of the slope of the failure plane. According to Mohr-Coulomb failure theory, which assumes straight failure surfaces, the slope of the failure planes to the horizontal are given by the following formula: $\theta_a = 45° + \frac{\phi}{2}$ and $\theta_p = 45° - \frac{\phi}{2}$ limiting the active and the passive failure wedges, respectively.

The slope of the failure planes in the sand and in the clay are visible in the plastic strain distributions adjacent to the cantilever system shown in Figure 4.5 and Figure 4.6, respectively. These figures are contour plots of equivalent plastic strain (variable PEEQ = $\int \sqrt{\frac{2}{3} d\varepsilon^{pl} \, d\varepsilon^{pl}}$) which indicate the regions where the state of stress has reached the failure condition. The various degrees of shading indicate the amount of plastic strain developed. The contour plots are superimposed onto the displaced shape of the mesh in order to demonstrate the displacement pattern of the wall and soil. As can be seen from these plots the soil tends to slide downwards along the failure surface in a wedge type fashion on the active side while on the passive side the soil in pushed upwards along a

curved failure surface. The slopes of the failure surfaces can be determined by measuring the gradient of the surfaces indicated by the region of plastic strain.

The failure wedges are initiated early in the analysis and increase in size throughout the excavation. Successive, parallel failure surfaces developed as the excavation depth increase in accordance with Rankine theory. The situations, in the respective soils immediately prior to failure are shown in the contour plot.

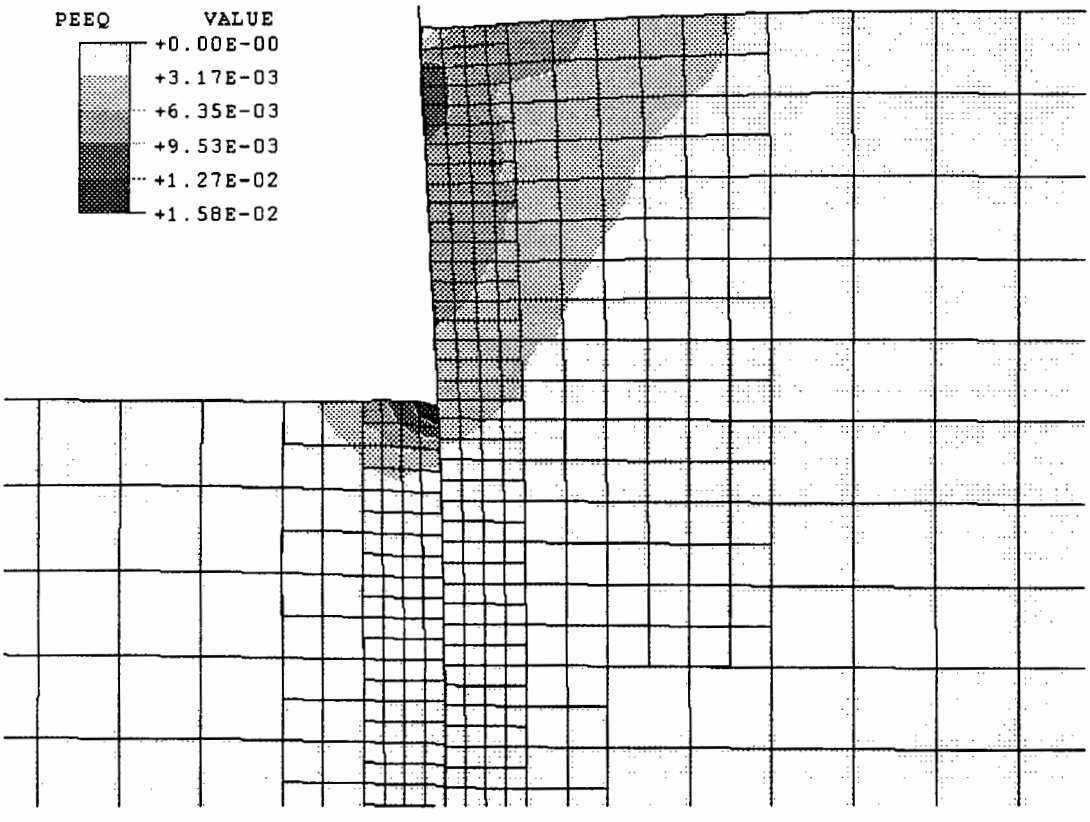

Figure 4.5: Contour plot of plastic strain of a cantilevered system in anisotropic sand superimposed on the displaced shape.
(Displacement magnification factor = 10)

The passive failure wedge developed early in the analysis of the cantilever wall in clay but the failure on the active side developed rapidly as the maximum depth of excavation is approached. The failure is initiated at the position of the darkest contour level shading behind the wall and developed in a narrow band from the region at the wall base towards the ground surface. Deformation that occurs in a narrow band is a phenomenon called strain localization. This type of failure has been observed in soft clays (Finno, 1989) and can only be modelled with the use of a non-associated flow rule. For a more detailed study of strain localization see Ortiz *et al*, (1987).

The failure surfaces for the sand, particularly on the passive side, are not straight but curved whereas the failure surfaces are straight for the clay. This supports the recommendation to use Mohr-Coulomb failure equations where $\phi < 35°$ and Caquot and Kérisel equations for soils of $\phi \geq 35°$.

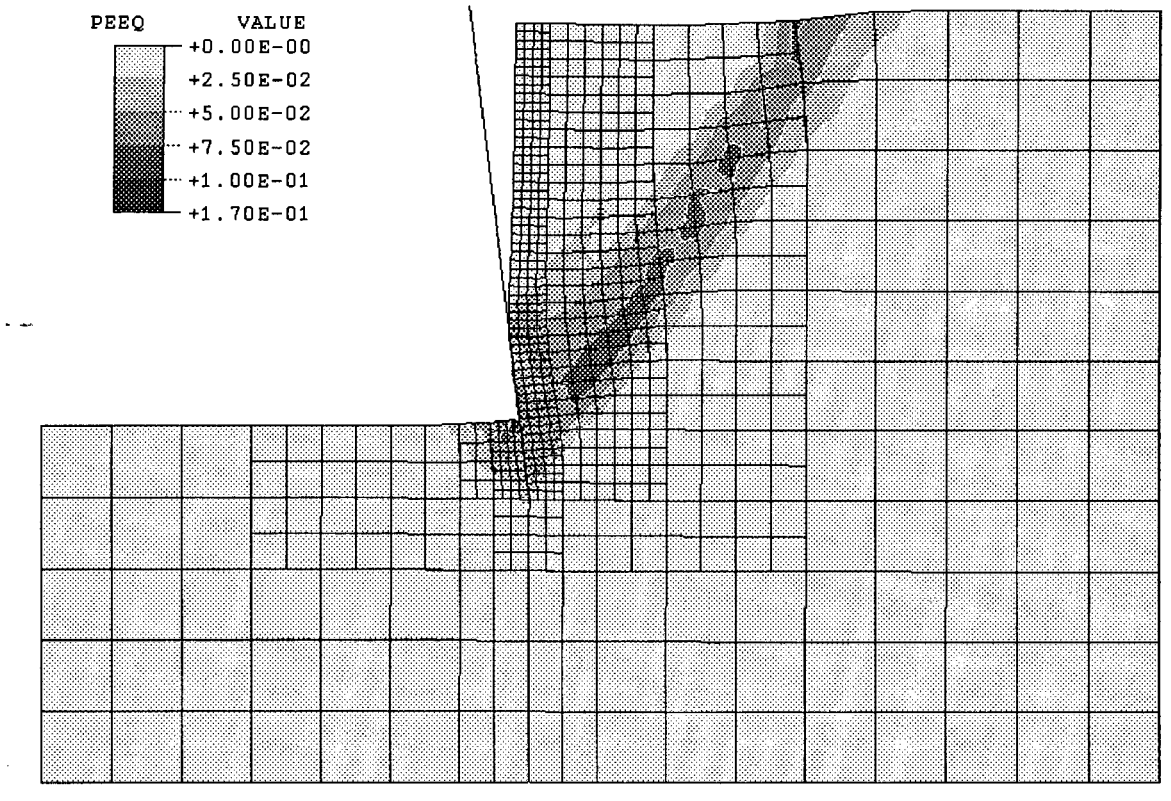

Figure 4.6: Contour plot of plastic strains of a cantilevered system in clay superimposed on the displaced shape.

(Magnification factor of the displacements = 2)

The respective measurements from the finite element analyses and the results calculated from theory are presented in Table 4.3 (b). The slope determined from the finite element results could not be measured accurately, therefore a range of values is presented. There is good agreement between analysis and theory which confirms the adequacy of the model and the assumptions made.

Description	Calculations based on Mohr-Coulomb failure criterion		Determined from results by the finite element method	
	θ_a	θ_p	θ_a	θ_p
Anisotropic sand	62.5°	27.5°	52-55°	39°*
Clay	57.5°	32.5°	50-54°	32-35°

Table 4.3 (b): Table of comparison between values calculated from the finite element analysis results and values calculated from Coulomb theory.

* This measurement is only approximate since the failure surface is curved.

b) Excavation depth

An analysis of an excavation with a cantilever sheet pile wall support system was performed for each soil type. Each analysis was executed until the excavation depth was the maximum depth that could be achieved. The maximum excavation depths achieved for the isotropic sand, the anisotropic sand and the homogeneous clay are 4 m, 5 m and 12 m, respectively. The maximum excavation depths for the sandy material are within the accepted measures for cantilever systems. The maximum depth for the clay appears to be an extreme example of a cantilever wall in a cohesive material.

When comparing the results of the isotropic sand and the anisotropic sand it is apparent that the maximum excavation is greater for the anisotropic sand. The anisotropic sand is a more realistic representation of the condition of a sand since it is likely that the increased gravitational pressure with depth causes the sand grains to be more closely packed, which is reflected in an increase in the Young's modulus.

c) Wall displacements

The wall displacements of the cantilevered sheet pile wall in all three soils are shown in Figure 4.7 (a). For purposes of comparison the excavation is at a depth of 4 m in all considerations. An examination of the wall displacements for the isotropic and the anisotropic sand reveals the effect of the increasing stiffness with depth in the anisotropic sand. In both cases the wall displacement is a combination of parallel translation and bending. Due to the higher stiffness of the anisotropic sand below the excavation level, the measure of parallel translation is reduced. Since the base of the wall is more firmly fixed the amount of bending is greater and therefore the wall tip displacement is also greater.

It is interesting at this point to note that the displaced shape of the wall for these two cases indicates that more redistribution of stress is allowed by the isotropic sand which is on average less stiff. This suggests that the maximum bending moment is less than for the anisotropic case. This is found to be true with the maximum bending moment of 50 kNm/m for the isotropic case and 57 kNm/m for the anisotropic case. Both of these values occurred just below the excavation depth of 4 m at the depth 4.75 m below the ground level. The maximum excavation depth is 1 m more for the anisotropic sand because of its increased stiffness below the excavation level.

The wall displacements for the analysis of the clay suggests that the mode of wall displacement is rotation about the top of the wall. This displacement mode is caused by the absence of active earth pressures behind the wall to a depth of about 3 m as shown by the lateral earth pressure distributions in Figure 4.8. Most of the supported soil behind the

wall is free standing due to the effect of cohesion. The situation changes as excavation continues down to the maximum excavation depth. Wall displacements are shown at this stage in Figure 4.7 (b) which clearly display a wall displacement mode of rotation about the bottom of the wall. The displacement of the soil relative to the wall is shown by the displaced shape of the mesh in Figure 4.6. The cohesion of the clay is responsible for the soil separating from the wall so that it stands freely to a depth of 9 m. Therefore the wall remains straight above that level. The maximum bending moment occurs at a depth of 12.75 m and has a magnitude of 122 kNm/m.

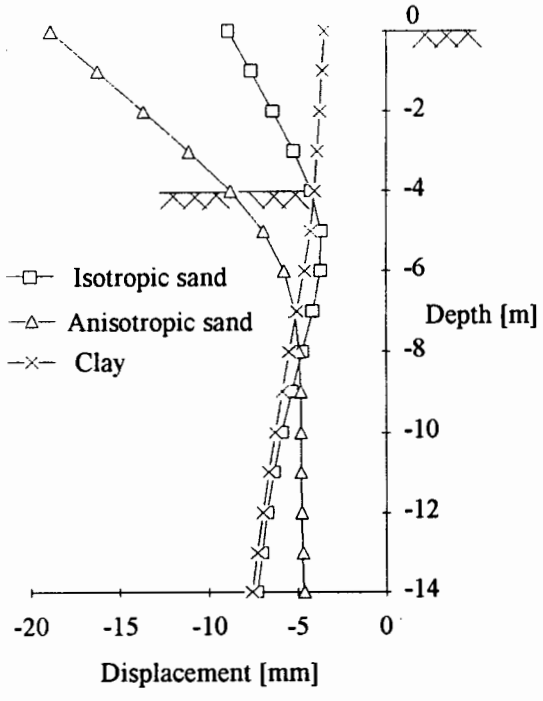

Figure 4.7 (a): Wall displacements for all three soil types at 4 m excavation depth.

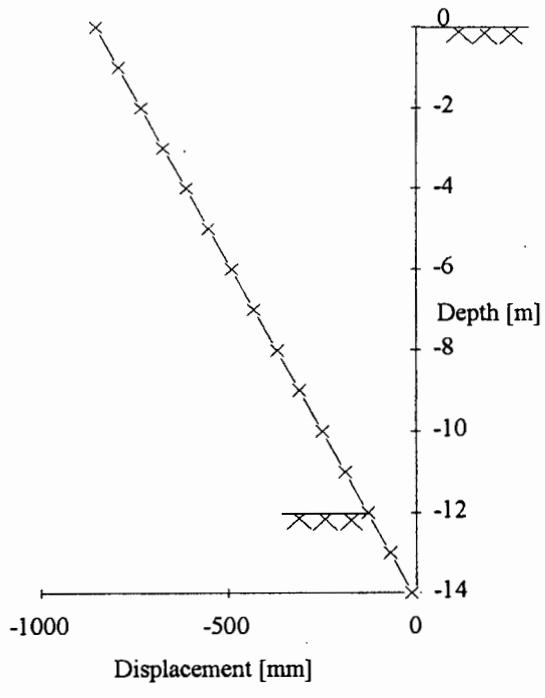

Figure 4.7 (b) Wall displacements for the homogeneous clay at maximum excavation depth.

d) Lateral earth pressures

The effect of cohesion on the lateral earth pressures is depicted in Figure 4.8 (a) and Figure 4.8 (b) where the earth pressure distributions are shown in the clay and sand at an excavation depth of 4 m and the maximum excavation depth, respectively. The immediate increase in passive resistance in front of the wall is clearly visible for the clay. The cohesion of the clay also enables it to stand freely until the shear stress limit is exceeded. For this reason there are zero stresses behind the wall to a depth of 9 m for the 12 m excavation. In conventional analysis the lateral passive earth pressures are expressed by two components representing a contribution from displacement (strain) and cohesion. A cohesional component $e_{pch} = 2c\sqrt{K_{ph}}$ is added to the horizontal passive earth pressures

and a component $e_{ach} = -2c\sqrt{K_{ah}}$ to the horizontal active earth pressures. The passive pressures in the clay at an excavation depth of 4 m are dominated by the cohesive component since there has not been sufficient wall displacement at this stage in the excavation to mobilize passive pressures.

In the sands it is evident that the earth pressures in front of the wall are mobilized to a slightly greater extent in the isotropic sand thus allowing a further 1 m in excavation before failure occurs. Behind the wall the full active pressures are mobilized all the way down and beyond the excavation level in both the isotropic and the anisotropic sand.

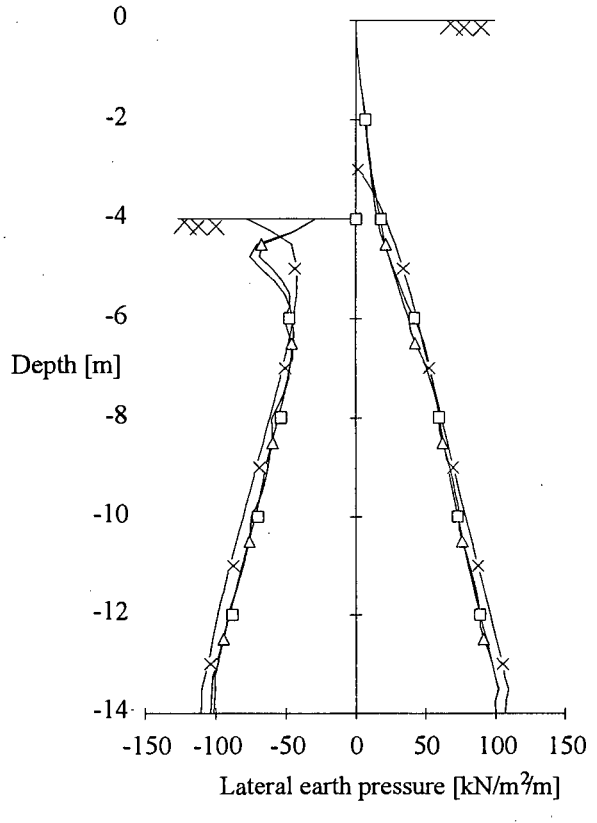

Figure 4.8 (a): Lateral earth pressures for all three soil types at 4m excavation depth.

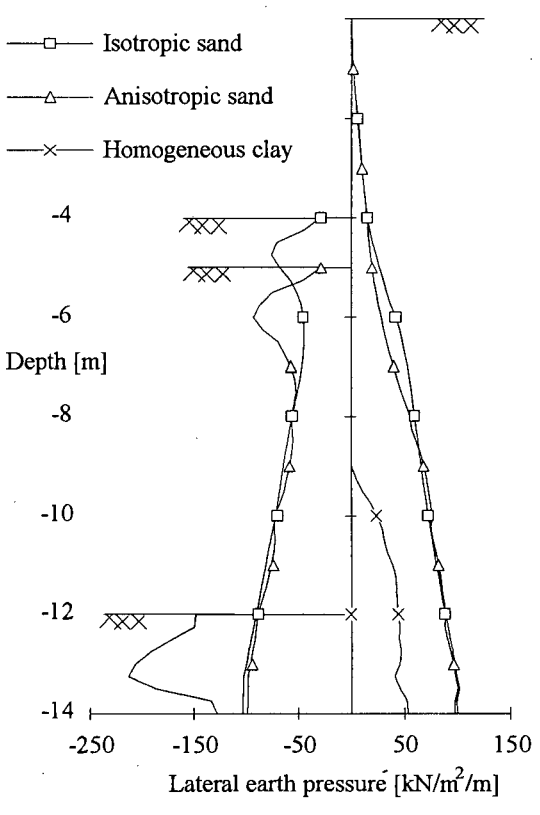

Figure 4.8 (b): Lateral earth pressures for all three soil types at maximum excavation depth

The lateral earth pressure distributions in the clay at 12 m excavation depth calculated by the finite element method are compared with the distributions assumed by the conventional method in Figure 4.9. As described earlier the active lateral earth pressures can be calculated by $e_{ah} = K_{ah}\gamma Z - 2c\sqrt{K_{ah}}$, therefore $e_{ah} = 0$ when $Z = \frac{2c}{\gamma\sqrt{K_{ah}}}$. The soil will be in tension above this level as illustrated in Figure 4.9. The tension crack extends, in this case, to a depth Z = 5.3 m which occurs at the excavation depth where $e_{ah} = -2c\sqrt{K_{ah}}$. The depth, Z, at which the earth thrust is zero can be calculated from the equation $Z = \frac{4c}{\gamma\sqrt{K_{ah}}}$, which for this case is 10.7 m. An inspection of the active earth pressures

behind the wall for the finite element analysis results indicate that the height of unsupported soil is 9 m.

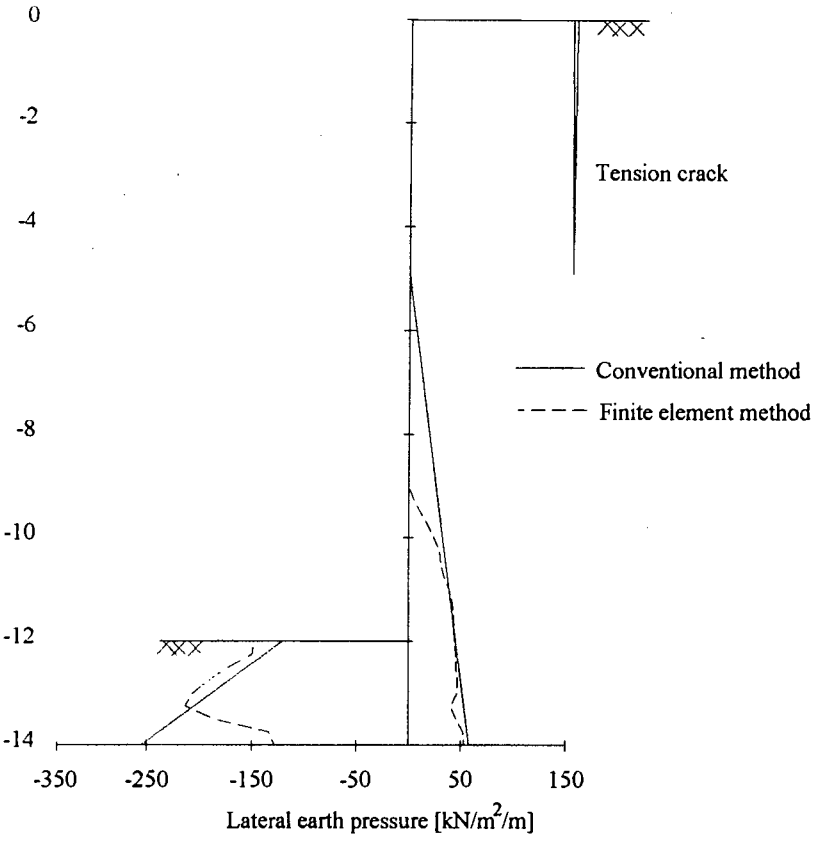

Figure 4.9: Lateral earth pressure distributions in the clay from the finite element and conventional analysis.

e) Settlements behind the wall

A big advantage in finite element analysis of support systems as opposed to the limit state analysis is that the surface movements of the material adjacent to the wall can be evaluated in the vertical as well as the horizontal direction. Generally of interest are the settlements of the supported material and the heave of the subsoil in the excavation. The heave of the subsoil is here not considered important and will not be discussed.

The issue of settlements was initially a problem in the performance of the finite element model. When the soil was described as isotropic the heave of the material below the base of the excavation was causing the soil on the surface behind the wall to heave. This behaviour does not agree with the observations made in practice where settlements are measured. To illustrate the problem a plot of the displaced shape is shown in Figure 4.10.

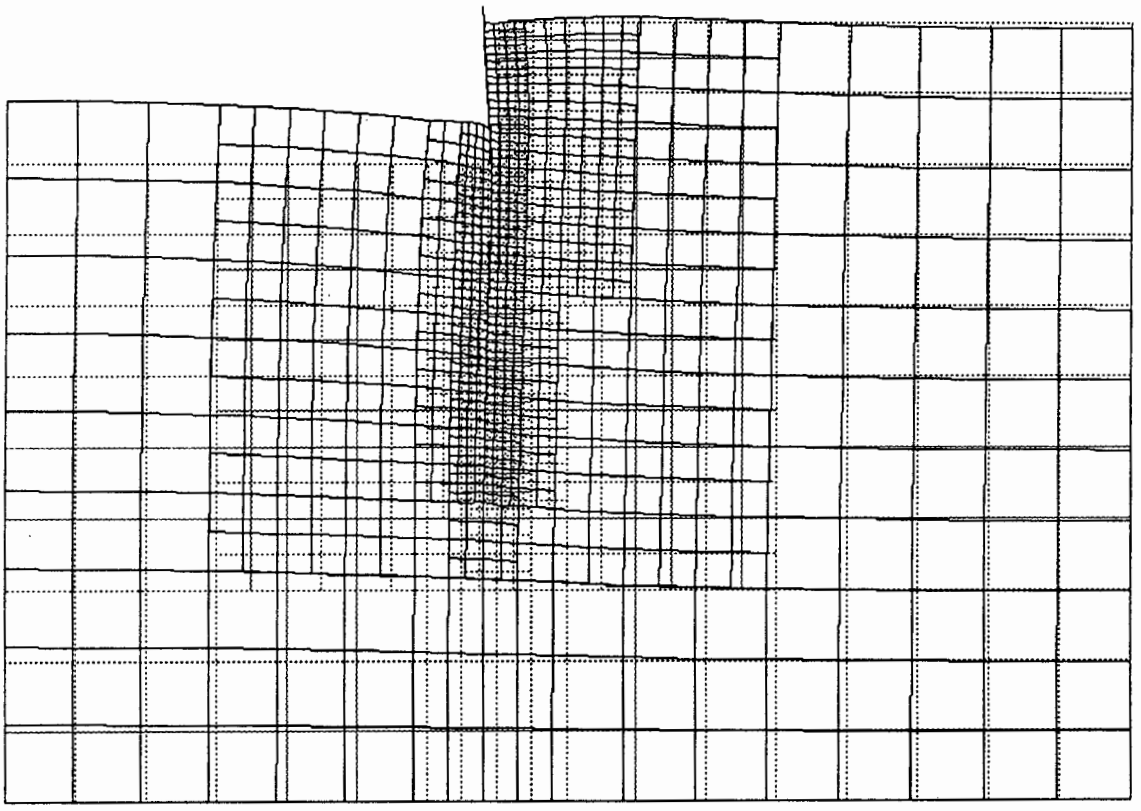

Figure 4.10: Displaced shape of the support system in isotropic sand.
(Magnification factor of displacements = 20)

In order to realistically simulate the surface settlements the soil characteristics were more accurately described. It is for this reason that an anisotropic sand was introduced with a Young' modulus increasing with depth. This approach was successful and gave a more realistic settlement pattern which is shown in Figure 4.11 (a). The surface settlements of the supported soil materials of all three selected types are shown for an excavation depth of 4 m in Figure 4.11 (a). The shape of the settlement pattern remains similar but the magnitude of settlements increases for the anisotropic sand. The soil in contact with the wall does not settle as much as the sand just behind the wall because of the influence of friction between the sand and the wall.

The ground surface of the clay heaves after 4 m excavation as shown in Figure 4.11 (a) but thereafter settles with increasing excavation depth and wall displacements as shown in Figure 4.11 (b).

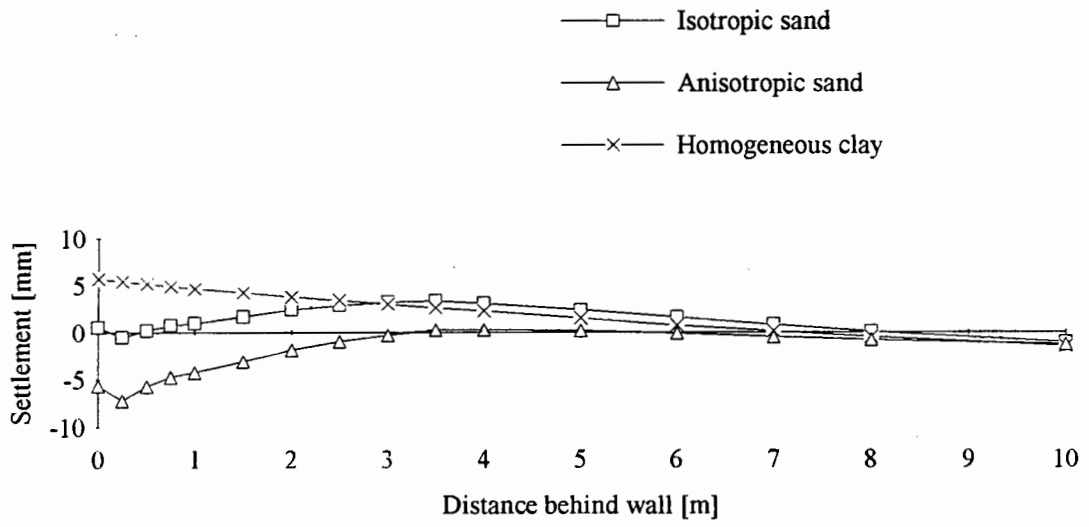

Figure 4.11 (a): Settlements patterns for all three soil types at 4 m excavation depth.

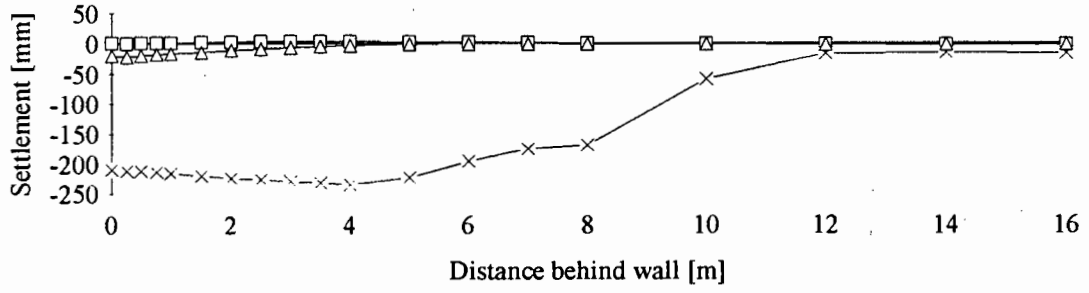

Figure 4.11 (b): Settlement patterns for all three soil types at maximum excavation depth.

CHAPTER 5
STUDY OF VARIOUS INFLUENCES ON MULTIPLE LEVEL SUPPORTED SYSTEMS

5.1 INTRODUCTION

The excavation depths for cantilever walls are limited by, amongst other reasons, the rigidity of the wall sections and therefore practical design, in general, concentrates on supported retaining wall systems. Thus, this chapter deals with multiple level supported systems the investigation of various input parameters with regard to the wall responses. The parameters considered are the wall stiffness, prop stiffness and applied prop loads. Based in the studies in Chapter 4 a particular flow rule, wall friction and soil type was selected for the investigation in this chapter.

It would be of help to the designer to know how the various parameters effect the shape of the redistributed earth pressures. These parameters are investigated in terms of lateral wall displacements, earth pressures, prop forces, bending moments, plastic strain distributions and surface settlements and the major trends are exposed. It should be appreciated that the influences are to some extent interrelated with respect to the overall behaviour of the support system. In order to allow comparisons between results where parameters have been varied all excavation analyses are carried out to a depth of 9.5 m.

5.2 BASIC CONFIGURATION OF THE MULTI-LEVEL SUPPORTED SYSTEM

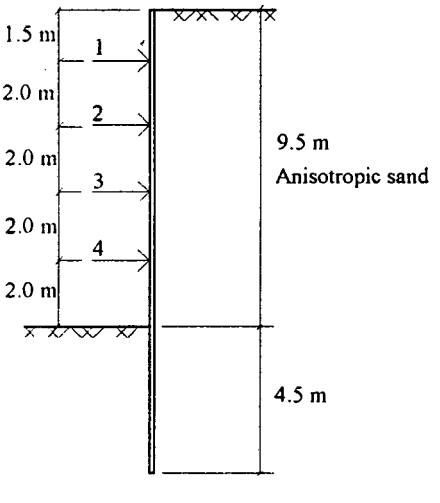

Figure 5.1: Schematic showing the basic configuration of the multi-level supported system.

The analyses of the multi-level supported systems in this chapter use the model with the basic configuration shown in the schematic in Figure 5.1. The prop spacing is chosen to be 2 m with the first prop at 1.5 m depth below the ground surface. All the props are assigned the same stiffness. The lateral support systems are installed in an anisotropic sand described by the Drucker-Prager constitutive model with a non-associative flow rule ($\psi = \frac{1}{2}\beta$). Wall friction of $\mu = \tan\frac{2}{3}\phi$ is included to approximate the soil-structure interaction.

5.3 WALL STIFFNESS

The type of lateral support system structures are generally grouped into two main categories, namely rigid walls and flexible walls. Typical examples of flexible walls are again sheet pile walls or soldier pile walls with horizontal lagging. Rigid walls are usually diaphragm walls or concrete pile walls. As the term indicates, the magnitude of wall displacements is less for rigid walls than for flexible walls and are therefore suitable for situations where settlements behind the wall need to be restricted. The construction of a rigid wall is generally more expensive than a flexible wall.

In order to investigate how wall stiffness has a bearing on the behaviour of support systems, analyses of four systems with walls of different stiffness were performed. The four walls included:

- an extremely 'rigid' wall of fictitious rigidity,
- a typical 1 m thick concrete diaphragm wall,
- a typical sheet pile wall and
- an extremely 'flexible' wall of fictitious flexibility.

The extreme cases have a value of bending stiffness that would not usually be encountered in reality but are analysed for comparative purposes. In Table 5.1 the specifications are listed for each wall. The sheet pile wall section is assumed to be rectangular in the analysis which is different to the real section used in practice. Therefore the thickness of the rectangular section is calculated so that the moment of inertia corresponds to the moment of inertia of a standard LARSSEN 4B section.

	'Rigid'	Diaphragm	Sheet pile	'Flexible'
Young's modulus, E [kPa]	2.8×10^9	2.8×10^7	2.06×10^8	2.06×10^8
Thickness [m]	1.0	1.0	0.1675	0.1063
Moment of Inertia, I [m^4/m]	8.33×10^{-2}	8.33×10^{-2}	3.92×10^{-4}	1.0×10^{-4}
Bending stiffness, EI [kNm^2/m]	2.33×10^8	2.33×10^6	8.07×10^4	2.06×10^4

Table 5.1: Specifications of the four selected wall types.

The results for the 'rigid' wall and the diaphragm wall were obtained using the finite element mesh for 'diaphragm wall' as described in Chapter 3, whereas for the sheet pile wall and the 'flexible' wall the analyses were carried out using the 'sheet pile wall' finite element mesh. Because of the greater stiffness of the rigid type walls the prop spacing can be made greater than for the flexible walls. However, for the purposes of comparison, a four-level propped wall with a prop spacing of 2 m is used for all cases. The value of the

stiffness coefficient for the props is chosen to be similar to values used by other researchers (Smith and Ho, 1992; Fourie, 1990) at 10 000 kN/m/m in all cases.

a) Wall displacements

The wall displacements from all four analyses of the support systems with selected wall stiffness are shown in Figure 5.2. The displacement mode for the rigid type walls is basically a combination of parallel translation and rotation about the top. The wall displacements are about 3.5 mm / 10 m excavation along the whole wall. The diaphragm wall deflects slightly due to the prop supports relative to the 'rigid' wall which remains straight. This causes the lateral earth pressure distributions are almost identical. The rigid type walls displace effectively as rigid bodies, i.e. changing position in space without changing shape. This results in greater wall tip displacements than the more flexible walls which undergo bending.

The flexible type walls displace by parallel translation below the excavation level but also bend about a point just above the excavation level. The bending that occurs at the point of rotation is also reflected in the bending moment diagram which is shown is Figure 5.4. The 'flexible' wall bulges out just above the excavation level more than the sheet pile wall and the tip displacements are slightly less. The wall displacements above the excavation level are about 11 mm / 10 m excavation. This is comparable to the general observation of about 7 mm / 10 m for flexible type walls (Ostermayer, 1981).

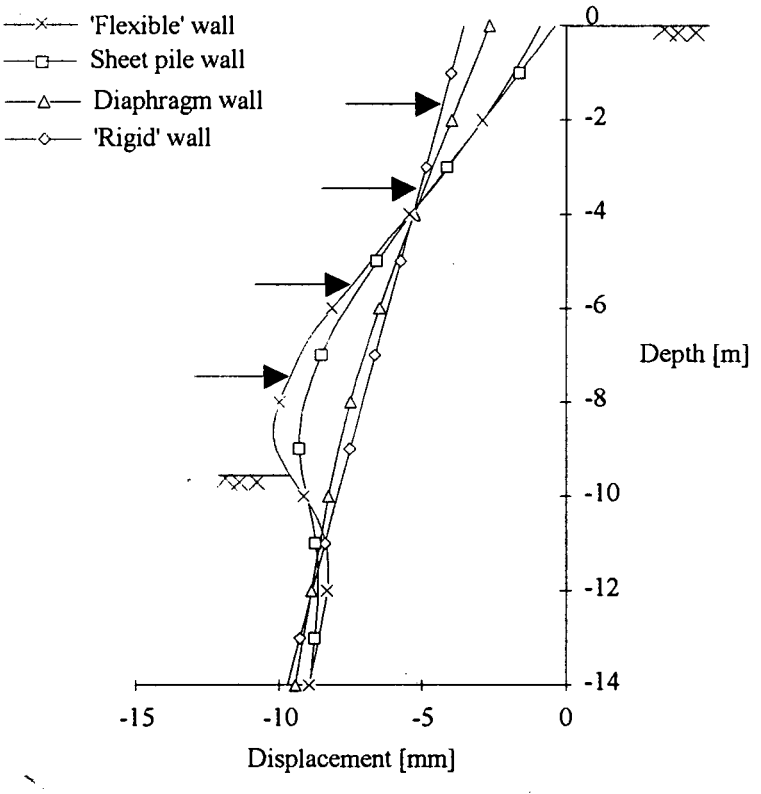

Figure 5.2: Wall displacements of supported walls of various stiffness.

b) Lateral earth pressures for the rigid walls

The lateral pressure distributions are shown for all the rigid type walls in Figure 5.3(a). The 'classical' triangular shape of the earth pressure distributions are depicted over the depth where active and passive earth pressures have been mobilized. Because of the wall rigidities, no significant earth pressure redistribution has taken place on the active side due to the prop forces. Therefore, the conventional methods of analysis which assume a classical earth pressure distribution can be used to give a reasonably accurate solution.

The lateral earth pressure distributions for the flexible type walls are shown in Figure 5.3(b). These demonstrate the redistribution of earth pressures that occur with flexible type walls. There is an increase in lateral earth pressure behind each prop and this effect is more pronounced for the 'flexible' wall. Earth pressures are redistributed from between the supports to the supported levels. The overall shape of the lateral earth pressure distribution is similar to that of the rigid type walls, however, the earth pressure redistribution that takes place has important implications.

It is expected that the increase in wall flexibility will cause the more flexible walls to attract smaller bending moments. The implications for the designer are that more flexible walls, which have the benefit of being more economically viable, can be used in the design on condition that the wall is stable and that the wall displacements and surface settlements behind the wall are within the limits that are required for that particular design situation.

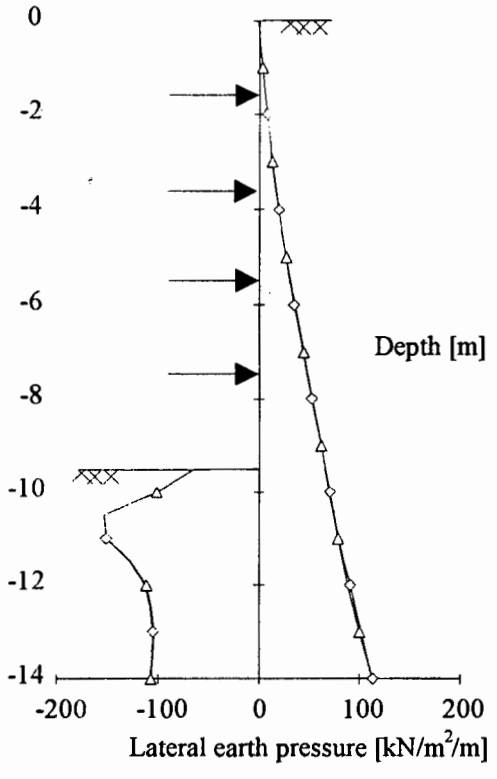

Figure 5.3 (a): Lateral earth pressure distributions for the rigid type walls.

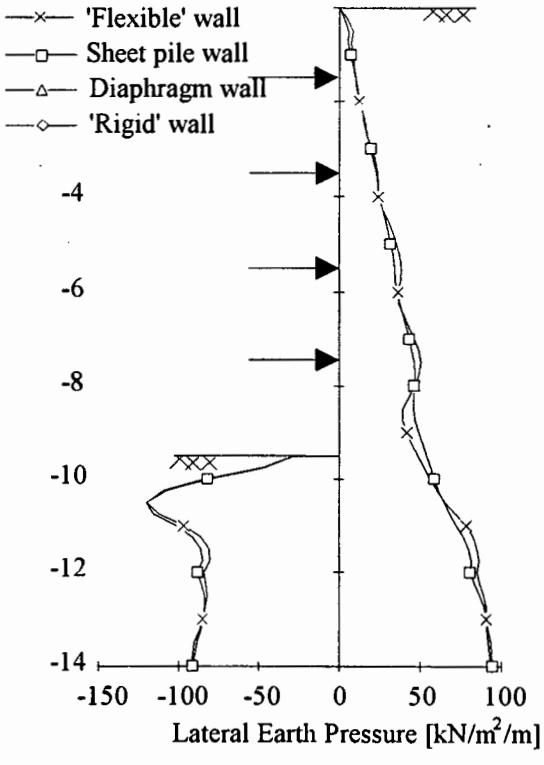

Figure 5.3 (b): Lateral earth pressure distributions for the flexible type walls.

c) Bending moments

The effect that wall stiffness has on the bending moments for the flexible type walls is demonstrated clearly in Figure 5.4. There is a significant reduction in the local peak bending moments that occur at each prop level with the decrease in wall stiffness. The more flexible walls allow the lateral earth pressures to be redistributed to the supported parts of the structure. It is therefore expected that the forces developed in the props will be greater in the case of flexible walls. The highest bending moments occur in the 'rigid' wall between the lowest prop level and the excavation level.

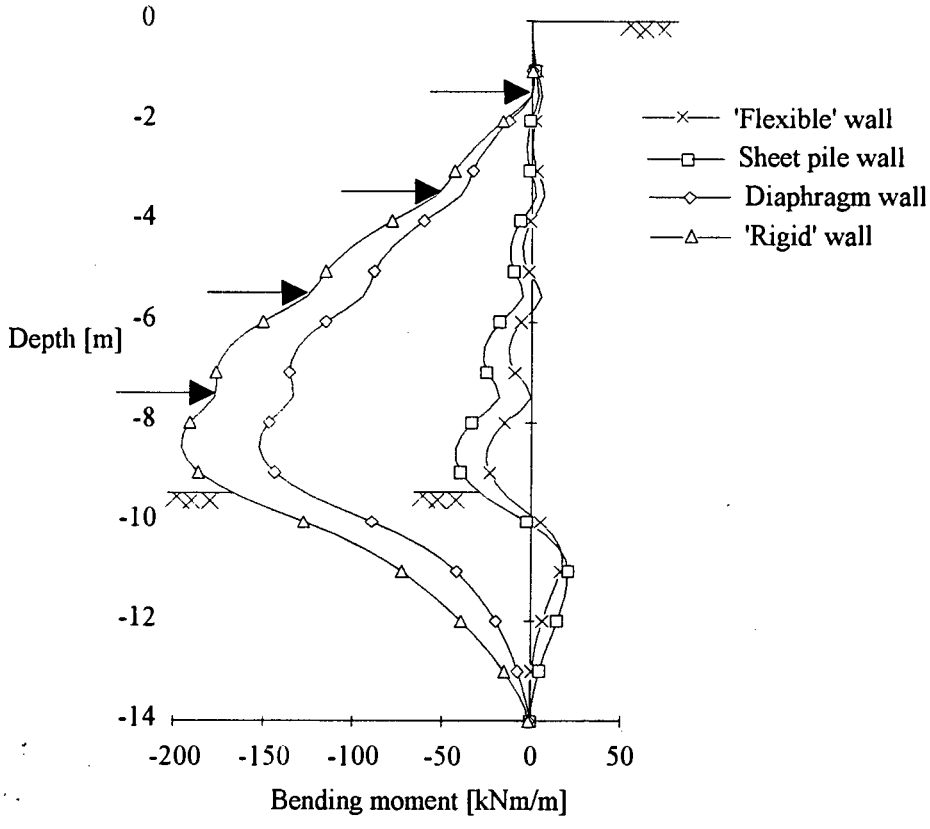

Figure 5.4: Bending moment distributions along supported walls of various stiffness.

d) Prop forces

The prop forces are higher at the top and lower at the bottom on the rigid type walls since the walls displace as rigid bodies. For the flexible type walls, the 'flexible' wall has higher prop forces than the sheet pile wall because the lateral earth pressures are redistributed to the supported levels. The prop forces are tabulated in Table 5.2 as well as the sum of the prop forces and the active earth thrust. The sum of the prop forces are basically in balance with the active earth thrust with little contribution from the passive earth thrust. Therefore, the embedment depth of the wall need only be about 2 m.

Prop Forces [kN/m]	'Rigid'	Diaphragm	Sheet pile	'Flexible'
Prop 1	42	37	22	23
Prop 2	51	50	47	47
Prop 3	60	62	71	75
Prop 4	69	73	89	96
Total prop force	222	222	229	241
Active earth thrust	287	282	272	275

Table 5.2: Prop forces for four walls of different bending stiffness.

e) Plastic strain distributions

The contours of equivalent plastic strain are plotted on the displaced mesh in the case of the 'flexible' wall and the sheet pile wall in Figures 5.5 (a) and 5.5 (b), respectively. The regions of plastic strain indicate where the soil has yielded. These regions, therefore, point out the failure zones within the soil in each case. The amount of deformation and plastic strain is greater for the 'flexible' than for the sheet pile wall, as would be expected.

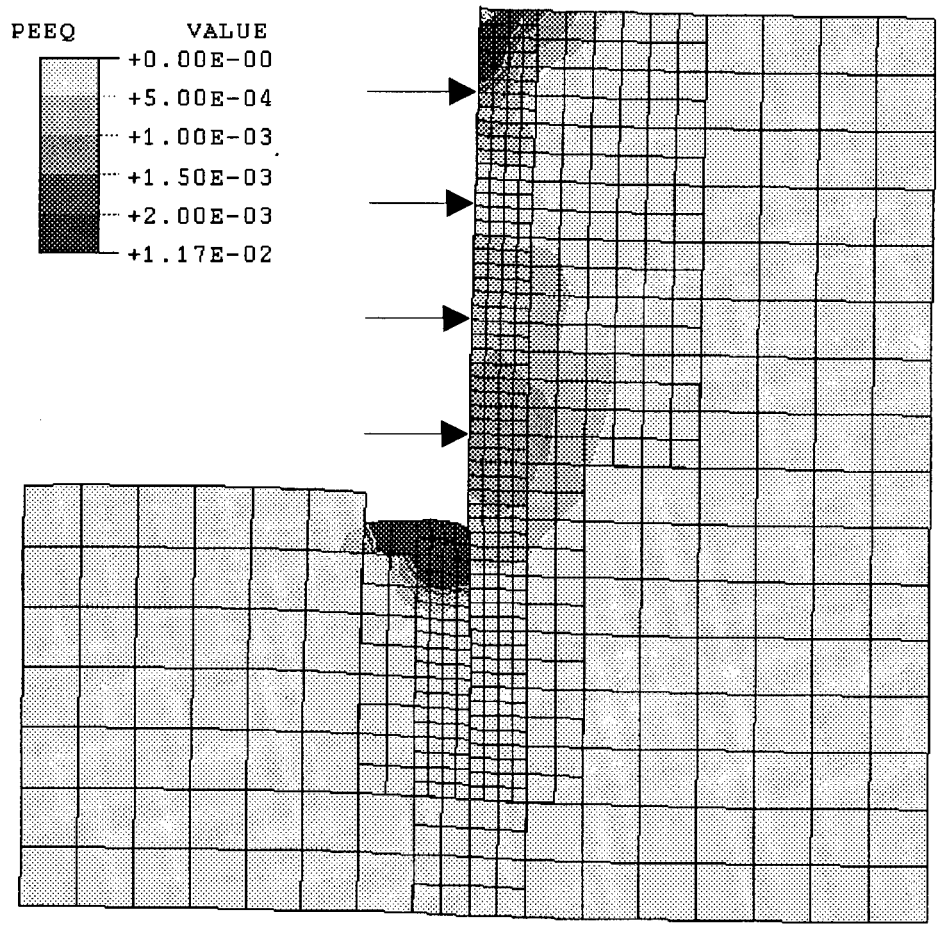

Figure 5.5 (a): Contour plot of plastic strains plotted on the displaced shape of the mesh for the 'flexible' wall.

(Displacement magnification factor = 20)

The wedge shape regions of failure behind the top of the wall are similar to those of the cantilever walls since this part of the wall is in principle a cantilever system. The plastic strain pattern that occurs is also a function of the prop stiffness. This is investigated in the subsequent
section.

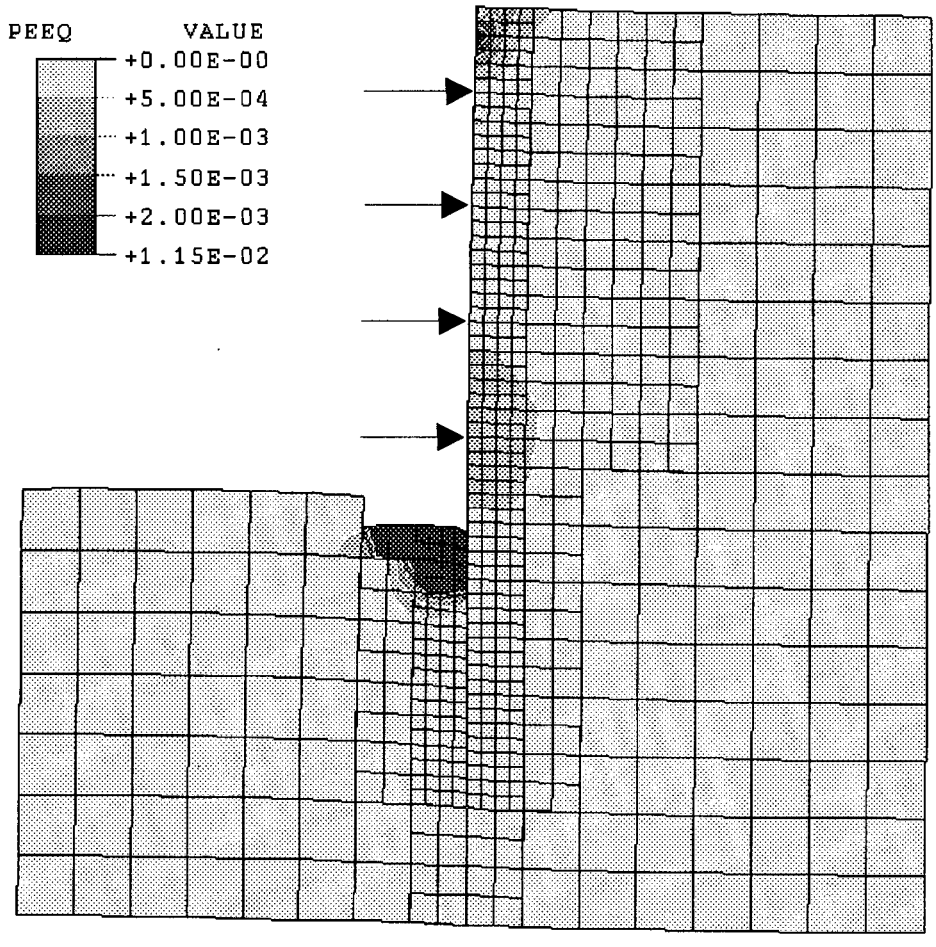

Figure 5.5 (b): Contour plot of plastic strains plotted on the displaced shape of the mesh for the sheet pile wall.
(Displacement magnification factor = 20)

f) Settlement patterns

The settlement pattern behind the 'rigid' wall is almost identical to the one behind the diaphragm wall and is not included in Figure 5.6. The surface displacements behind the flexible walls indicates that the soil heaves immediately behind the wall which gradually reduces until settlements develop beyond a distance of approximately 5 m behind the wall. The situation is different for the diaphragm wall with no heave occurring behind the wall and a more uniform settlement pattern. This pattern develops because the rigid walls displaced as rigid bodies causing wall tip displacements to occur. The bending that

The heave behind the wall is caused by the heave of the subsoil in the excavation lifting the wall and transferring across to the soil behind the wall. Observations of heaving behind the wall in the field have not been recorded yet, the results from the finite element analysis predict heaving behind the support systems. The finite element model may need to be improved in this regard. Two possible ways of modifying the model are:

- based on a similar problem experienced in the cantilever wall study the anisotropic soil stiffness parameters can be modified to increase the Young's modulus with depth.;
- The wall friction coefficient can be increased on the active side and reduced on the passive side which will both cause an increase in the resultant downward force on the wall.

The surface movements behind the rigid wall also indicate that the magnitude of the settlements are greater for the diaphragm wall than for the flexible type walls. Rigid walls are often employed in a situation where surface settlements need to be restricted because of the close proximity of excavations to adjacent buildings. There appears to be a discrepancy between these results and practice since the settlements behind the rigid walls are greater than for the flexible walls. The reason is that when rigid walls are employed in practice they are constructed with greater embedment depths than the case investigated here. The greater embedment reduces the magnitude of the parallel translation wall displacements. Consequently, the reduction in lateral movements of the wall restricts in the settlements of the ground surface behind the wall. Increasing the embedment depth of the flexible walls will not reduce the magnitude of the settlements much because the lateral wall movements are largely as result of bending.

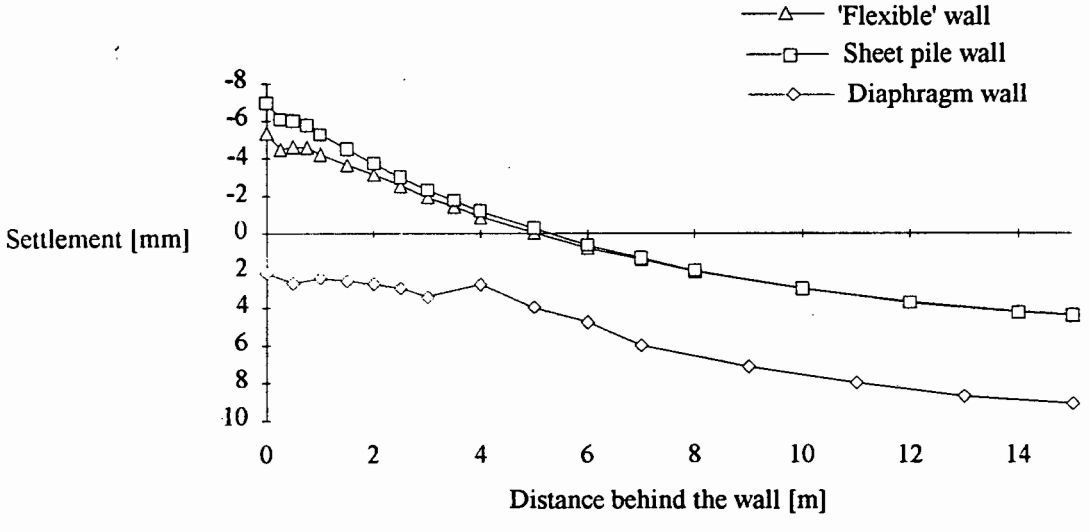

Figure 5.6: Settlement pattern behind walls of various stiffness.

5.4 PROP STIFFNESS

In the following investigation, the prop stiffness is varied at all four prop levels and the performance of the multiple supported wall studied. The wall stiffness was chosen to be that of the sheet pile wall investigated in the previous section. Three different support systems were analysed, each of different coefficient of prop stiffness but constant over all levels. As an upper limit,

- a value of k = 30 000 kN/m/m is assumed to represent a 'stiff' prop of high stiffness,
- a prop stiffness coefficient of 10 000 kN/m/m is assumed for an 'intermediate' case and
- a prop stiffness coefficient of 3000 kN/m/m is assumed to represent a 'soft' prop of low stiffness on the other extreme.

These values are in the order of magnitude as the stiffness used by Smith and Ho, (1992).

a) Wall displacements

It is expected that the wall displacements are greatest for the wall system which is supported by 'soft' props. The trend of wall displacements increasing as the prop stiffness decreases is shown in Figure 5.7. The displacement distribution of the wall with props of low stiffness depict a bulge over the midsection of the wall and shows a relatively large tip and embedment displacement in comparison to the other cases. The gradient of the walls reveal a lateral wall displacement of about 6 mm / 10 m excavation for the wall supported by the stiff props and about 12 mm / 10 m for the wall supported by the props of 'intermediate' stiffness.

For this particular case of the wall supported by 'soft' props results in a situation where the excavation depth of 9.5 m is just before the failure of the system.

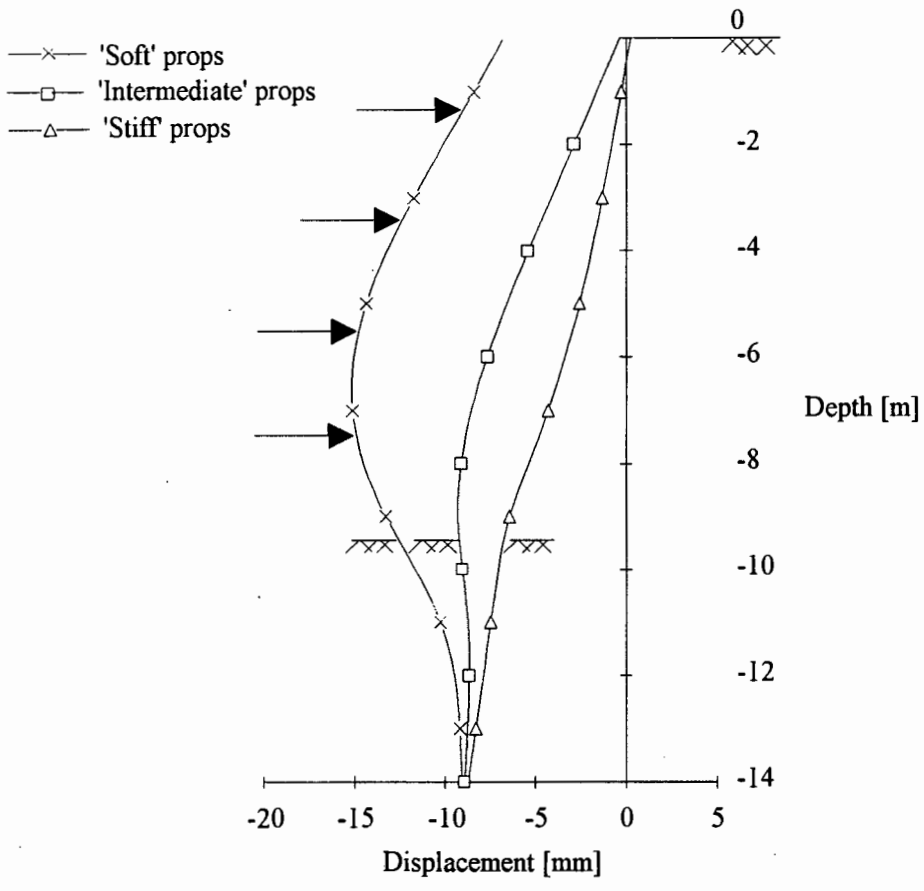

Figure 5.7: Wall displacements for support systems with props of three different coefficients of stiffness.

b) Lateral earth pressures

The wall displacements showed that the increase in prop stiffness results in the wall being more restrained and this is reflected in the lateral earth pressure distributions. The earth pressures increase behind the wall and decrease in front of the wall embedment with prop stiffness shown by the respective lateral earth pressure distributions for the three cases in Figure 5.8.

The gradient of the earth pressure distributions behind the wall, above the lowest prop level indicate active earth pressure conditions for the wall supported by soft props, through to earth pressures approaching at-rest conditions for the wall supported by stiff props. The stiff props therefore offer almost the same support as the supporting soil did before excavation. There is some deviation from these conditions below the prop level since the passive earth resistance is less than the prop support and acts below the level of excavation.

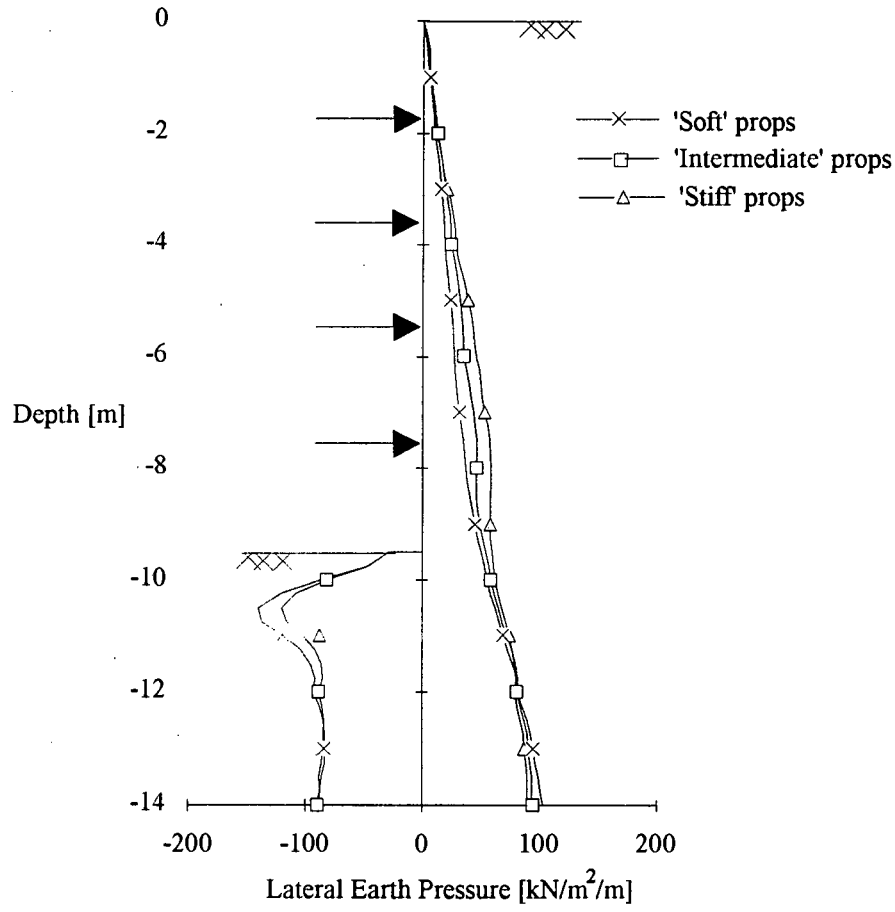

Figure 5.8: Lateral earth pressure distribution for support systems with props of three different coefficients of stiffness.

c) Bending moments

The bending moment diagram for all three cases, shown in Figure 5.9, demonstrates the significant effect of prop stiffness on the design of the support structure. Local maxima occur at each prop level and the magnitude of the bending moments at these levels are lower as the prop stiffness increases for the range of prop stiffness coefficients examined. The trend indicates that higher prop stiffness coefficients would increase the magnitude of the bending moments. Since the props of high stiffness restrict the movement of the wall as a whole, the maximum bending moment, which occurs between the lowest prop level and the excavation level, is lower than for the other cases. Of the cases considered the most efficient solution with respect to bending moments is the wall supported by stiff props.

Having investigated the influence of wall and prop stiffness on the bending moments of the wall, it is apparent that a design optimization procedure would need to be carried out by varying the wall stiffness and the prop stiffness to find the optimum design.

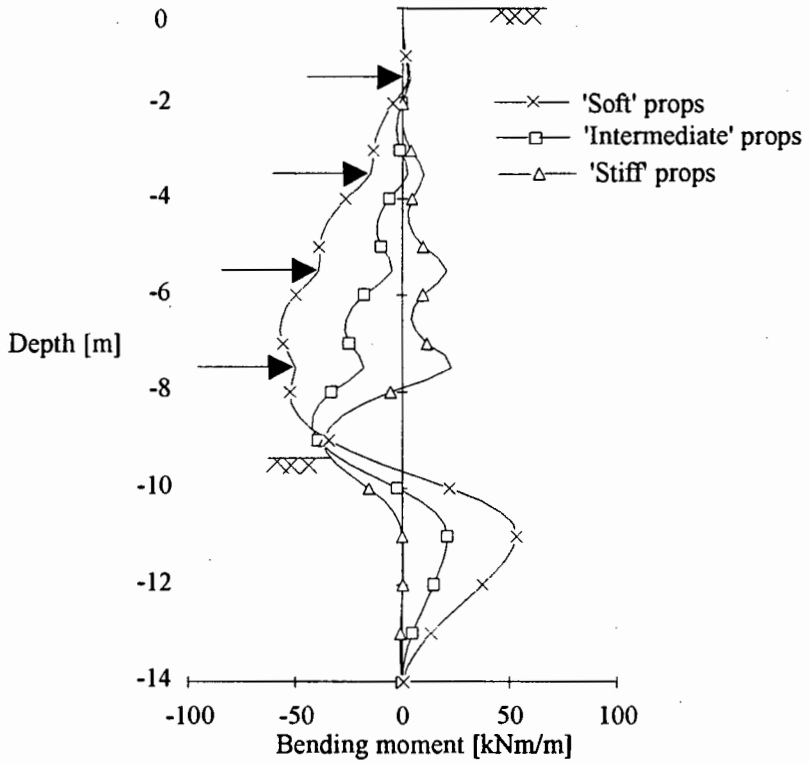

Figure 5.9: Bending moment diagram for support systems with props of three different coefficients of stiffness.

d) Prop forces

In general, the trend of variation in prop forces is that the stiffer props develop less force upon wall movement near the top of the wall and greater force near the excavation level. The forces are greater nearer the excavation floor because the earth pressures behind the wall in this region are greater. The wall displacements are greater near the top for walls with softer props and therefore greater forces are developed. The prop forces at all levels of support that act on the walls are listed in Table 5.3 including the sum of the prop forces and thrust of the earth pressures behind the wall and above the excavation level. Once again, most of the earth pressure behind the wall is balanced by the total prop force. The difference represents the passive earth thrust in front of the embedded wall which is greatest in the case of 'soft' prop support and lowest in the case of 'stiff' prop support.

Prop Forces [kN/m]	'Soft' Props	'Intermediate' Props	'Stiff' Props
Prop 1	28	22	16
Prop 2	38	48	48
Prop 3	44	71	88
Prop 4	44	89	144
Total prop force	154	230	296
Total earth thrust	217	273	323

Table 5.3: Prop forces for props of three different stiffness.

e) Plastic strain distributions

The contour plots of plastic strains, which indicate regions where the soil has failed are plotted for the support systems with stiff props and soft props in Figure 5.10 (a) and Figure 5.10 (b), respectively. In the case of the assumption of stiff props some plastic strain has only occurred due to the cantilever action at the top of the wall and at the base of the excavation where passive resistance is offered by the soil. Nowhere else do the stresses in the soil behind the wall reach the yield surface due to the restriction of wall displacements by the stiff props.

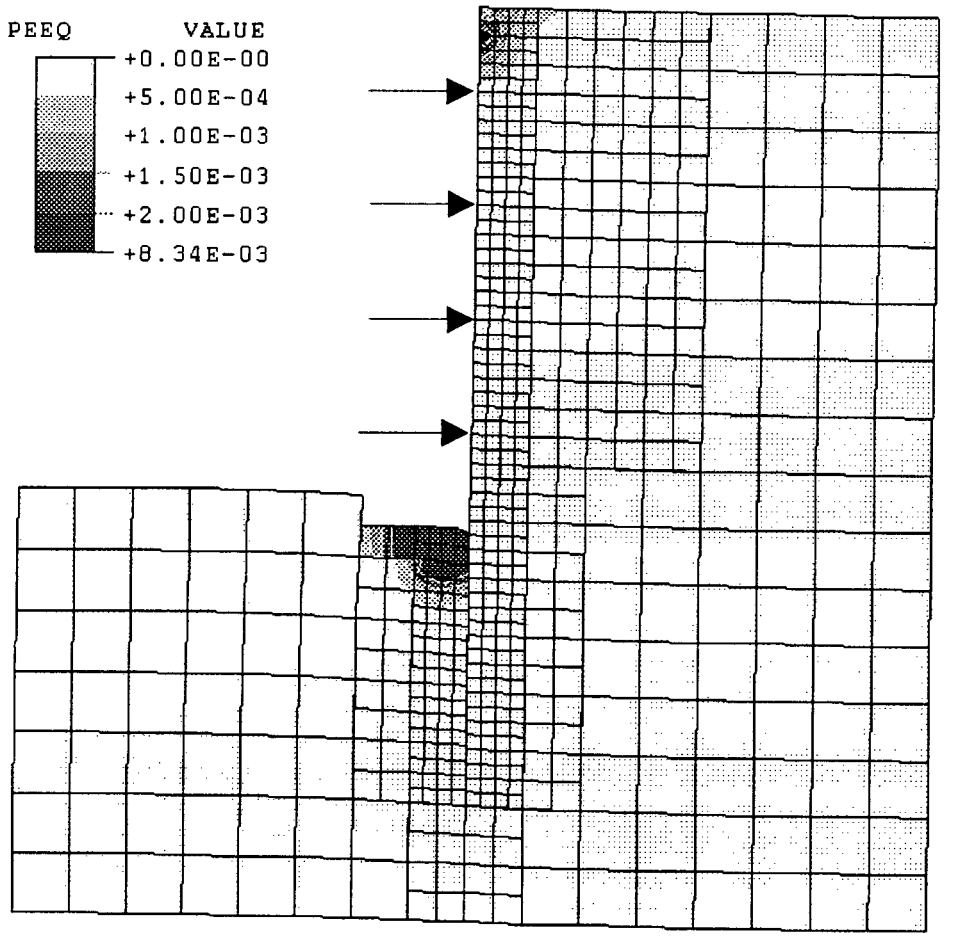

Figure 5.10 (a): Contours of plastic strain for the support system with 'stiff' supports plotted on the displaced mesh.

(Displacement magnification factor = 20)

The situation for the support system with soft props is quite different. The deformations are far greater and therefore plastic strain has occurred over a greater region and to a greater extent. The highest plastic strains develop between the prop supports indicating the redistribution of earth pressures as discussed earlier The contours shown in the plot are not continuous over element boundaries because the soil parameters have been defined with a Young's modulus increasing with depth in 2 m thick layers.

These two contour plots can be compared to the plot in Figure 5.5 (b) which is of the sheet pile wall supported by props of an 'intermediate' stiffness coefficient. The area and magnitude of plastic strain is between the two extreme cases as expected.

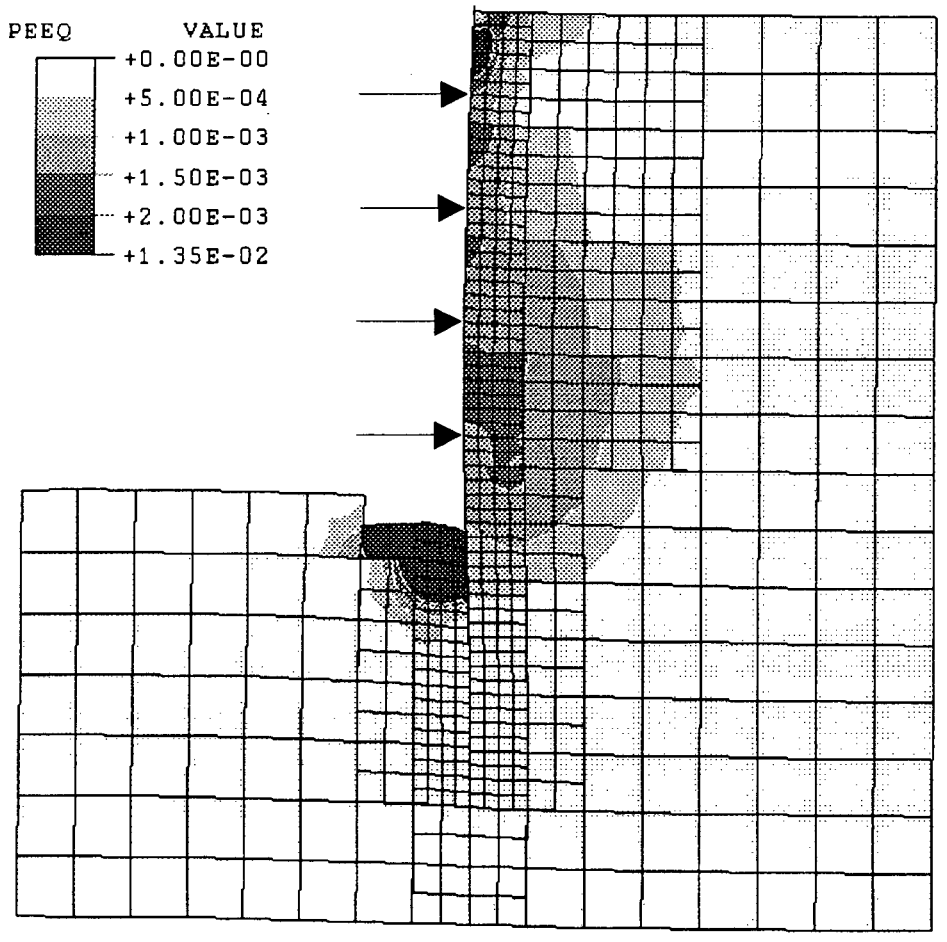

Figure 5.10 (b): Contours of plastic strain for the wall supported by 'soft' supports plotted on the displaced mesh.

(Displacement magnification factor = 20)

f) Settlements

The settlement patterns for the analyses involving the props of different stiffness are shown in Figure 5.11. The surface settlement behind the wall is a function of the lateral wall movements at the level of the ground surface. If the lateral wall movements are restricted then so will the magnitude of the settlements. It is apparent from Figure 5.11 that an increase in prop stiffness increases the magnitude of heave that occurs immediately behind the wall. Heave occurs due to the decrease in wall displacements at the top of the wall with an increase in prop stiffness (see also Figure 5.7).

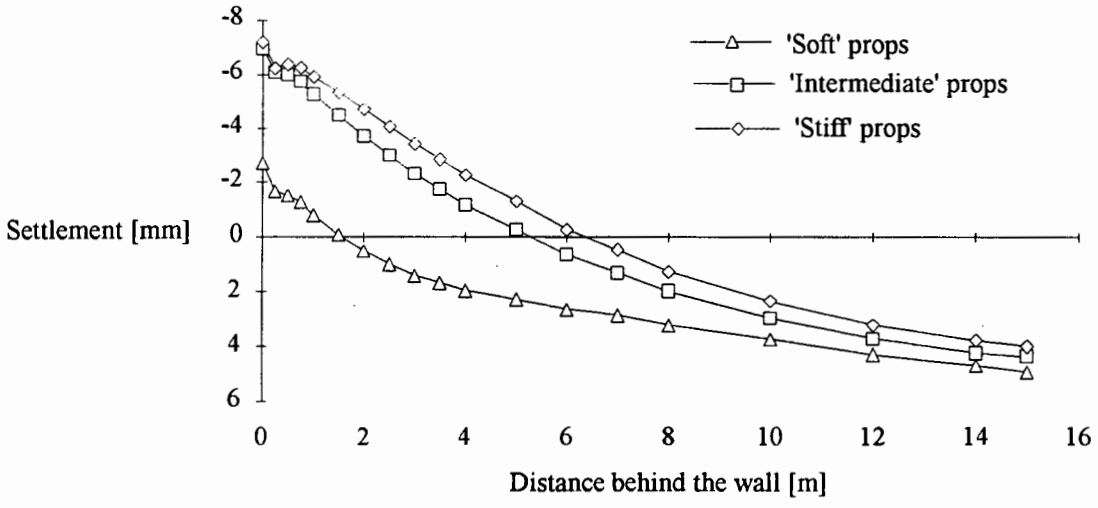

Figure 5.11: Settlement pattern for supported walls with props of three different coefficients of stiffness.

5.5 APPLICATION OF ADDITIONAL PROP LOADS

The procedure for applying prop loads has been described in Chapter 3. The purpose of applying prop loads is to simulate a similar soil/structure interaction which takes place when soil anchors are prestressed. Prestressing of anchors is generally performed after the installation of anchor supports in lateral support system engineering. The investigation of applied loads provides some insight into the influence that prestressing has on the behaviour of the support system.

The performance of a support system with the basic configuration described earlier in this chapter with props of 'intermediate' stiffness was studied. Again, the wall stiffness was chosen to be that of the sheet pile wall examined in the investigation of wall stiffness. An analysis of the support system without any applied loads was performed. Table 5.4 presents the initial loads that the props exerted at prop installation, due to initial wall movements and the loads due to the wall displacements that occur at the final excavation depth. A proportion of 80% of the difference in these forces was chosen to apply to the props in a subsequent analysis, in addition to the forces exerted due to the wall movement. These forces are listed in the table including the ratio $\frac{\text{initial load}}{\text{final load}}$ expressed as a percentage.

b) Bending moments

The bending moment distributions shown in Figure 5.13 are more revealing as to the influence of loads applied at the supports. There is a reduction in the local maxima of bending moments, which occur at the supported levels, when loads are applied. There is, however an increase in the maximum bending moment which occurs between prop level 4 and the excavation level. This increase in bending moment, relative to the case without applied loads, could be reduced by increasing the load applied at prop level 4. This would cause a shift of the bending moment distribution in this region in the positive direction and therefore reduce the magnitude of the bending moment at and below prop level 4.

The influence that applied loads have on bending moments is considered to be the most important in terms of economics because it determines the size of the wall section that is required in a design. Clearly the designer needs to take into consideration the application of loads and the magnitude of the applied loads when optimizing the design by minimising the bending moments.

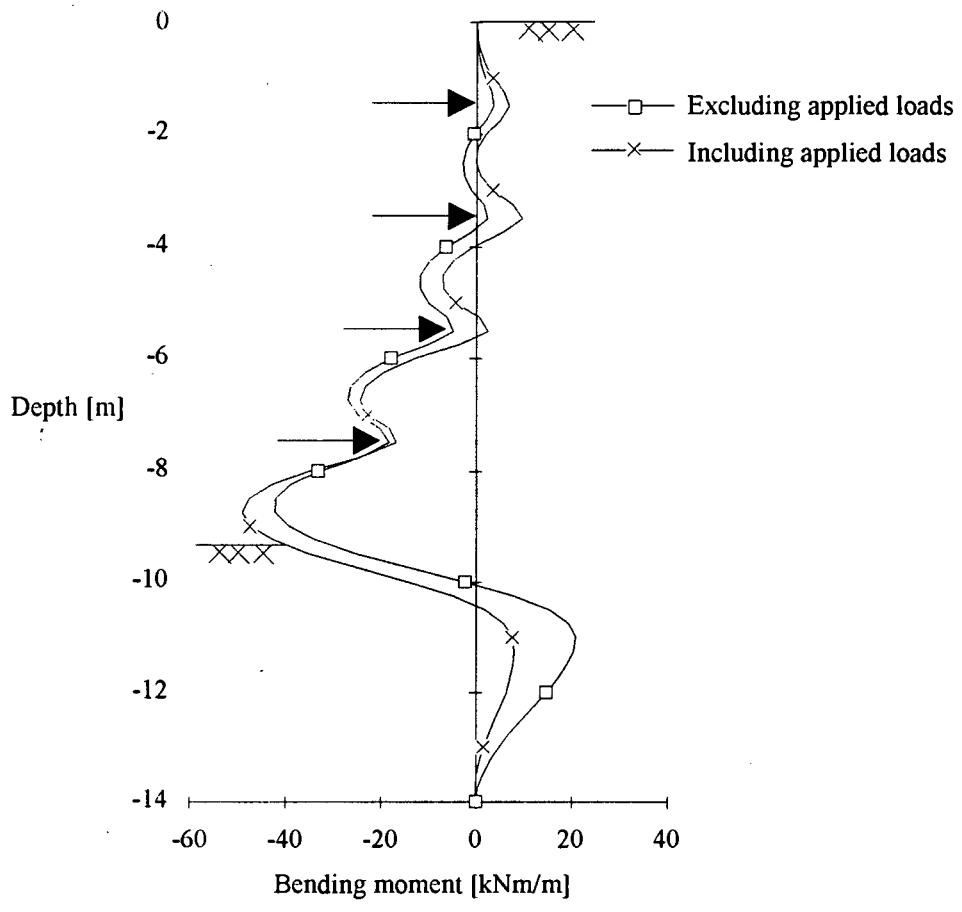

Figure 5.13: Bending moment distributions for the support system with and without applied loads.

c) Plastic strain distributions

The contours of plastic strain are plotted on the displaced shape of the mesh in Figure 5.14. This contour plot can be compared to the contour plot of the sheet pile wall without applied loads shown in Figure 5.5 (b). The amount of plastic strain is less for the case which includes applied forces because the wall displacements are more restricted. This case is similar to the situation where 'stiff' props were used to support the wall structure.

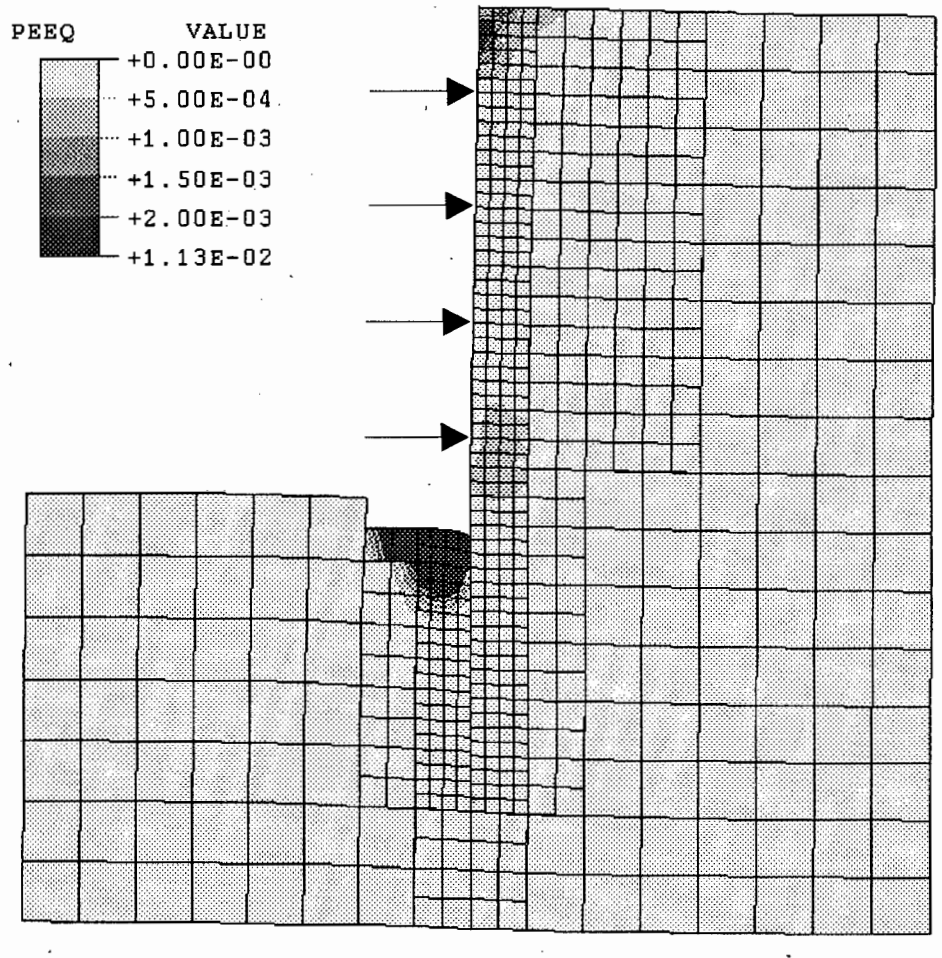

Figure 5.14: Contours of plastic strain for the support system including applied loads.
(Displacement magnification factor = 20)

d) Settlements

A comparison was made between the settlements for the cases with and without applied prestress forces. The reduction in lateral wall displacements caused by the applied loads resulted in the amount of heave immediately behind the wall being slightly higher than in the case where no additional prop loads were applied.

CHAPTER 6
CASE STUDIES

6.1 INTRODUCTION

The design of cantilever support systems carried out by the conventional method involves an assumption concerning the earth pressure distribution. The assumption is that the earth pressures are acting at the limit state i.e. full active and passive pressures have been mobilized. The earth pressure in multiple level supported systems deviates significantly from the classical distribution and it is recommended (Code of Practice, 1989) that, for design purposes, a redistributed active earth pressure of simple geometrical shape be assumed. The simplified redistributions represent either rectangular, trapezoidal or triangular approximations of the theoretical earth pressure distributions behind the wall.

In order to demonstrate the potential of the finite element method in lateral support design, a specific case study of a cantilever wall and a multiple supported wall were chosen and analysed using both the conventional method and the finite element technique. The results are compared and discussed with particular emphasis on how the different earth pressure distributions influence the results of the two methods, i.e. the moment distribution along the wall in the cantilever study and the moment distribution and prop forces in the multiple level supported study.

6.2 CANTILEVER WALL CASE STUDY

The dimensions and properties of the cantilever system were assumed to be the same as those used in the investigation of the influence of soil types on cantilever support systems. The wall section has a bending stiffness of EI = 8.07 x 10^4 kNm^2/m. The soil parameters of the isotropic sand chosen are listed in Table 4.2. The design excavation depth was 4 m.

The conventional method used for the design was based on Blum's method (1950) which involves three steps to calculate the:

1) penetration depth, which is the depth below the excavation level that the wall penetrates,
2) maximum moment (and its location along the sheet pile wall), and
3) wall deflections.

The wall deflections were not calculated and are therefore not considered in the following comparative study. The design was based on the assumption of limit state considerations, i.e. the wall penetrates below the excavation level to a depth at which the sum of the overturning and resisting moments is zero. The values for the earth pressure coefficients

K_{ah} = 0.23 and K_{ph} = 7.6, respectively, were obtained from the tables published by Caquot and Kérisel, (1948). A factor of safety of 1.5 was chosen and applied to the passive earth pressure coefficient, thus $K_{ph\ reduced}$ = 5.0.

a) Lateral earth pressures

The lateral earth pressure distributions from Blum's method and the finite element analysis are shown in Figure 6.1. At the limit state the earth pressures act to the depth at which moments are zero, which is assumed as the point about which the wall rotates. This was found to occur at a depth of 6.23 m. In Figure 6.2 which shows bending moment distributions, this depth is indicated by the intersection of the dashed line with the vertical axis. The earth pressures below the point of rotation depth were assumed to be fully passive behind the wall and fully active in front of the wall. The total penetration depth is then calculated (shown in Figure 6.1) as $u + t_1 + \Delta t_1$ = 2.64 m, where u is the distance from below the excavation level to where the sum of the active and passive earth pressures is zero and, t_1 is the distance below this point to the point of rotation. An additional length $\Delta t_1 = 0.2t_1$ is added. Thus the total length of the cantilever sections calculated by the conventional method is 6.64 m.

The comparison of lateral earth pressures illustrates one of the main differences in the design approach between the conventional method and the finite element method. The first objective in the conventional design is to find the required penetration depth of the wall, whereas the assumption of a total wall length is required in the finite element method at the onset of the analysis. In this case study the penetration depth assumed in the finite element method is 10 m compared to the penetration depth calculated by the conventional method at 2.24m. For this reason the earth pressures below the point of rotation in the finite element method are not mobilized at all, i.e. earth pressure conditions below the point of rotation are at-rest rather than in active or passive failure situations.

The finite element results demonstrate that the conventional method overestimates the passive earth pressures above the point of rotation even though a reduced coefficient of passive earth pressure was introduced. On the other hand, the finite element analysis clearly reveals that the passive earth pressure has only been mobilized up to 0.5 m below the excavation level. Below that level the earth pressures drop off to the at-rest condition.

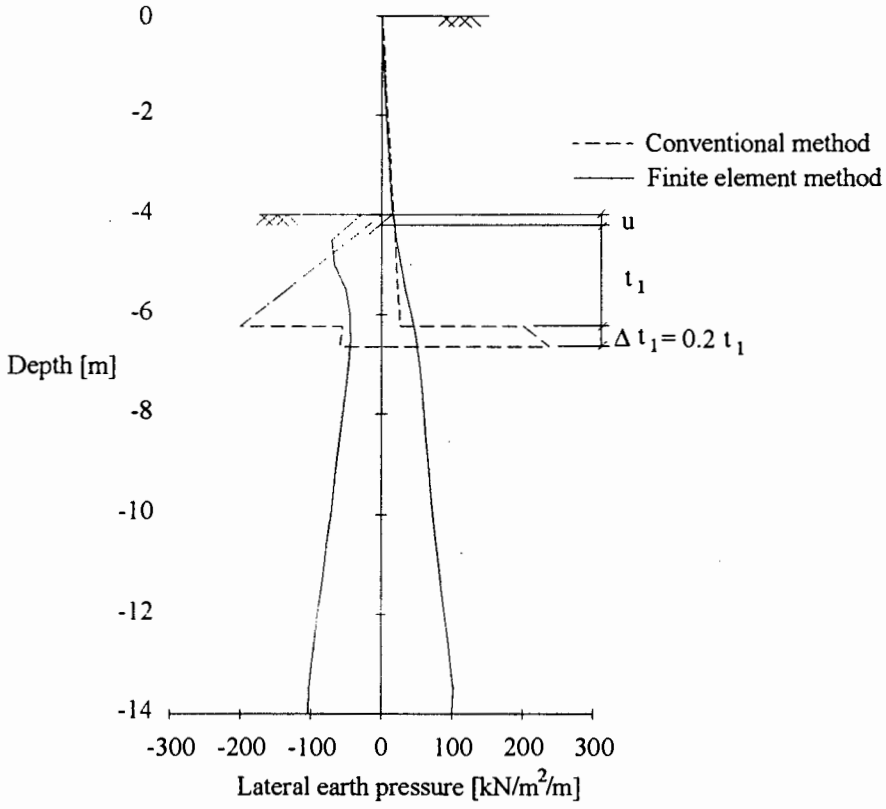

Figure 6.1: Lateral earth pressures from both methods of analysis.

b) Bending moments

The effect of the greater passive resistance, assumed in the conventional method, on the bending moment distribution is depicted in Figure 6.2. The comparison between bending moments calculated by both methods also shows that the maximum bending moment is overestimated by the conventional method. The maximum bending moment calculated in the conventional analysis is 71.3 kNm/m compared to 49.7 kNm/m in the finite element analysis. The depth at which the bending moment is zero is also significantly different due to the difference in passive earth pressures and wall length.

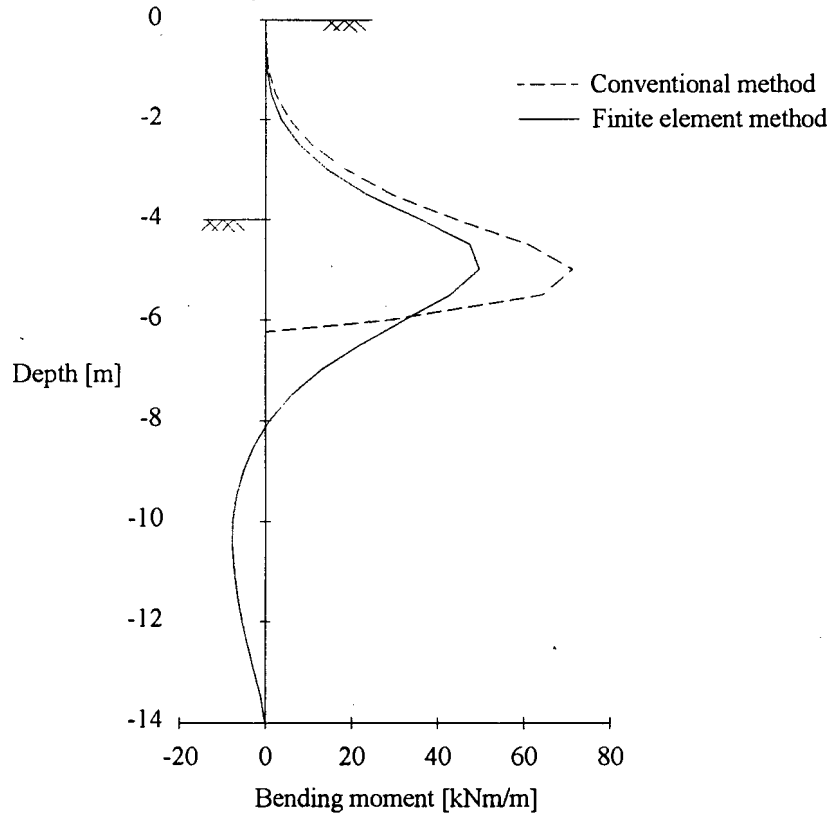

Figure 6.2: Bending moment distributions from both methods of analysis.

6.3 MULTIPLE LEVEL SUPPORTED WALL CASE STUDY

6.3.1 Description of the Problem

The case study undertaken was of a four-level propped sheet pile wall embedded in a stratified soil. The elevation is schematically depicted in Figure 6.3 and the pertinent soil parameters required for the design calculation are listed in Table 6.1. A layer of silt is being supported which is underlain by a medium dense sand. The groundwater table is 1 m below the excavation level.

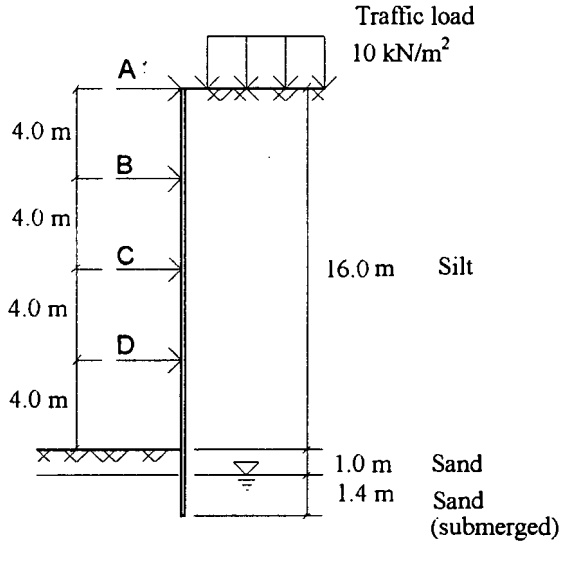

Figure 6.3: Schematic in elevation of the multiple level sheet pile support system.

The wall structure consists of HOESCH 155 sections, with a stiffness of EI = 6.18×10^{-4} kNm^2/m, driven to a depth of 18.4 m prior to the excavation. A traffic load of 10 kN/m^2 is applied at ground level behind the wall. The props are vertically spaced at 4m intervals.

Soil parameters	Silt	Sand	Sand (submerged)
Unit weight γ	19 kN/m^3	17.5 kN/m^3	9.5 kN/m^3
Internal friction angle φ	25^o	35^o	35^o
Cohesion c	5 kN/m^2	1 kN/m^2	1 kN/m^2
Poisson's ratio ν	0.3	0.3	0.3
Young's modulus E	15 MPa	40 MPa	40 MPa

Table 6.1: Summary of soil properties.

6.3.2 Finite Element Model Specifications

The finite element mesh and boundary conditions are shown in Figure 6.4. The elements used to represent the soil, wall and supports were the same as those described in Chapter 3 for the sheet pile wall model. The soil-structure interaction was modelled with interface elements associated with an interface boundary, as before. The coefficient of wall friction prescribed at the interface was calculated using $\mu = \tan \delta$, where the friction angle δ was set to $\delta_a = \frac{1}{3}\varphi$ on the active side and $\delta_p = \varphi$ on the passive side where φ is the internal angle of friction of the soil.

The initial stresses in vertical and horizontal direction were described by $\sigma_v = \gamma H$, where H is the depth, and $\sigma_h = K_0 \sigma_v$, respectively, with a coefficient at-rest of $K_0 = 0.5$ which was assumed constant and representative for both silt and sand.

The investigation of the influence of the flow rule in Chapter 4 showed that the associative flow rule enables a greater maximum excavation depth for cantilevers and therefore should enable a greater prop spacing for supported walls. A preliminary analysis was performed using a non-associative flow rule with a dilation angle of $\psi = \frac{3}{4}\phi$. This analysis did not achieve a solution for this problem with a prop spacing of 4 m as required by the design. A solution was only possible using a fully associative flow rule, although this is not an accurate description of the soil behaviour. The implication of using an associative flow rule is that a solution can be achieved for a higher prop spacing than would be possible when using a non-associative flow rule. The requirement of an associative flow rule would therefore lead to the recommendation that the design is not stable and that either a higher applied prop load is required or the prop spacing should be reduced.

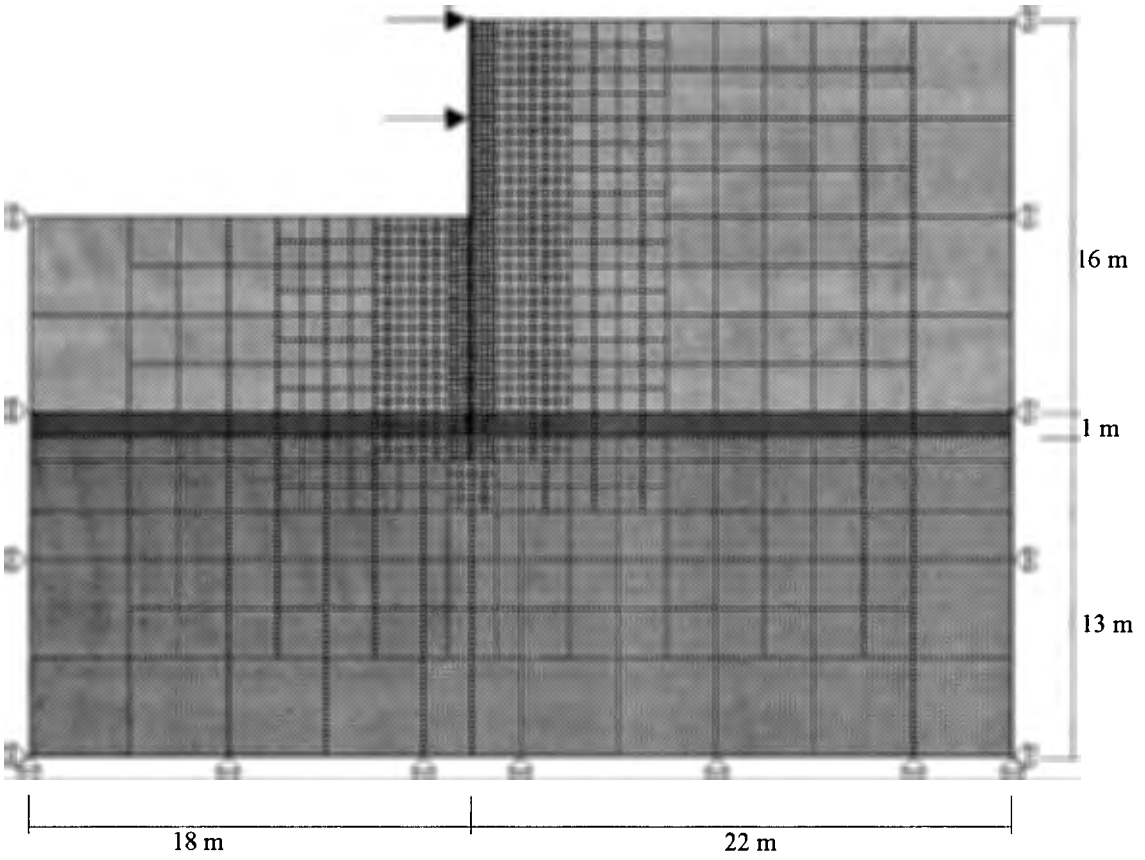

Figure 6.4: Finite element mesh (after 8 m excavation) including dimensions and boundary conditions.

6.3.3 Finite Element Analyses of the supported wall

For the purposes of the study, the relevant response characteristics of the problem derived by the conventional and finite element methods are evaluated. For a meaningful comparison, the basis of the two methods should be on common grounds. This means that the prop supports need to be closely represented by spring elements or the known prop forces applied as concentrated loads (a method not yet undertaken). For this reason, three different strategies were undertaken in the analysis of the problem to provide a basis for the comparative studies:

1) Concentrated loads equal to the design prop forces, as calculated by the conventional method, were applied to model the props.

2) Spring elements were employed to represent the prop supports with variable stiffness coefficients 10 000, 20 000, 20 000 and 30 000 kN/m/m for prop levels A, B, C and D, respectively. The increase in prop stiffness was introduced to simulate a greater support with increasing excavation depth.

3) Spring elements with constant stiffness at all levels were installed with a coefficient of stiffness 10 000 kN/m/m, and specific prop loads applied. The applied prop loads were chosen to be one third of the calculated design load based on the conventional design

method (without implementing any additional factor of safety). The values of the applied prop loads are tabulated in Table 6.2.

Prop level	Design load from conventional method [kN/m]	Applied prop load (⅓ of design load) [kN/m]
Prop 1	23	8
Prop 2	245	82
Prop 3	242	81
Prop 4	330	110

Table 6.2: Design and applied prop loads.

Some difficulties were experienced during the finite element analyses by these three methods:

The initial analysis by method 1) was unsuccessful due to a problem with the removal of the soil layers during the simulation of excavation after a concentrated load had been applied. A similar problem has been reported by Brown *et al* ,(1985) and Whittle *et al*, (1992) and the need for an accurate solution algorithm for the simulation of excavation was emphasised, particularly for situations involving applied concentrated loads. The procedure for removing elastic-plastic elements recommended in the ABAQUS User Manual was used as described in Chapter 3. This procedure was successful when the applied prop loads were below a critical value but failed when the loads were above this critical value. The analysis was re-run using four-noded, quadrilateral, full integration elements to represent the soil, instead of the reduced integration elements used in the previous investigations. The use of these elements resolved the problem and the results are presented in the next section.

A similar problem occurred during the analysis approach described in method 2) when the prop stiffness at level B exceeded about 18 000 kN/m/m. This prop stiffness resulted in the prop load exceeding the critical value. The use of full integration elements again removed this limitation.

The analysis by method 3) was successful with reduced integration elements and the results are shown and discussed in the following section.

6.3.4 Results of conventional and finite element analyses

a) Conventional analysis

A conventional analysis of the example was performed by Nendza (1989) and the results are presented below. The resultant classical distribution is shown in Figure 6.5(a) and the chosen trapezoidal shaped redistribution of earth pressure in Figure 6.5(b), as

recommended in Code of Practice (1989). The passive earth pressures are replaced by a single force, E_{ph}, acting at a depth of 17.6 m. The value of K_{ph} was acquired as before. A factor of safety of 1.5 was introduced and thus the reduced value of K_{ph} was 5.57.

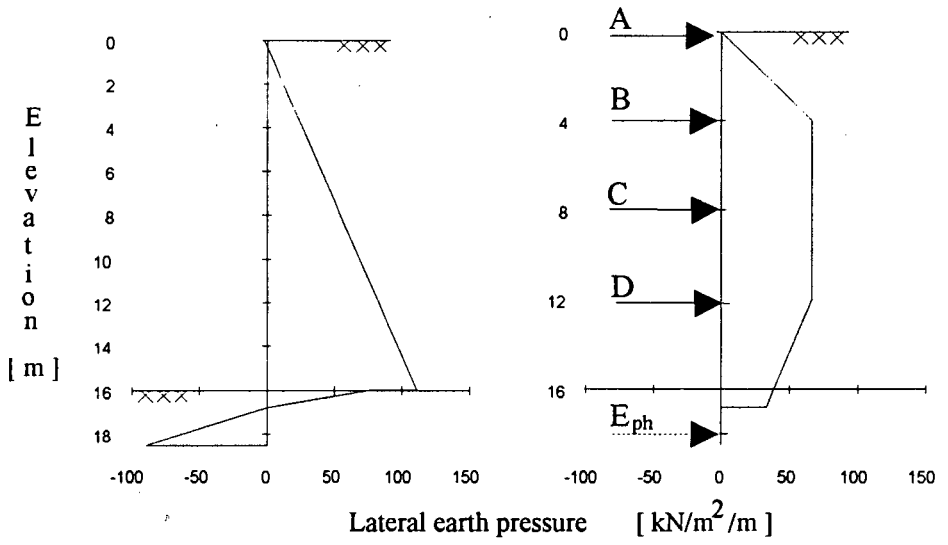

(a) Resultant classical distribution (b) Selected redistribution

Figure 6.5: Lateral earth pressure distribution from the conventional analysis.

b) Comparison between lateral earth pressures from the conventional analysis and the finite element analyses

The focus of the investigation is the evaluation of the prop forces based on the assumption of an earth pressure distribution. The comparison between lateral earth pressures calculated from the conventional analysis and the three methods of finite element analyses are shown in Figure 6.6. The redistributed earth pressure from the conventional method, shown by the dashed line, is superimposed on the pressure distributions from the finite element analyses. Considering that the recommended shape of the conventional method is of simple geometric configuration for practical design purposes, the earth pressure distributions behind the wall are in reasonably good agreement from the ground surface down to prop level D. The best agreement is obtained from method 1) since the prop loads are the same as those calculated by the conventional method. Method 2) represents a very stiff support option and therefore produces the highest earth pressures whereas the earth pressure distribution from method 3) is intermediate to the other two.

The main difference between the finite element results and the assumed earth pressure distribution is observed at the level of prop D and greater depth. The earth pressures from all three methods by the finite element method indicate higher pressures in this region. They also demonstrate the redistribution of earth pressures at the prop levels. The effect of the difference in earth pressures is reflected in the bending moments and prop forces

shown in Table 6.3 and Table 6.4, respectively. A more reasonable assumption of earth pressures behind the wall would have been to extend the rectangular shape from prop level D to below the excavation level rather than the decrease that was assumed over this depth.

From the earth pressures mobilized in front of the wall a value for the passive earth pressure coefficient was derived. This value of K_{ph} = 6.85, compared to the value K_{ph} = 8.35 published by Caquot and Kérisel, (1948), indicates that the passive pressures have not been fully developed.

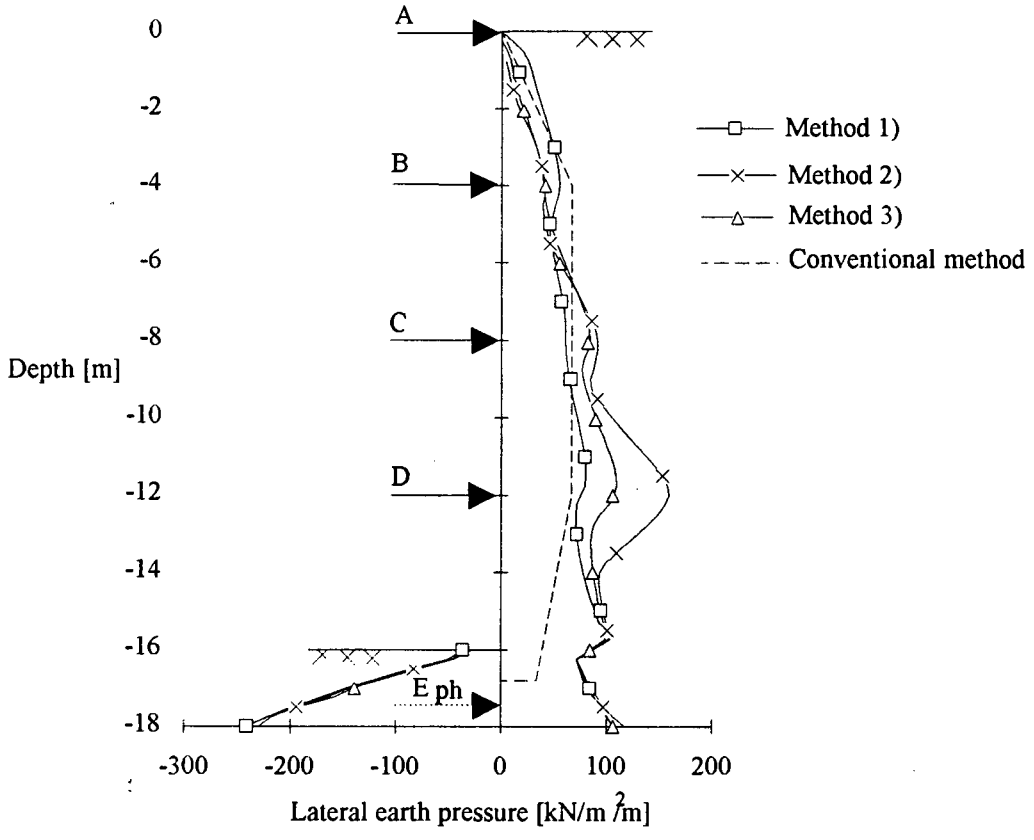

Figure 6.6: Earth pressure distributions from the finite element and conventional (dashed line) analyses.

c) Comparison of the bending moments

In Figure 6.7, it can be observed that the bending moments for method 3) are intermediate to the other two methods. This was expected judging from the results of the lateral earth pressures which indicated the stiffness of the three schemes. The prop forces applied at prop level D were calculated from the assumed earth pressure distribution which under predicted the earth pressures at this level. Thus the bending moment at this level is lowest for method 1). The maximum moment for all three methods is observed close to the midspan between level D and the excavation level.

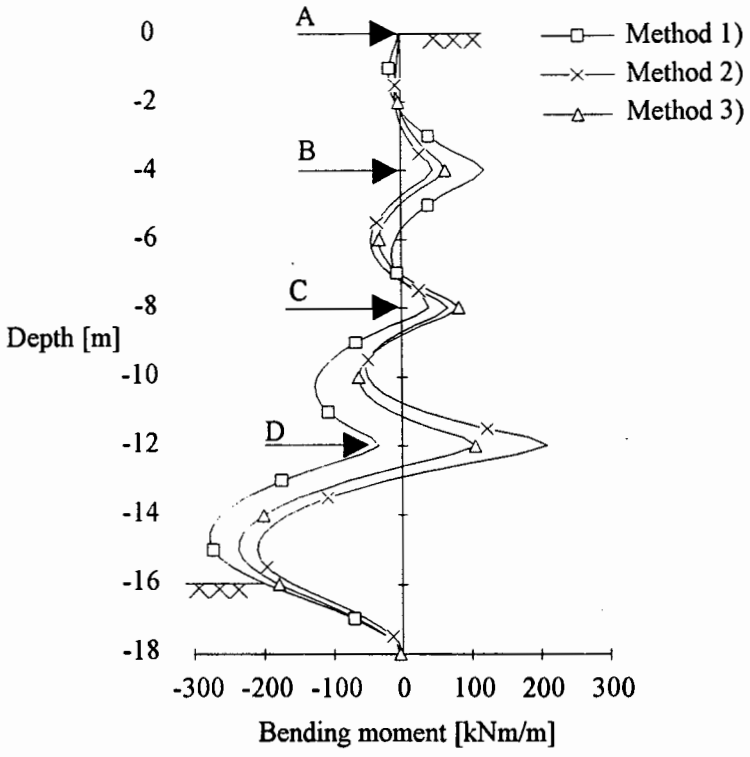

Figure 6.7: Bending moment distributions calculated by the finite element method.

A comparison of the bending moments from the conventional analysis and the finite element analyses, listed in Table 6.3, indicate that the conventional method generally underpredicts the bending moments including the maximum bending moment. This is obviously due to the underestimation of the earth pressures, which emphasises the importance of accurately predicting the earth pressure distribution. The maximum bending moment is the value that determines the required stiffness of the structure. Method 2) gives the lowest maximum bending moment of the schemes considered.

Support Level	Conventional analysis	Finite element analysis (Method 1)	Finite element analysis (Method 2)	Finite element analysis (Method 3)
A	0	0	0	0
B	83.4	119	45	63
C	72.7	39	67	82
D	155.5	-34	209	105
D-E_{ph}	-108.8	-274	-210	-237

Table 6.3: Bending moments from the conventional and finite element analyses.

d) Comparison of the prop forces

The difference in the earth pressure distribution between the two methods also results in a difference in prop.forces, shown in Table 6.4. The prop forces from the finite element analyses by methods 2) and 3) are lower at the top and higher at the bottom than those

found by the conventional analysis. Method 2) uses the stiffest prop supports and attracts the highest prop forces.

Of particular interest is the value used for E_{ph} in the conventional method which is lower than the value calculated from the results by the finite element analyses (i.e. the area of the passive earth pressure distribution). This is partially due to the application of a factor of safety to the passive pressures in the conventional method as well as the under prediction of the earth pressures behind the wall. This demonstrates that the application of the factor of safety did not yield a conservative result because of the under-prediction of the earth pressures. The low value of E_{ph} also contributed towards a low prediction of the bending moment between prop level D and the excavation level.

Support Level	Conventional analysis	Finite element analysis (Method 1)	Finite element analysis (Method 2)	Finite element analysis (Method 3)
A	23	23	7	5
B	245	245	157	94
C	242	242	302	225
D	330	330	643	358
E_{ph}	63	284	279	273

Table 6.4: Prop forces from the conventional and finite element analyses.

e) Contours of plastic strain

The contours of plastic strain, indicating regions where the soil has failed, plotted on the displaced shape of the mesh is shown in Figure 6.8 for the analysis by method 1). Results from method 1) proved to be intermediate with less plastic strain developing than method 2) but more than method 3). A local failure is indicated below the excavation level due to the high wall displacements in this region. Although the coefficient of passive earth pressure is not fully developed, the curved passive failure surface is clearly depicted as well as the onset of the active failure surface. This would suggest that the soil in front of the wall embedment is highly unstable.

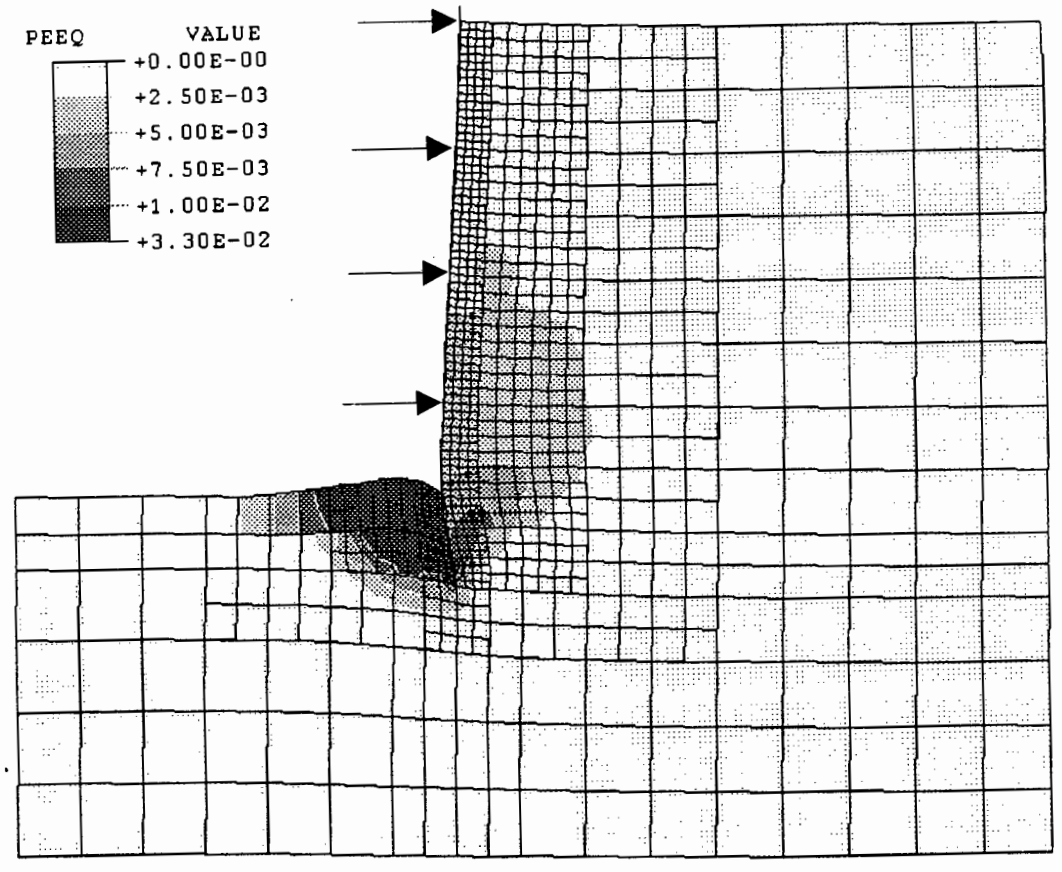

Figure 6.8: Contours of plastic strain plotted on the displaced mesh (method 1).
(Magnification of displacements = 20)

CHAPTER 7
FACTOR OF SAFETY

7.1 FACTORS OF SAFETY USED IN PRACTICE

Brinch Hansen (1953) set out a philosophy of geotechnical design in which separate considerations are given to the selection of design loads and design values of soil strength. Partial coefficients were proposed to factor characteristic loads and soil strength parameters to derive design values. This approach of adjusting parameters was influential on certain conventional design practice applications. In the finite element context partial factors can be easily and readily applied. The soil strength parameters, generally the peak values, are factored down to design parameters with which the analysis is undertaken.

However, this approach focuses only on an estimate of loads and resistances for design and ignores the effect of deformations. In lateral support problems the excavation of supporting soil causes the development of plastic strain in the soil adjacent to the wall. The areas of plastic strain represent areas where the soil has failed. The amount of failed soil depends on the amount of deformation of the support system. In the finite element method a factor of safety can be developed taking account of these kinematic effects.

In this chapter, some consideration is given towards a definition of a factor of safety based on the quantity dissipated plastic strain energy. Due to the lack of a clear definition of failure for the case of multiple level supported walls, the application of the proposed factor of safety is limited to cantilever walls installed in selected soil types.

A preliminary effort is also made to extend the application of the safety factor to multiple level supported walls. This involved a study of how the quantity dissipated plastic strain energy evolved during multiple level support system analyses. A complete study of the factor of safety and its precise definition is beyond the scope of this investigation.

7.2 CONSIDERATIONS FOR A FACTOR OF SAFETY IN FINITE ELEMENT ANALYSIS

For a specific engineering problem of a metal plate in tension, an energy based generalized factor of safety (GFS) was proposed by Hsu (1991). It is defined as $GFS = \left(\frac{TUSE}{TSE}\right)^{\frac{1}{n}}$ where TUSE is the total ultimate strain energy at failure, and TSE is the current strain energy and n is a material related parameter. The calculation of the total strain energy accounts for the material properties of soil and wall directly. This may be acceptable for structural components of fixed domain, but not for geotechnical applications. A

shortcoming of using the strain energy is that it is dependent on the total size of the area meshed since total strain energy is integrated over the entire discretized area. In the case of the analysis of support systems, this is not a useful definition since the size of the area meshed is not fixed.

It appears that a more suitable approach is to use dissipated plastic strain energy as a quantity in an expression of the factor of safety.

Plastic work at a point in the material model is defined by:

$$W^{pl} = \int \sigma \, d\varepsilon^{pl}$$

Plastic work is done when the elastic limit has been exceeded. This occurs only in the regions where sufficient deformation has taken place. The regions that have undergone plastic strain indicate the zones of failure. The dissipated plastic strain energy, for convenience hereafter referred to as dissipated energy, is the integral of plastic work over the whole volume and is written as:

$$DE = \int_V W^{pl} dV$$

A proposed expression for the factor of safety can therefore be written as:

$$FS = \left(\frac{UDE}{DE} \right)^{\frac{1}{n}}$$

where UDE is the ultimate dissipated energy at failure and DE is the dissipated energy at the design depth of excavation. This expression gives a measure of the energy still to be dissipated before failure is reached. It is also independent of the area meshed since, for an accurate solution, the mesh has to incorporate at least all areas in which plastic strain occurs.

The factor of safety ranges from infinity at zero excavation to unity when at the maximum depth of excavation DE and the UDE have the same magnitude. The following section involves a study of the dissipated energy and the application of the proposed factor of safety to cantilever walls.

7.3 STUDY OF DISSIPATED PLASTIC STRAIN ENERGY

7.3.1 Cantilever Walls

The development of the dissipated energy is investigated for the cantilever wall installed in three different soil types as presented in Chapter 4, namely the isotropic and anisotropic sand and the homogeneous clay. In Figure 7.1 (a) and 7.1 (b) the development of the dissipated energy in the three different soil types is shown. (It should be noted that the

scales on the vertical axes are different). For the case of a cantilever wall installed in clay, shown in Figure 7.1 (a), a sudden increase in plastic strain is observed just prior to failure of the support system.

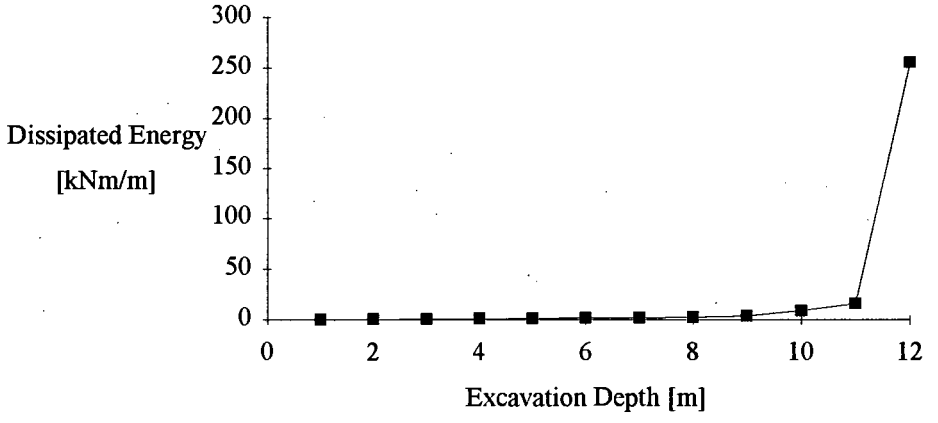

Figure 7.1 (a): Dissipated energy versus excavation depth for a homogenous clay.

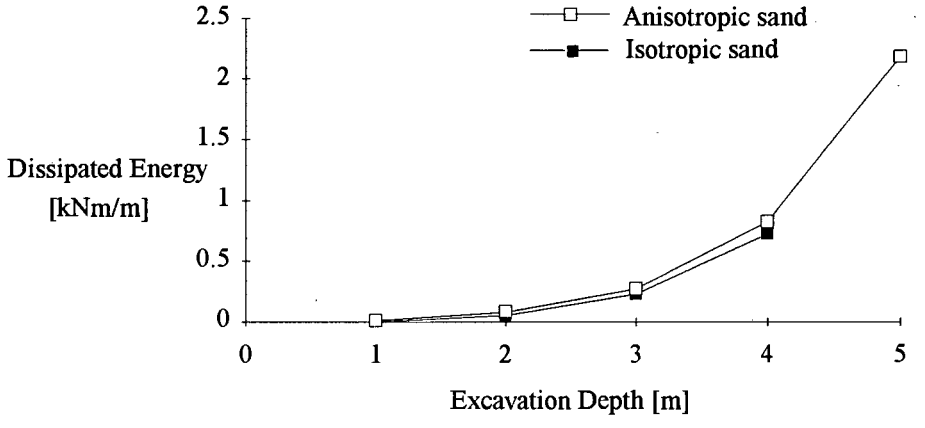

Figure 7.1 (b): Dissipated energy versus excavation depth for an isotropic and anisotropic sand.

For this reason the definition of the factor of safety was modified so that the area under the graph of dissipated energy versus excavation depth is being used in place of the value of the dissipated energy itself. The rate of change of the area under the relationship with respect to the excavation depth is less than the rate of change of the quantity dissipated energy. Thus, the calculation of the measure $\int_0^z \mathrm{UDE}\, dz$ as the maximum depth is approached is less sensitive than the measure UDE. The factor of safety can now be expressed as

$$FS = \left(\frac{\int_0^z \mathrm{UDE}\, dz}{\int_0^z \mathrm{DE}\, dz} \right)^{1/n},$$

The graphs of the factor of safety versus excavation depth are shown in Figure 7.2. Values of $n = 2$ and $n = 5$ in the expression were chosen arbitrarily to demonstrate the influence of n on the modified factor of safety. The values of the factor of safety were limited to the range between 1 and 2.5 and the respective excavation depths shown. As an example, the maximum depths of excavation allowed assuming a factor of safety of 1.5 are indicated on the graph. The higher value of n restricted the maximum excavation depth to a greater extent. Thus, an increase in the value of n results in a more conservative result. The value of n should possibly be higher for cohesive soils, as opposed to non-cohesive soils, because of the rapid increase in plastic strain just prior to failure.

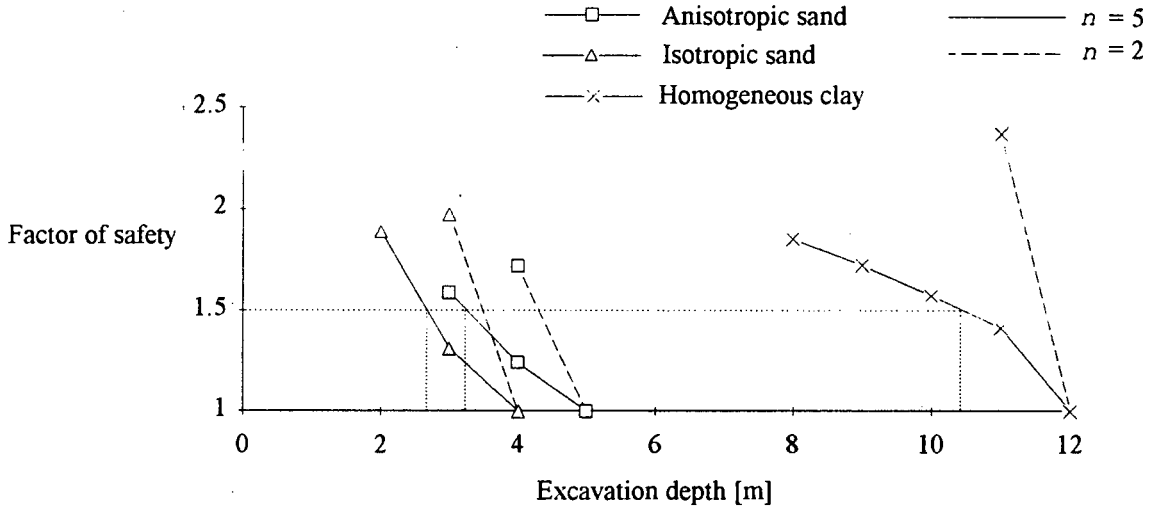

Figure 7.2: Factor of safety versus excavation depth for the three different soils types.

In order to determine if these maximum depths given by the proposed safety factor definition are reasonable, the analyses of the cantilever walls were redone with partial safety factors applied to the soil strength parameters. According to the Brinch Hansen approach , the parameters of internal friction angle, ϕ, and of cohesion, c, are reduced by a recommended factor. To enable a comparison to the above results a factor of safety of 1.5 was applied to both of these shear parameters. The reduced values in terms of the equivalent Drucker-Prager parameters are listed in Table 7.1.

Description	Friction angle, β	Cohesion, d [kPa]	Dilation angle, ψ	Reduced friction angle, β	Reduced cohesion, d [kPa]	Reduced dilation angle, ψ
Homogeneous clay	35.8°	46.4	17.9°	26.3°	32.7	13.1°
Isotropic sand	44°	1.39	22°	34.1°	1.0	17.1°
Anisotropic sand	44°	1.39	22°	34.1	1.0	17.1°

Table 7.1: Drucker-Prager soil strength parameters and the factored equivalents for the three selected soil types.

The maximum excavation depths (to the nearest 0.5m) allowed by the proposed factor of safety with n = 5 and those achieved from the analyses involving factored soil strength parameters are compared in Table 7.2. The results indicate that the application of partial safety factors yield more conservative excavation depths than the dissipated energy based factor of safety.

Soil type	Maximum depth allowed by proposed safety factor [m]	Maximum depth allowed by partial safety factors [m]
Homogeneous clay	10	7.5
Isotropic sand	2.5	2
Anisotropic sand	3	2.5

Table 7.2: Maximum excavation depths allowed by the proposed energy based factor of safety and the conventional partial factors of safety.

7.3.2 Multiple Level Supported Walls

In terms of the cantilever wall system, the approach to the problem of introducing a factor of safety expression in the finite element method depends on achieving a solution just prior to failure so that the quantity UDE can be calculated. However, the failure of a multiple level supported system cannot be based on the consideration of simply the maximum excavation depth. With the provision of prop support such a straight forward criteria of support system failure is not available.

The solution of the numerical scheme just prior to failure of the system can be defined by an analysis in a number of possible ways. One is to allow excavation to continue below the design depth until a solution cannot be converged upon. This method is not a satisfactory way of defining the failure of the system since, in reality, additional props would be introduced when the next prop level was reached. Another would be to introduce additional props when the next prop level is reached and continue this process until a converged solution cannot be achieved. This is still not satisfactory since it extends the computer time and the maximum depth obtained would be dependent on the parameters for prop stiffness and applied prop forces.

The application of the proposed factor of safety to multiple level supported systems was not undertaken, however, the evolution of dissipated energy as a function of the excavation depth was considered. The purpose being to assess dissipated energy as a suitable measure on which to base an expression for a factor of safety for support systems in general.

suitable measure on which to base an expression for a factor of safety for support systems in general.

The examples considered were those of the four level supported sheet pile wall in anisotropic sand presented in the first section of Chapter 5, and the multiple level supported wall case study presented in Chapter 6. The evolution of dissipated energy with excavation depth for the standard sheet pile wall is shown in Figure 7.3. The rate of change of dissipated energy decreases slightly each time a prop is introduced. This demonstrates that the quantity dissipated energy responds directly to the effect that supports have on improving the stability of the system.

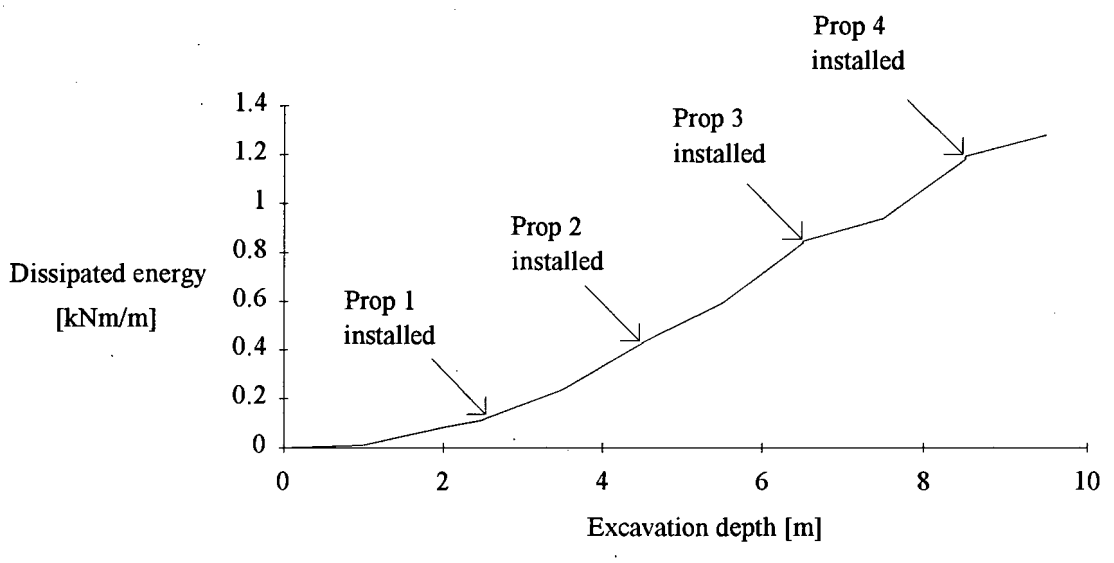

Figure 7.3: Dissipated energy as a function of excavation depth for the sheet pile wall in anisotropic sand.

Figure 7.4 shows the evolution of dissipated energy for the case study. The effect of supports and soil properties on the quantity of dissipated energy is demonstrated by this example. The effect of prop supports is similar to the previous example where the rate at which the dissipated energy increases is reduced indicating that the system has been made more stable.

The influence of soil properties is more interesting and responsible for the behaviour of the dissipated energy around the installation of prop 4. The decrease in value of the dissipated energy implies that there has been a reduction in the amount of plastic strain. This means that the material that was removed had undergone more plastic strain than the amount that occurring in the supporting material that remains. This decrease in the amount of plastic strain that developed in the supporting soil occurred as the excavation depth approached the level of sand and then began to increase once again. The Young's modulus for sand was greater than for the silt and therefore as the excavation level approached the

underlying sand, the supporting sand deformed less than the silt had been deforming. This example shows that the quantity dissipated energy also captures the effect that soil properties have on the stability of the system.

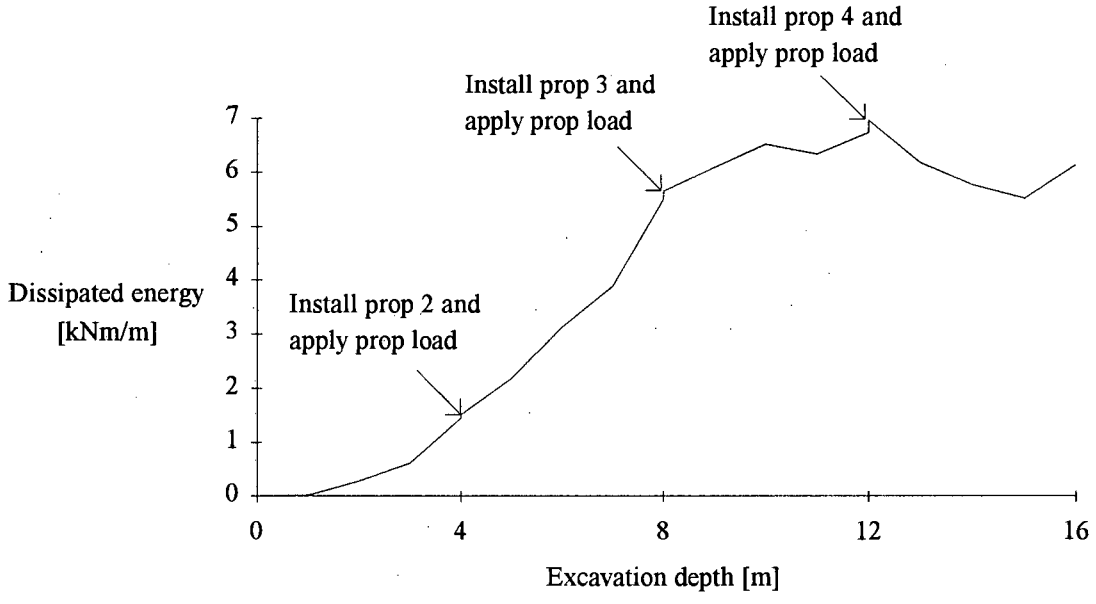

Figure 7.4: Dissipated energy as a function of excavation depth for the four-level supported system case study.

A complete study of the factor of safety for application to the finite element method is required if the finite element method is to be used in general design practice. The definition of the safety factor should be applicable to a wide range of situations. The preliminary study undertaken in this chapter suggests that dissipated energy is a good measure on which to base the definition.

CHAPTER 8
CONCLUSIONS AND RECOMMENDATIONS

8.1 CONCLUSIONS

A number of conclusions can be drawn from the finite element studies done in this investigation.

Based on the investigation using cantilever walls it was found that:

1. The choice of plastic flow rule has a significant influence on the maximum depth of excavation that can be achieved before failure. A fully associative flow rule allows the greatest depth of excavation. This influence can be extended to multiple level supported walls where a greater prop spacing would be enabled by a flow rule approaching fully associative flow.
2. Wall friction has an influence on the soil-structure interaction. Greater passive earth pressures are mobilized with an increase in the coefficient of wall friction and therefore deeper excavations are possible.
3. The accurate description of the soil properties is an important aspect of the finite element model. The shear strength parameters influence the stability of the system and the soil stiffness is particularly relevant to the magnitude of surface settlements behind the wall.
4. Earth pressures seldom act at the limit state as assumed in conventional design methods.
5. The main disadvantage of finite element method is that the length of the structure needs to be assumed at the onset of the analysis whereas this is calculated in conventional analysis.

The parameters investigated using the multiple level supported systems are all inter-dependent and should not be considered in isolation. However, the approach of varying one parameter whilst keeping the others constant revealed that:

1. Flexible walls attract smaller bending moments than stiffer walls because they allow the redistribution of earth pressure. There is an increase in the amount of plastic strain that occurs in the soil adjacent to walls of increasing flexibility. A more flexible wall system is therefore less stable than a system with a stiffer wall. The magnitude of surface settlements behind the wall are greater for stiff walls when compared to flexible walls of the same length. An increase in embedment depth will, however, reduce the settlements behind a stiff wall which is not the case for flexible walls.

2. Stiffer props tend to increase the bending moments that occur at the support levels. The trend with respect to bending moments is that a lower bending moment occurs between the lowest prop level and the excavation level for stiffer props. This is an important consideration because the highest bending moment often occurs in this region.
3. The application of additional support loads can be implemented to simulate the effect of prop prestress. Applying support loads has a similar effect to increasing the stiffness of the support without requiring a stiffer support.
4. The parameters of wall and prop stiffness and the application of additional support loads can be easily varied so that the design of the support system can be optimized.
5. The main advantages of the finite element method over conventional methods are that the earth pressures are calculated taking account of all the important variables and that the behaviour of the whole system can be reliably predicted which includes information about the soil as well as the structure.

Concerning a factor of safety that can be applied to the finite element method:

A proposed definition for a factor of safety is based on the quantity of dissipated plastic energy. The definition yields less conservative results to those when Brinch Hansen partial safety factors are applied to the soil properties in the case of cantilever walls. The measure dissipated plastic strain energy includes the effects of material strength parameters and wall supports and its performance suggests that it is suitable for the definition of a factor of safety.

8.2 RECOMMENDATIONS

Based on the investigation that was undertaken the following recommendations can be made:

1. The finite element model of a lateral support system should include:
   - a non-associative flow rule;
   - wall friction to simulate soil-structure interaction;
   - an accurate description of the soil properties and
   - an appropriate solution algorithm for simulating the excavation procedure.
2. A conventional analysis should always be done in conjunction with the finite element analysis. This will give the analyst information on which to base a choice of the embedment depth of the structure and will minimize the time spent on optimizing the design. The redistributed shape of the lateral earth pressures should, in turn, be assessed in terms of the earth pressure distributions calculated by the finite element method.

3. A definition of a dissipated energy based factor of safety needs to be developed and extended to multiple level supported walls. A reliable expression of a factor of safety, applicable to a wide range of situations would serve to encourage the use of the finite element method in general practice.

This investigation has shown that the finite element method has a lot to offer in terms of lateral support system design and it is recommended that it is used as a routine design tool.

REFERENCES

ABAQUS Version 5.2 Users Manual, Hibbitt, Karlsson and Sorensen, Inc., Providence, R.I. (1992)

ABAQUS Version 5.2 Theory Manual, Hibbitt, Karlsson and Sorensen, Inc., Providence, R.I. (1992)

Bjerrum, L., Frimann Clausen, C.J., and Duncan, J.M., (1972), Earth pressures on flexible structures, *Proc. 5th ECSMFE*, Madrid, State of the Art Paper, 169-196

Blum, H., (1950), Beitrag zur Berechnung von Bohlwerken, *Bautechnik*, **2**, 45

Bowles, J.E., (1988), *Foundation Analysis and Design*, McGraw-Hill, New York

Brinch Hansen, J., (1953), *Earth pressure calculation*, DGI, Copenhagen

Brown, P.T., and Booker, J.R., (1985), Finite element analysis of excavation, *Computers and Geotechnics*, **1**, 207-220

Caqout and Kérisel, (1948), *Tables de poussée et butée*, Gauthier-Villars, Paris

Code of Practice, (1989), *Lateral Support in Surface Excavations*, SAICE, Geotech. Div., Yeoville

Edelman, T. et al., (1958), Comparitive sheet piling calculations, *Proc. Brussels Conference on Earth Pressure Problems*, **2**, 71-81

Egger, P., (1972), Influence of wall stiffness and anchor prestressing on earth pressure distribution, *Proc. 5th ECSMFE*, Madrid, State of the Art Paper, 259-264

Félix, B., Frank, R., and Kutniak, M., (1982), F.E.M. calculations of a diaphragm wall, influence of the initial pressures and of contact laws, *Int. Symposium on Numerical Models in Geomechanics*, 643-652

Finno, R.J., (1989), Field measurements of strain localization in soft clay, *Cracking and Damage*, Mazars, J. and Bazant, Z.P. (Eds), Elsevier Applied Science, N.Y.

Finno, R.J., and Harahap, I.S., (1991), Finite element analysis of HDR-4 excavation, *Journal of Geotechnical Engineering, ASCE*, **117**, 1590-1609

Fourie, A.B., (1992), Statically indeterminate retaining walls - Analysis by the finite element method, *Proc. FEMSA*, 187-200

Hsu, T. ,(1991), A generalized factor of safety under energy basis, *Computers in Structures* **39**, 609-613

Murakami, H., Yuki, Y., and Tamano, T., (1988), Perfomance and analysis of anchored sheet pile wall in soft clay, *Numerical Methods in Geomechanics*, 1341-1346

Nendza, H. (Eds.), (1989), Tunnelbau, *Dt. Ges. f. Erd-u. Grundbau*, pp. 43-63

O'Rourke, T.D., and Jones, C.J.F.P., (1990), Overview of earth retention systems: 1970-1990, *Proc Speciality Conf. on Soil Mech. and Foundation Eng., ASCE*, 22-51

Ortiz, M., Leroy, Y., and Needleman, A., (1987), A finite element method for localized failure analysis, *Comp Meth in Applied Mech and Eng*, **61,** 189-214

Ostermayer, H., (1981), Lecture notes, *Techn. Universität München*

Potts, D.M., and Day, R.A., (1990), Use of sheet pile retaining walls for deep excavations in stiff clay, *Proc. Institution Civil Engineers*, **88**, 899-927

Potts, D.M., and Fourie, A.B., (1985), The effect of wall stiffness on the behaviour of a propped retaining wall, *Géotechnique*, **35**, 347-352

Rowe ,P.W.,(1952), Anchored sheet pile walls, *Proc ICE*, **1**, 27-70

Smith, I.M., and Ho, D.K.H., (1992), Performance of a braced excavation in a marine clay, *Int. J. Num. Analyt. Methods in Geomech.*, **16**, 845-867

Terzaghi, K., (1943), *Theoretical Soil Mechanics*, New York, Wiley, 510

Terzaghi, K., (1954), Anchored bulkheads, *ASCE Transactions*, **119**, 1243-1324

Terzaghi, K. and Peck, R.B., (1967), *Soil Mechanics in Engineering Practice*, John Wiley Sons, New York.

Tsui, Y., and Clough, G.W., (1974), Plane strain approximations in finite element analyses of temporary walls, *Proc. Bi-annual ASCE Geotech. Conf., Austin, Texas*

Whittle, A.J., Hashash, Y., and Whitman, R.V., (1993), Analysis of deep excavation in Boston, *Journal of Geotechnical Engineering, ASCE*, **119**, 69-90

Winterkorn, H.F. and Fang, H.(Ed), (1975), *Foundation Engineering Handbook*, Van Nostrand Reinhold, New York.

APPENDIX

EXAMPLE INPUT DECK

```
*HEADING, UNSYMM
RETAINING WALL ANALYSIS
**
**
** NODE DEFINITIONS
**
*RESTART, WRITE, FREQUENCY=30
**
**Input all nodal coordinates
*NODE, INPUT=/j1/clrtro01/nodelm/sw.nod
**
**Define node sets on the boundaries
*NSET, NSET=LHS, GENERATE
1,7,1
.....
.....
*NSET, NSET=RHS, GENERATE
3134,3140,1
.....
.....
*NSET, NSET=BOT
1,12,23,34,168,179,457,791,6858,
.....
.....
**Define node set of wall
*NSET, NSET=WALL, GENERATE
6747,6778,1
.....
.....
**Define node set of ground surface behind the wall
*NSET, NSET=SETT
6218,6243,6268,6293,6318,
6404,6417,6498,6511,6524,6537
**
**Define node sets of the nodes on the interface of soil and wall for each layer
*NSET, NSET=CONN1, GENERATE
5958,5962,1
*NSET, NSET=SLID1, GENERATE
6799,6803,1
*NSET, NSET=CONN2, GENERATE
5954,5958,1
*NSET, NSET=SLID2, GENERATE
6795,6799,1
.....
.....
**Define node set of prop positions
*NSET, NSET=PROP
6795,6785,6774
**
** ELEMENT DEFINITIONS
**
*ELEMENT, TYPE=B21, ELSET=WALL, INPUT=/j1/clrtro01/nodelm/freeb.elm
```

```
**
*ELEMENT, TYPE=CPE4R, ELSET=SOIL, INPUT=/j1/clrtro01/nodelm/freee.elm
*ELEMENT, TYPE=CPE4R, ELSET=SOIL, INPUT=/j1/clrtro01/nodelm/freep.elm
**
**Define slide line interface elements
*ELEMENT, TYPE=ISL21, ELSET=BCONT
4001,6218,6217
.....
.....
**
*ELEMENT, TYPE=ISL21, ELSET=FCONT
3009,5769,5770
.....
.....
**
*ELGEN ,ELSET=BCONT
4001,23,-1
.....
.....
*ELGEN ,ELSET=FCONT
3009,23,1
.....
.....
**
**Define spring elements for props
*ELEMENT, TYPE=SPRING1, ELSET=PROP1
5001, 6795
*ELEMENT, TYPE=SPRING1, ELSET=PROP2
5002, 6785
*ELEMENT, TYPE=SPRING1, ELSET=PROP3
5003, 6774
*ELSET, ELSET=PROPS
PROP1, PROP2, PROP3
**
**Define element sets for ouput purposes
*ELSET ,ELSET=ACTIVE, GENERATE
4001,4056,1
*ELSET ,ELSET=PASSIVE, GENERATE
3008,3056,1
**
*ELSET ,ELSET=WHOLE
SOIL, WALL
*ELSET ,ELSET=ALL
WHOLE, BCONT, FCONT
**
**Define element sets for layers to be excavated
*ELSET, ELSET=LAYER1, GENERATE
1812,1884,24
.....
.....
**
*ELSET, ELSET=LAYER2, GENERATE
1808,1880,24
.....
.....
**
**Define element sets of layers of soil elements throughout the model for
**increasing Young's modulus with depth
```

```
*ELSET, ELSET=E1, GENERATE
2054,2061,1
*ELSET, ELSET=E1
LAYER1, LAYER2,
.....
.....
*ELSET, ELSET=E2, GENERATE
2046,2053,1
.....
.....
**
**Define the slide lines for the interfaces on each side of the wall
*SLIDE LINE, ELSET=BCONT, TYPE=LINEAR, GENERATE
6803,6780,-1
6778,6747,-1
6866,6863,-1
6861,6858,-1
*SLIDE LINE, ELSET=FCONT, TYPE=LINEAR, GENERATE
6858,6861,1
6863,6866,1
6747,6778,1
6780,6803,1
**
**Input all multi-point constraints
*MPC, INPUT=/j1/clrtro01/nodelm/free.mpc
**********************************************
**Element properties
**Define soil properties for each layer throughout depth of model
*SOLID SECTION, ELSET=E1, MATERIAL=PSOIL1
*SOLID SECTION, ELSET=E2, MATERIAL=PSOIL2
*SOLID SECTION, ELSET=E3, MATERIAL=PSOIL3
*SOLID SECTION, ELSET=E4, MATERIAL=PSOIL4
*SOLID SECTION, ELSET=E5, MATERIAL=PSOIL5
*SOLID SECTION, ELSET=E6, MATERIAL=PSOIL6
*SOLID SECTION, ELSET=E7, MATERIAL=PSOIL7
*SOLID SECTION, ELSET=E8, MATERIAL=PSOIL8
*SOLID SECTION, ELSET=E9, MATERIAL=PSOIL9
*SOLID SECTION, ELSET=E10, MATERIAL=PSOIL10
*SOLID SECTION, ELSET=E11, MATERIAL=PSOIL11
**
**Define interfaces and associated friction
*INTERFACE, ELSET=BCONT
1.,0.,0.,1.
*FRICTION
0.0,
*INTERFACE, ELSET=FCONT
1.,0.,0.,1.
*FRICTION
0.0,
**
**Define wall section properties
*BEAM SECTION, SECTION=RECT, MATERIAL=STEEL, ELSET=WALL
1.,0.1675
0,0,-1
**
**Define spring properties
*SPRING, ELSET=PROP1
1
```

```
3000
*SPRING, ELSET=PROP2
1
3000
*SPRING, ELSET=PROP3
1
3000
**********************************************
**Material properties
*MATERIAL, NAME=PSOIL1
*ELASTIC
6.0E3,0.3
*DRUCKER PRAGER
43.3,1.0,43.3
*YIELD, TYPE=SHEAR
1.37,0.0,
*DENSITY
2.039
**
*MATERIAL, NAME=PSOIL2
*ELASTIC
18.0E3,0.3
*DRUCKER PRAGER
43.3,1.0,43.3
*YIELD, TYPE=SHEAR
1.37,0.0,
*DENSITY
2.039
**
.....
.....
**
*MATERIAL, NAME=STEEL
*ELASTIC
206.E6,0.3
*PLASTIC
300.0E3,0.0
*DENSITY
2.039
**********************************************
**Boundary conditions
*BOUNDARY
LHS,1,,
BOT,2,,
RHS,1,,
**********************************************
**Initial conditions
*INITIAL CONDITIONS, TYPE=STRESS, GEOSTATIC
SOIL, 0.0,22.0, -440.0,0.0, 0.5
**********************************************
**Gravity Loading
*STEP
*GEOSTATIC
*DLOAD
SOIL,GRAV,-9.81,0.0,1.0
*PRINT, CONTACT=YES
*EL PRINT, ELSET=PASSIVE, POSITION=AVERAGED AT NODES
S11,S12
```

```
*NODE PRINT, FREQUENCY=0
*END STEP
**********************************************
**Deactivate Anchors
*STEP
*STATIC
0.1, 1.
*MODEL CHANGE, REMOVE
PROP1,PROP2,PROP3
*EL PRINT, FREQUENCY=0
*NODE PRINT, FREQUENCY=0
*END STEP
*****************************************
**Fix all nodes in contact and remove contact element
*STEP, INC=1
*STATIC
1. ,1.
*CHANGE MATERIAL, ELSET=BCONT
*FRICTION
0.43,
*CHANGE MATERIAL, ELSET=FCONT
*FRICTION
0.43,
*BOUNDARY, FIXED
CONN1,PINNED
SLID1,PINNED
*MODEL CHANGE, REMOVE
3063,3062,3061,3060
*EL PRINT, FREQUENCY=0
*NODE PRINT, FREQUENCY=0
*END STEP
*****************************************
**Remove two layers of elements
*STEP, INC=30
*STATIC
0.1, 1.
*BOUNDARY, OP=NEW
LHS,1,,
BOT,2,,
RHS,1,,
*MODEL CHANGE, REMOVE
LAYER1,
*EL PRINT, ELSET=ACTIVE, FREQUENCY=30, POSITION=AVERAGED AT NODES
S11,S12
*EL PRINT, ELSET=PASSIVE, FREQUENCY=30, POSITION=AVERAGED AT NODES
S11,S12
*NODE PRINT, NSET=PROP, FREQUENCY=30
RF,U
*END STEP
*****************************************
.....
.....
```